Population ecology of mesopelagic fishes

Thorvaldsen, Kjetil Gjeitsund

Publication date:
2022

Document Version
Publisher's PDF, also known as Version of record

Thesis title/Author: Population ecology of mesopelagic fishes/ Kjetil Gjeitsund Thorvaldsen

Page, line	States	Should state
7,1	mesopelagic fish species	the mesopelagic fish species
8,14	were	where
14, 1	understood(Webb	understood (Webb
14,3	gigaton(Proud	gigaton (Proud
14,4	gigaton(FaO	gigaton (FaO
14,6	unknown.(Hidaka	unknown (Hidaka
14,12	Identify mesopelagic	Identify the mesopelagic
14,15	Use triangular	use triangular
14,14	(TS(F)to identify signatures (II,II), Use	(TS(F)to identify signatures (I), use
15,1	Calanusfinmarchicus	*Calanus finmarchicus*
15,5	In this chapter I	in this chapter, I
15,14	depth(Kaartvedt	depth (Kaartvedt
15,16	bathtpelagic(Duvall	bathypelagic (Duvall
16,3	limited(Webb	limited (Webb
16,8	et al., 2014)	*et al., 2014*).
16,12	zooplankton(Barham	zooplankton (Barham
16,14	piscivorous(Salvanes	piscivorous (Salvanes
17,6	Norway(Grimaldo	Norway (Grimaldo
17,8	assumed(Iririgoien	assumed (Irigoien
18,1	communities are	Communities is
18,3	fishes(Marshall…)(figure 1	fishes (Marshall..) (Figure 1)
18,4	enormous(Irigoien	enormous (Irigoien
18,7	spatially(Kaartvedt	spatially (Kaartvedt
18,9	ontogeny(Giske	ontogeny (Giske
18,title 2.2	2.2 maurolicus muelleri	2.2 *Maurolicus muelleri*
18,14	abundant(Rees	abundant (Rees
19,6	distribution(Ikeda	distribution (Ikeda
19,9	mounts(Toyokawa	mounts (Toyokawa
19,13	year(Gjøsæter	year (Gjøsæter
19,18	spring(Gjøsæter	spring (Gjøsæter
20,1	aquaculture(Alvheim	aquaculture (Alvheim
20,3	catchability(Kaartvedt	catchability (Kaartvedt
21, title	3.1 acoustics	3.1 Acoustics
22,1	studies(Simmonds	studies (Simmonds)
21,6	1966) .	1966).
22.2	consequences(St.John	consequences (St.John
22.6	morphologies(Godø	morphologies (Godø
22.7	backscatter(Toyokawa	backscatter (Toyokawa
22,11	estimates(Nakken	estimates (Nakken
22, 19	ex situ	*ex situ*,
23,4	fish(Nakken	fish (Nakken
23,10,	scattering(Figure 3a	scattering (Figure 3a
23,11	peak(Figure 3b	peak (Figure 3b
23,12	Stabilizes(Figure 3c	stabilizes (Figure 3c
23,16	animal(Sundnes	animal (Sundnes
24,1	estimation(Kloser	estimation (Kloser
24,5	The Three dimentional	The three dimentional
25,12	Frequency(Olav Handegard	frequency (Handegard et al., 2009
25,19	Thesis (I,II,III,)	Thesis (I, II, III(
26,3	methods (I,II,III)	methods (I, II, III)
26,4	Strength (I,III)	strength (I, III)
27, figure 4	Figure 4: example	Figure 4: Example
28, figure 5	Example of Maurolicus	Example of pearlside
25.14	behaviour (cech	behaviour (Cech
28, section 3.3.1 line 2	fishes(Proud	fishes (Proud

29,17	contac(Hosia	contact (Hosia
30,3	camera(Dias	camera (Dias
30,6	;(I)),(I)	;I)
30,7	pearlside(Giske	pearlside (Giske
34, 5 and 6	*C.finmarchicus*	*C. finmarchicus*
34.17	mm(Visser	mm (Visser
34,19	kilometres(Rizzo	kilometres (Rizzo
35,3	export(Davison	export (Davison
35,8	predators(Bjelland	predators (Bjelland
36,Title	4.11 quantifying….self overlap	4.11 Quantifying…self-overlap
36.16	encounters(Bianco et al., 2014. .	encounters (Bianco et al., 2014).
36.17	Flight(Viswanathan	flight (Viswanathan
38,2	calculations of	Calculations see
38,4	There are	there is
38,5	organism have	organism has
38,9	monte carlo	Monte-Carlo
38,13	radiuses are	radiuses is
38,14	Where,	Here,
38.15	self overlap	self-overlap
37,11	factors(Aksnes	factors (Aksnes
38,16	self-overlap(Bianco	self-overlap (Bianco
39, title	Movement ecology of maurolicus	Movement ecology of pearlside
39, 2	Comfort zone(Staby	comfort zone (Staby
39,8	regimes(Kaart	regimes (Ka
39,10	pattern(figure 5 and 8). as	pattern (figures 5 and 8). As
39,9	differences(Giske	differences (Giske
39,17	copepods(Rasmussen… Thorvaldsen et al	copepods (Rasmussen…. II;III)
40,title	4.21 Self overlap with maurolicus muelleri	4.2.1 Self-overlap behaviour of pearlside
40,4	Self overlap model (equation x	self-overlap model (equation 3)
40,3	mortality(Giske	mortality (Giske
41,2	studies(Christiansen	tudies (Christiansen
43,2 and 3	low(III……fishes(II	low (III….. fishes (II
44.1	Cfinmarchicus	*C.finmarchicus*
44,4	density(II,III	density (II, III
45,10	surface(Bagøien	surface (Bagøien
45,17	-1(Yen	-1 (Yen
48, 7	classes(Martin	classes (Martin
48, 14	samples(goviandarajan	samples (Govindarajan
49,3	properties(Agersted	properties (Agersted
49,7	trawl(Underwood	trawl (Underwood
49,8	process(Allken	process (Allken
49,10	problematic(Hosia	problematic (Hosia
51,1	identified	identified as
51,6	studies,	studies
51,9	Trophic layers	trophic levels
51,15	escape(Yen	escape (Yen
52,5	error(Ehrenberg	error (Ehrenberg
52.12	prey(Edward	prey (Edward
52,16	seal(Goulet	seal (Goulet
53,2	evolution (Bianco	evolution (Bianco
53,3	stueis	studies
53,4	properties	properties,
53,10	distribution(III)	distribution (III)
54,1	models(LOtka	models (Lotka
54.12	2020)fish	2020), fish
54,13	mussels(Pastor	mussels (Pastor

DTU Aqua
National Institute of Aquatic Resources

Population ecology of mesopelagic fishes

Kjetil Gjeitsund Thorvaldsen

PhD Thesis

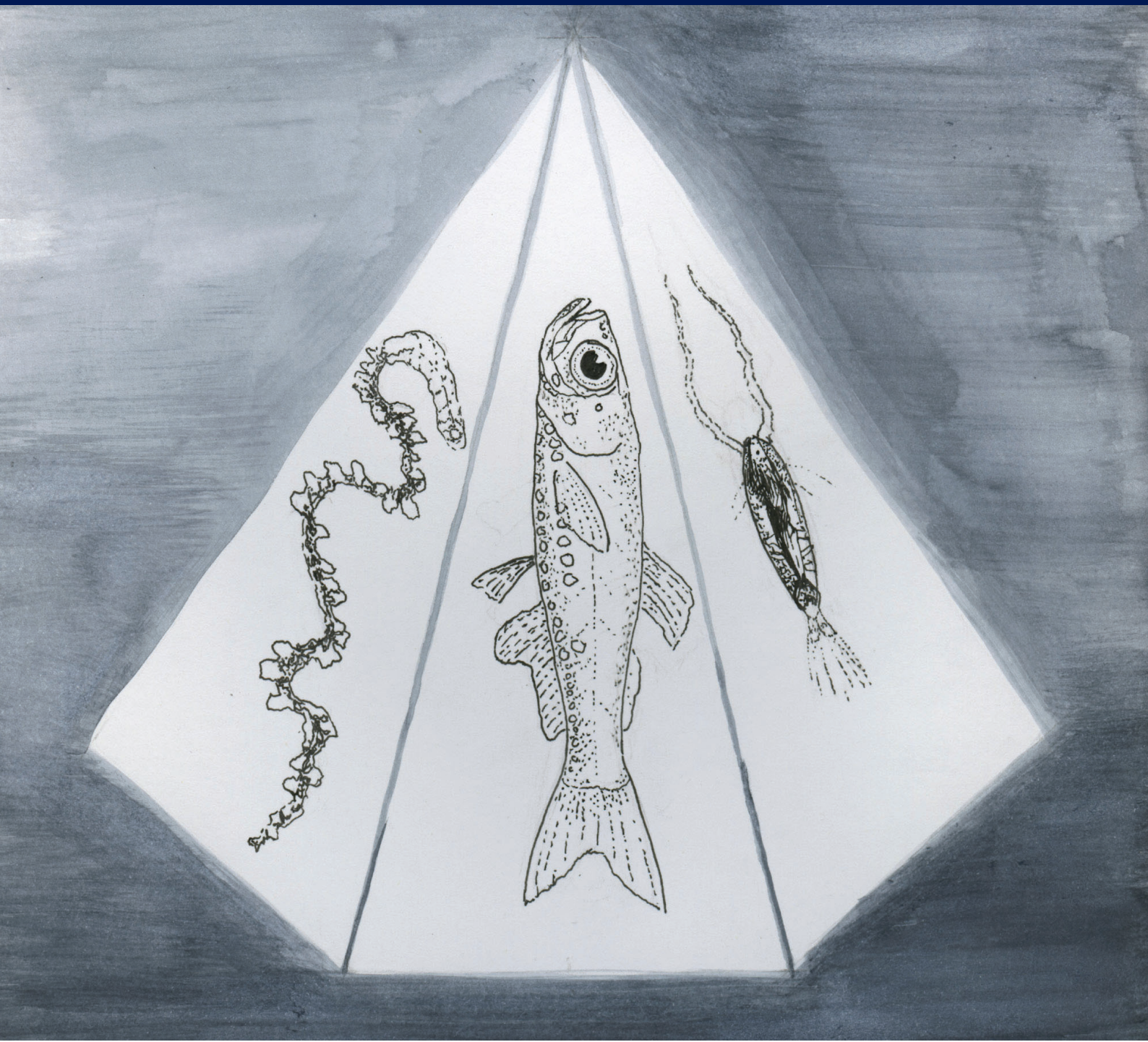

Cover art – Ingvild Mandrup

Population ecology of mesopelagic fishes

Kjetil Gjeitsund Thorvaldsen

Preface

This PhD project was carried out at The National Institute of Aquatic Resources DTU Aqua, Sections for Oceans and arctic, Technical Unversity of Denmark (DTU). The PhD was funded by EU-project “H2020 MEESO” with grant number 817669, and EU-project “H2020 PANDORA” with grant number773713. The presented work in this thesis have been carried out under the main supervision of Senior researcher Stefan Neuenfeldt, and co-supervision of Professor Patrizio Mariani, and Professor J. Rasmus Nielsen. The PhD project also includes a stay abroad at the Max Planck institute. Presented in this thesis are three scientific papers, and an introduction summarizing the work done in the respective papers.

-Kjetil Gjeitsund Thorvaldsen

Acknowledgments

I would like to offer a special thanks to my main supervisor Senior researcher Stefan Neuenfeldt for everything for these three years. I remember you told me "A PhD should be fun", and I have tried to live by that every day for three years, and I can confirm it has been fun from the first day, through the entire pandemic and to the final day. I am very thankful for the daily supervision, and being able to discuss fisheries biology, guitar solos and how to park my bike correctly on a German intercity-train. I have seen these years as somewhat transformative as you have helped me to identify my own strengths and interests, and primarily lets me use those in the PhD. I have always felt that I could ask about anything, and you have always been very open minded to new approaches which I am extremely grateful for.

I would like to thank my Co-supervisors Rasmus and Patrizio for fantastic input in the last two manuscripts. I would like to thank Rasmus for the time in the PhD-committee, where I learned a lot about the administrative processes throughout a PhD, and for all your supervision. I would like to thank Patrizio for including me in the aquatic field-work course as a teaching assistant. The annual trips with Havfisken, observing shipwrecks with echosounders, catching cod, and the following fish bbq with the students is always one of the highlights of the year.

I would like to thank my office-mate Fletcher. I am so happy we started the same week. First: Thanks for helping me with python, and all sorts of programming, saving me

valuable time so I could focus at fish behaviour. Second I would thank you so much on spending 95% of our time with obscure movie references, eating Korean fried chicken, and looking at memes both before, during and after the pandemic.

I have had an amazing social experience working at DTU aqua, and I have always felt valued at section for Oceans and Arctic. This is mainly thanks to our boss Karen Edelvang that really has made hard effort of making our work environment fun and down to earth arranging seminars, Friday bars and picnics together with Maj-Britt. Thanks to Christian starting and finishing the same day as me. It has been a lot of fun both at and outside work, and I will always remember that smell of fermented sand eel we experienced in the North Sea. Thanks to Anshul, Philip and Costanza for the lunches, coffee breaks, and for normalizing enormous lunch plates, I am very happy to have shared office with you three for the later parts of the PhD.

I would also extend huge thanks to all my PhD-friends Anders, Anton, Amalia, Regitze, Aurelia, Marie, Remy, Berthe, Caroline, Delove, Paco and visitors Cian and David, and all the other PhD-students at DTU Aqua. I would like to thank Bo Lundgren for all his help with fisheries acoustics. I would like to thank Alex and Kaz for integrating me into the social life of the Max Planck University and for all our animal behaviour discussions. Thanks Karin for all kind help with the administrative part of submitting the PhD. I have gotten a lot of friends outside of work in Copenhagen. You are all appreciated and I would like to extend my thanks to Mikael, Mia, Kenneth, Mathea, Elin, Sarah, Sarah,

Amina, Iben, Nicolaj, Heidi and Julia. Thanks for making sure I literally have no spare time off work!

Finally and most importantly I would like to thank my girlfriend and domestic partner Frida, for agreeing that moving to Copenhagen and bringing our pets (thanks Linni and Jenny for emotional support) along to be a great idea, and for the wonderful eventful daily life we have shared these past 3 years. Thanks for making the most out of every day even during three bouts of Corona-lockdown. It has been an adventure! Thank you so much!

Summary

This thesis focuses mainly on mesopelagic fishes, and mesopelagic fish species *Maurolicus muelleri.* Mesopelagic fishes are found in the oceanic twilight zone starting at the end of the euphotic zone down to approximately 1000 meters. The mesopelagic zone is found in all world oceans, and the fishes that inhabit them potentially occupy the highest vertebrate biomass on earth, dwarfing the annual commercial fishery landings. Their low trophic level and high abundance suggests that they can become important as a sustainable source of protein and lipids for an increasing human population. However, they play a part in active carbon sequestering, which means overexploitation can possibly have disastrous consequences. Mesopelagic fishes are also important ecologically as the mid-trophic link between primary production and commercial species.

In this thesis, I have used a lowered hydro acoustic observation platform to identify and separate mesopelagic fishes from other taxa. I have used the a split beam echosounder to provide three dimensional locations of the target to track and quantify behaviour of common mesopelagic fish *Maurolicus muelleri (*pearlside) and their prey *Calanus finmarchicus*, and my findings are relevant for mesopelagic fish ecology, abundance estimation and potentially carbon binding.

Mesopelagic fish and physonect siphonophores have similar backscattering properties. By observing the backscatter of both siphonophores and fish at Vøringplatået at the coast of Norway over a from 35 to 160 kHz with some of the targets visually identified by a photo camera , I have shown that siphonophores species *Nanomia cara* likely can be separated from pearlside. This is because *Nanomia cara*'s observed backscattering signature obtained with broadband echosounders differed from pearlside. This can provide more precise biomass estimates in the future, and highlights the importance of alternative ground-truthing methods to verify acoustic data. However, there are still large challenges in the ground truthing process that needs further work.

The three-dimensional position data provided by the split beam echosounder can also be used to observe behaviour. By observing both juvenile and adult pearlside at close range in Sørfjorden in Norway and tracking them for more than 60 seconds I found that some of the fish showed specific swimming patterns. The 3D position data I obtained were used in a path geometry model were I could quantify the degree of overlap within the tracks. By fitting the trajectories to the path geometry model, I saw that the juvenile pearlside fish took larger risks near the surface compared to the overwintering adults in the deeper water layer. Some of the mesopelagic fishes moved in a way which enabled efficient foraging within their own visual range, while still staying hidden within the visual range of the predators.

Studying interactions with their preferred prey, I managed to resolve 3mm long copepods *Calanus finmarchicus* as single target tracks with the echosounder and observe their behaviour in three dimensions. By applying the self-overlap model, previously only applied on copepods in laboratories, and calculating their numerical density, and estimate relative light extinction, I learned that the *C.finmarchicus* in the surface took higher risks compared to two other depths. Their behaviour were likely a compromise between food search and anti-predator behviour, while behaviour in the intermediate depths were more convoluted. Higher light intensity and higher degrees of copepod movement led the fish to migrate to a lower density of prey to forage

Dansk resumé

Denne Ph.d.-afhandling omhandler hovedsageligt mesopelagiske fisk med særligt fokus på arten *Maurolicus muelleri.* Mesopelagiske fisk findes i den oceaniske twillight zone, som starter ved den nederste del af fotiske zone og forsætter til en dybde af omkring 1000m. Den mesopelagiske zone forekommer i alle verdenshave, og er hjemsted til den største del av verdens samlede fiskebiomasse. Deres lave trofiske niveau og høye utbredelse antyder, at de potentielt kan blive en vigtig bæredygtig kilde til proteiner og lipider for at facilitere en stigende verdensbefolkning. De spiller imidlertid en betydelig rolle i aktiv kulstofbinding, som betyder at overudnyttelse af disse arter muligvis kan bevirke katastrofale konsekvenser. Mesopelagiske fisk er også essentielle for marin økologi, da de mellem trofiske lag forbinder primærproduktionen og kommercielle arter.

I denne afhandling har jeg brugt en sænket hydroakustik observationsplatform for at identificere og adskille mesopelagiske fiskearter fra andre dyrgrupper. Jeg har brugt et split-beam ekkolod for at opnå tredimensionelle målinger af en målgruppe for at spore og muliggøre kvantificering af adfærdsmønstre hos almindelig mesopelagisk fisk såsom *Maurolicus muelleri (*pearlside) og deres bytte *Calanus finmarchicus,* og mit studie og mine resultater er relevante for mesopelagisk fiskeøkologi, biomasseestimation og potentielt bedre forståelse af interaksjoner som leder til kulstofbinding.

Mesopelagisk fisk og physonect sifonophorer har lignende backscatter signaturer. Ved at observere backscatter signaler fra både sifonophorer og fisk ved Vøringplatået ud for kysten af Norge i frekvensområdet 35 til 160 kHz, hvor flere individuelle mål blev artsbestemt med et optisk kamera, har jeg vist, at sifonophores arten *Nanomia cara* sandsynligvis kan blive adskilt fra pearlside individer. Dette skyldes, at de observerede backscatter signaturer af *Nanomia cara* målt med bredbåndsekkolod, adskilte sig fra pearlside. Dette kan understøtte mere præcise biomasseestimater i fremtiden, og fremhæver vigtigheden af alternative ground-truthing metoder for at validere akustiske data. Der er dog stadig store udfordringer i fremgangsmåden for ground-truthing, og yderligere studie er nødvendige.

De tredimensionelle positionsdata leveret af splitbeam-ekkolodet kan også bruges til at observere adfærd. Ved at observere både unge og voksne perleside på tæt hold i Sørfjorden i Norge og følge dem i mere end 60 sekunder fandt jeg ud af, at nogle af fiskene udviste specifikke svømmemønstre. De 3D-positionsdata, jeg målte, blev brugt i

en path geometry model hvor jeg kunne kvantificere graden af overlapning inden for banerne. Ved at tilpasse banerne til stigeometrimodellen så jeg, at de unge perlesidefisk tog større risici nær overfladen sammenlignet med de overvintrende voksne i det dybere vandlag. Nogle af de mesopelagiske fisk bevægede sig på en måde, der muliggjorde effektiv fouragering inden for deres eget synsvidde, mens de stadig holdt sig skjult inden for rovdyrenes synsvidde.

Ved at studere interaktioner med deres foretrukne bytte, lykkedes det mig at opløse 3 mm lange copepoder Calanus finmarchicus som enkelte målspor med ekkoloddet og observere deres adfærd i tre dimensioner. Ved at anvende selvoverlapningsmodellen, som tidligere kun blev anvendt på copepoder i laboratorier, og beregne deres numeriske tæthed og estimere relativ lysudryddelse, lærte jeg, at *C.finmarchicus* i overfladen tog højere risici sammenlignet med to andre individer i dybere lag. Deres adfærd var sandsynligvis et kompromis mellem søgning for føde og anti-rovdyradfærd, mens adfærd i de mellemliggende dybder var mere indviklet. Højere lysintensitet og højere grader af copepod-bevægelse fik fisken til at migrere til en lavere tæthed af bytte for at fouragere.

List of publications

I. Thorvaldsen, K. G., Neuenfeldt, S., Kubilius, R., and Ona, E. . Towards identifying broadband signatures of the Norwegian shelf's sound scattering layers(Submitted).

II. Thorvaldsen, K. G., Neuenfeldt, S., Mariani, P., and Nielsen, J. R. Hiding in plain sight: Predator avoidance behaviour of mesopelagic Maurolicus muelleri during foraging(Submitted).

III. Thorvaldsen, K. G., Neuenfeldt, S., Mariani, P., Hauss, H., and Nielsen, J. R. Deviations from functional predation responses Light and anti-predator behaviour are more important than density in encounters between the mesopelagic fish and its prey(In preparation).

Contents

1 Objectives

The mesopelagic zone is large, important, and poorly understood(Webb *et al.*, 2010; St.John *et al.*, 2016; Proud *et al.*, 2019; Grimaldo *et al.*, 2020; Paoletti *et al.*, 2021). The largest biomass estimates scenario are close to 19 gigaton(Proud *et al.*, 2019), while the total landing of fish globally are 0.097 gigaton(FaO, 2020). Mesopelagic fish contribute to the biological carbon transport, while precisely how much and how trophic interactions occur are still to a large degree unknown. (Hidaka *et al.*, 2001; Davison *et al.*, 2013; St.John *et al.*, 2016). Knowledge on spatial and temporal distribution and behaviour is needed both from a governance and industry-perspective as mesopelagic fish might be a sustainable resource, and even more importantly we need more knowledge to prevent overexploitation as they play a potential large role in climate regulation.

The aim of this thesis is to explore the usage of lowered hydro acoustic observation platforms to track and follow mesopelagic targets to (I) identify mesopelagic fish species *Maurolicus muelleri* in multi-specific mesopelagic layers using broadband-echo sounders, measure frequency dependent target strength (TS(f))to identify signatures (II,II), Use triangular position obtained by the split beam echosounder to observe 3d motion patterns,

quantifying behaviour of *Maurolicus muelleri* (II), and their prey *Calanusfinmarchicus* from now on referred as *C.finmarchicus*,(III), then apply trajectory data in path geometry models to explore behavioural patterns facilitating encounters between different trophic levels within the mesopelagic zone (II,III).

2 Mesopelagic fish

In this chapter I will define mesopelagic fishes, their general distribution and large scale behaviour phenomena diel vertical migration (DVM), before I introduce the species in focus in this thesis, *Maurolicus muelleri*, from now on referred in the text as pearlside. This is a very common mesopelagic fish with an almost global distribution, ecologically important as trophic link between primary production and exploitable species, and very high in nutrients and a potential fishmeal, lipid and protein source. I will briefly introduce distribution and life history of pearlside

2.1 Distribution and behaviour

The mesopelagic zone is one of the largest habitats on earth, covering 60% of the earth surface, and about 20 % of the total ocean volume. The mesopelagic zone is defined by light, and is typically found between 200-1000 meters depth(Kaartvedt *et al.*, 2019). The mesopelagic zone usually stretches from the end of the euphotic zone down to the bathypelagic(Duvall and Christensen, 1946; Marshall, 1951). This large volume is filled

with a wide variety of organisms. However, due to its size, technological limitations and accessibility, our knowledge on the mesopelagic zone and its inhabitants are very limited(Webb *et al.*, 2010). To increase our knowledge, we need to fully understand of the link between the micro nekton prevailing in the mesopelagic, primary production, and commercial species (Handegard *et al.*, 2013).

A significant proportion of the total biomass in the mesopelagic are believed to be bony fishes (Marshall, 1951; Gjøsaeter and Kawaguchi, 1980; Lam and Pauly, 2005; Irigoien *et al.*, 2014) There are 30 families of mesopelagic fishes with often a unique physical appearance, and some species of fish with epipelagic features that also live within the mesopelagic both permanently or occasionally (Salvanes and Kristoffersen, 2001). Mesopelagic fish co-exist with crustaceans, mesozooplankton and gelatinous zooplankton(Barham, 1963, 1966; Gjøsaeter and Kawaguchi, 1980; Pugh, 1984; Youngbluth *et al.*, 2008). Most mesopelagic fishes are relatively small (2-15) cm and are either planktivorous or piscivorous(Salvanes and Kristoffersen, 2001). Many mesopelagic fishes are important prey for commercially important species (Bjelland, 1995; Battaglia *et al.*, 2013; Olson *et al.*, 2014; Duffy *et al.*, 2017). Light is believed to be the main factor driving vertical distribution and behaviour for many mesopelagic species, and are believed to generally shape the vertical boarders of the mesopelagic zone (Giske *et al.*, 1990; Aksnes and Utne, 1997; Eiane *et al.*, 1999; Aksnes *et al.*, 2004; Staby and Aksnes, 2011; Staby *et al.*, 2013; Kaartvedt *et al.*, 2019; Langbehn *et al.*, 2019).

Recorded by echo sounders, the mesopelagic sound scattering layers is seen as one of the universal features of the open ocean, and are typically observed as a continuous veil several 100 meters tall. Mesopelagic fishes are very common in all oceans, especially in upwelling zones and along continental slopes, and less densely aggregated off shore and in the arctic (Knutsen *et al.*, 2017). There have been attempts of commercial fisheries in the Gulf of Oman, South of island and Western Norway(Grimaldo *et al.*, 2020). However, there have been indications that trophic efficiency is higher in the open oceans than first assumed(Irigoien *et al.*, 2014)

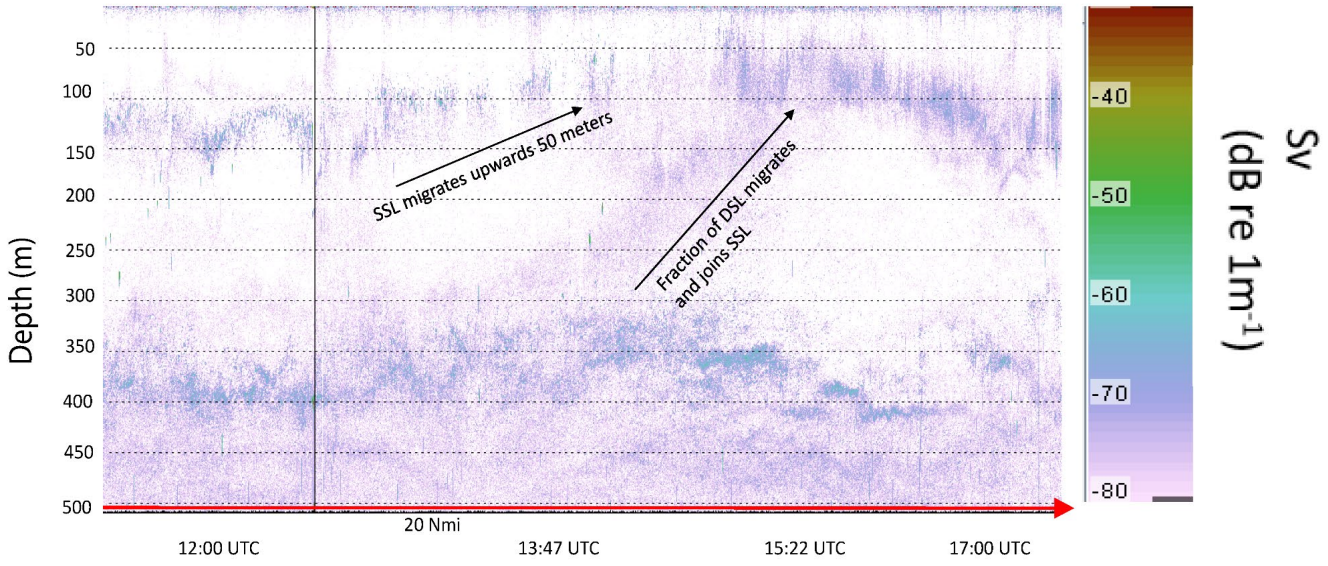

Figure 1. Example of mesopelagic layers observed by ship mounted echosounders (I). The echosounders provide a twodimentional image over time and distance showing volume scattering strength (dB re 1m re $1m^{-1}$). Two scattering layers are recorded by the echosounder. The upper layer were called shallow scattering layer and were found between 100-150 meters during day, and the deep scattering layer are found

between 350-500 meters. At approximately 13:47 a small fraction of the DSL migrates and joins the SSL closer to the surface also known as DVM.

One of the global features of mesopelagic communities are their extensive vertical migrations towards the surface to feed on epipelagic organisms or other mesopelagic fishes(Marshall, 1951)(Figure 1). This is also called diel vertical migration or DVM, as the gross weight of migrating mesopelagic fishes is enormous(Irigoien et al., 2014; Klevjer et al., 2016). The degree of migration varies both spatially(Kaartvedt et al., 1998; Klevjer et al., 2016; Knutsen et al., 2017), temporally, and intra and interspecifically. For some species this behaviour is determined by ontogeny(Giske and Aksnes, 1992; Prihartato *et al.*, 2015; Thorvaldsen *et al.*, II;III), gender (Kristoffersen and Salvanes, 2001) and internal state (Christiansen et al., 2021). Vertical migrations are an important ecological feature as they are a significant part in active carbon transport (Davison et al., 2013; Kelly et al., 2019). Mesopelagic fish are also important predators on mesozooplankton, and play a large role as a mediator of carbon transport to deeper waters (Hidaka *et al.*, 2001; Davison *et al.*, 2013; St.John *et al.*, 2016; Martin *et al.*, 2020)

2.2 maurolicus mulleri

2.2.1 Spatial and vertical distribution

The family *Maurolicus* is circumglobal, and abundant(Rees *et al.*, 2020). One of the most common fish species in this family are *Maurolicus muelleri*, also known as Muellers Pearlside or Pearlside. Pearlside are a small vertically migrating mesopelagic fish living in the shallow parts of the oceanic twilight zone. Its distribution has been often used to mark

the upper border to the mesopelagic zone (Kaartvedt *et al.*, 2019), as it usually form a scattering layer over the deep scattering layer (DSL) which is often distinguishable on echosounders (Giske *et al*, 1990; Bjelland, 1995; Godø *et al*, 2009; Staby and Aksnes, 2011; Staby *et al*, 2013; Kaartvedt *et al*, 2019). The life history strategies of pearlside are known to be highly diverse, possibly explaining its highly successful spatial distribution(Ikeda, 1996; Kristoffersen and Salvanes, 1998). However, copepods seem to be pearlside's most important food source worldwide (Ikeda, 1994). Pearlside are found in coastal areas as well as shallower off-shore areas such as ridges and sea-mounts(Toyokawa *et al.*, 1997). They are often common in deep fjords (Gjøsæter and Kawaguchi, 1980). The investigations highlighted in this thesis was focused around the Norwegian coast (I) and especially Sørfjorden in western Norway (II,III).

Pearlside usually have a life-span around 3-5, years, growing up to 5 cm and typically spawning after a year(Gjøsæter, 1981; Kristoffersen and Salvanes, 1998). The temporal behaviour of pearlside change with copepod abundance (Prihartato *et al.*, 2015), and in some cases , extreme light intensity can result in schooling behaviour (Kaartvedt *et al.*, 1998). During winter, adult and juvenile pearlside form two vertical depth layers (Figure 2a-b) where the juveniles migrate to feed on copepods in the surface to ensure to reach maturity before spring(Gjøsæter, 1981; Kristoffersen and Salvanes, 1998; II;III)) . Pearlside have been observed to spawn between March and October (Kristoffersen and Salvanes, 1998). The high protein and lipid content found in the fish combined with high abundances, potential harvest of pearlside have been suggested both for human

consumption and for fishmeal production for aquaculture(Alvheim *et al.*, 2020; Grimaldo *et al.*, 2020; Standal and Grimaldo, 2020). However, there are as challenges both with regard to identification(Proud *et al.*, 2019), low catchability(Kaartvedt *et al.*, 2012; Grimaldo *et al.*, 2020) economic challenges (Paoletti *et al.*, 2021), and ecological implications (Pauly *et al.*, 2002; St.John *et al.*, 2016).

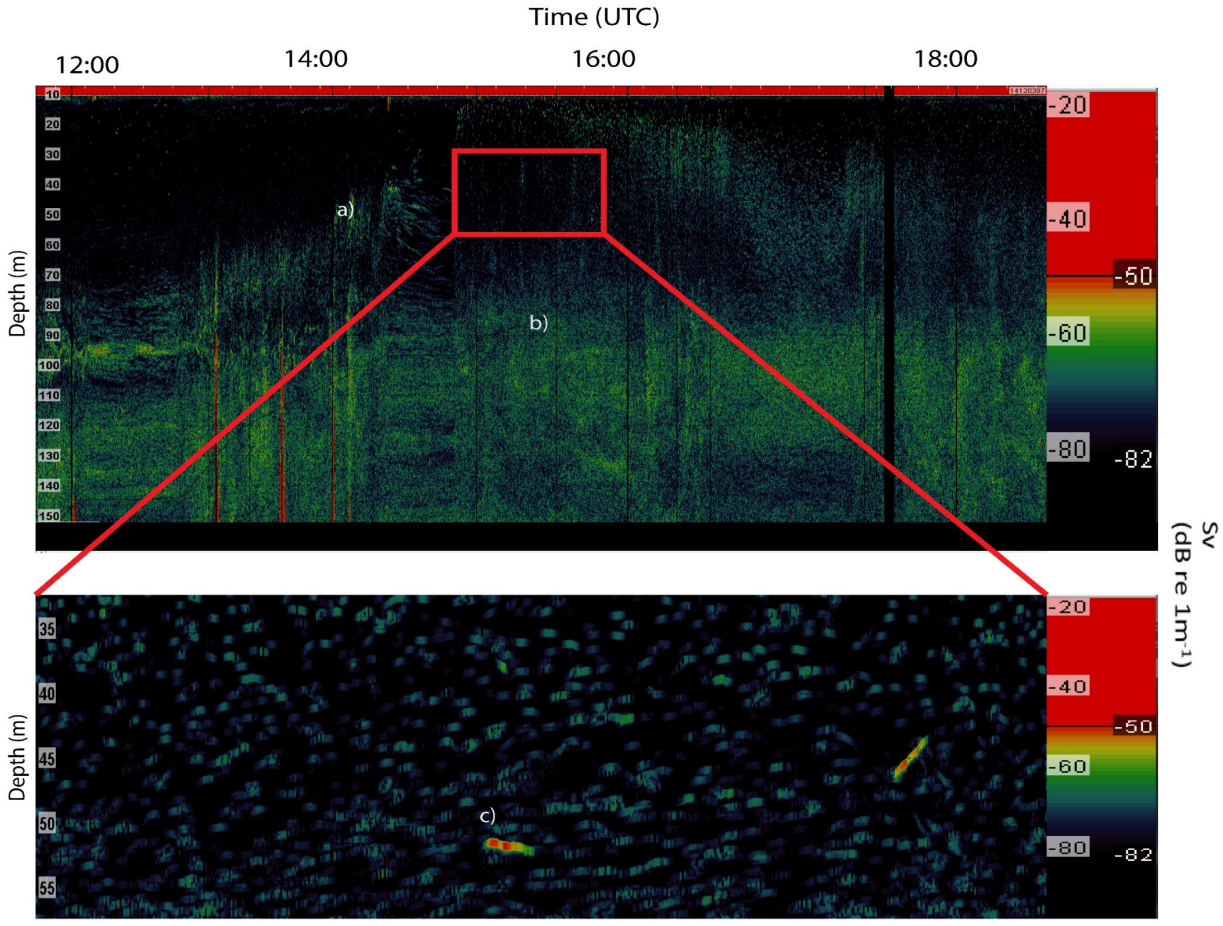

Figure 2. Example of pearlside behaviour in Sørfjorden recorded by 38 kHz Simrad EK80 echsosounder measured from research vessel G.O Sars. The echogram is showing volume backscattering strength (S_v dB re m^{-1}) Panel a is showing a layer of juvenile pearlside at 80-100 m migrating towards the surface during

dusk to forage(II). Panel b) is showing the scattering layer below consisting of both adult pearlside and glacier lanternfish (*Benthosema glaciale*). C) Is showing piscivorous fish observed in the echogram as largered traces within the layer of pearlside seen as green traces

3 Identifying pearlside in a multispecies mesopelagic layers

In this chapter I will briefly review acoustic methods to identify mesopelagic fishes and pearlside in particular, before I continue to introduce target tracking which is applied in all three studies in the thesis (I;II;III).

3.1 acoustics

For determining the distribution of mesopelagic fishes both in space and time, scientific acoustic echosounders have been applied since World War II (Duvall and Christensen, 1946; Marshall, 1951, 1960; Barham, 1963, 1966) . Echosounder transmits a sound pulse moving through water, hitting several targets that produces backscatter. This backscatter or echo is converted to an electrical signal. After transmitting several pulses, the received signals transforms into a 2-dimentional image (Figure 1 and 2). Scientific echosounders take advantage of the long penetration range of sound in waters providing possibilities to observe large depths including the mesopelagic zone in a non-intrusive way. Echosounders have been frequently used to observe the backscattering properties of pearlside (Torgersen and Kaartvedt, 2001; Scoulding *et al.*, 2015; Sobradillo *et al.*, 2019) and to observe their ecology (Giske and Aksnes, 1992; Torgersen and Kaartvedt, 2001; Staby and Aksnes, 2011a; S*taby et al*., 2013; Christiansen *et al*., 2019). Translating acoustic backscatter into the right group or species is crucial both for stock assessment and ecological

studies(Simmonds and MacLennan, 2007). Mesopelagic fishes are subject to exploitation, and potential over-exploitation can have extreme unforeseen consequences(St.John *et al.*, 2016). Uncertainties of biomass and climate impact are important aspects. Having better knowledge on species composition, behaviour and distribution can offset some of these challenges. There are several bottlenecks for identifying mesopelagic fishes, swimbladder morphologies(Godø *et al.*, 2009; Davison *et al.*, 2015; Kloser *et al.*, 2016; Dornan *et al.*, 2019; Proud *et al.*, 2019), and other taxa creating similar backscatter(Toyokawa *et al.*, 1997; Warren *et al.*, 2001; Lavery *et al.*, 2007; Warren and Wiebe, 2008; Proud *et al.*, 2019;(I)) .

3.2 Target strength

The backscattering properties of a single target are a crucial parameter to convert echo-integration values into credible biomass estimates(Nakken and Olsen, 1977; Ona, 1999; Simmonds and MacLennan, 2007). Target strength is the logarithmic measure of the reflectivity of the target compared to the incident wave made by the transducer, also called the backscattering cross section of a target σ_{bs} which is expressed as

$$\sigma_{bs} = R^2 I_b / I_i \quad (1)$$

Where R^2 is the range from the target, I_b is the intensity of the backscattered wave, and I_i is the intensity of the incident wave. σ_{bs} is converted to logarithmic form (TS) used to express the echo intensity of one single point (dB re $1m^2$). TS can be measured either *in* or *ex situ* or theoretically by creating backscatter models (Simmonds and MacLennan,

2007). 95% of the backscatter is produced by the swimbladder, and for most species there is a linear relationship between swimbladder, length, width and fish length, while fishes without swimbladder backscatter is produced by bones, oils, scales and other features of the fish(Nakken and Olsen, 1977). The relationship between the acoustic properties of the target and frequency can be used to identify different acoustic classes (Martin *et al.*, 1996; Stanton *et al.*, 1998; Korneliussen and Ona, 2002, 2003; Lundgren and Nielsen, 2002, 2008; Lavery *et al.*, 2007; Korneliussen *et al.*, 2016; Sakinan *et al.*, 2019). The scattering of a swimbladder or a pneumatophore found in siphonophores (Stanton *et al.*, 1998; Warren *et al.*, 2001; Knutsen *et al.*, 2018) follow a specific pattern. At low frequencies backscatter rise rapidly, also called Rayleigh scattering(Figure 3a), followed by a resonance peak(Figure 3b), and the geometric region, where the backscatter properties stabilizes(Figure 3c). A swimbladder has a natural oscillation, and when the frequency of that incident wave is similar to the natural oscillation, the swimbladder will produce a significantly larger backscatter, which is better known as resonance (Figure 3b). The resonance peak found in swimbladdered fishes and gas filled organisms can be used to identify , and potentially predict size of the animal(Sundnes and Sand, 1975; Medwin and Clay, 1998; Lundgren and Nielsen, 2002, 2008; Stanton *et al.*, 2010), and with the emergence of broadband methodologies, scattering properties can be observed over a large range of frequencies (Lundgren and Nielsen, 2002, 2008; Stanton *et al.*, 2010; Jech *et al.*, 2017; Agersted *et al.*, 2021; Khodabandeloo *et al.*, 2021)(Figure 6a-c). Most fishes are found within the geometric region at frequencies higher than 18 kHz. However, some mesopelagic fishes and fish larvae can be found within the resonance region at frequencies

applied at acoustic surveys, which can lead to a large bias in biomass estimation(Kloser *et al.*, 2002, 2016; Godø *et al.*, 2009; Davison *et al.*, 2015; Proud *et al.*, 2019).

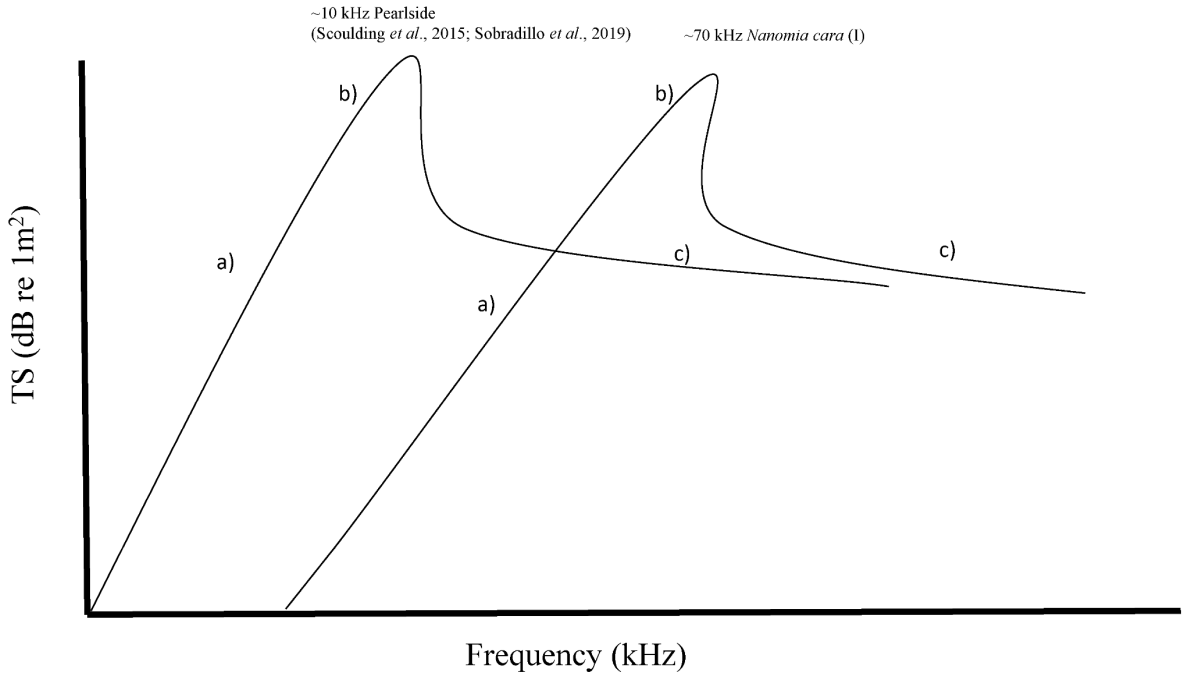

Figure 3) Simplified sketch of how target strengths change with frequency for pearlside (Scoulding *et al.*, 2015; Sobradillo *et al.*, 2019) and siphonophore *Nanomia cara* based on in situ measurements (I). where panel a) are showing the Rayleigh scattering region, b) the resonance peak and c) the geometric region. The differences in resonance peak could be used to separate pearlside from siphonophore *Nanomia cara.* and 38 kHz could be used to separate pearlside, as *Nanomia cara* would still be in the Rayleigh scattering region.

3.3 Acoustic target tracking

The emergence of the split beam echosounder enabled acoustic target tracking. Acoustic target tracking simply explained is identifying a single target, then tracking the same target for several pings when the target is alone in the sampled volume. The Three-dimensional

position of a target can be determined with a split beam echosounder. The distance to the target (r) from the center of the split beam transducer can be calculated as.

$$r = \frac{c\tau}{2} \quad (2)$$

where c is the speed of sound in seawater and τ is the time interval between the transmission of the pulse and the reception of the reflected pulse from the target. The phase differences between the signals received by the four quadrants of the transducer is then used together with the distance to calculate the positions x, y and z of the target relative to the axis of the transducer beam, where c and y is across axis and z is along the axis. The triangular positions derived from the split beam echosounder can be used to observe how TS changes over time (Ehrenberg and Torkelson, 1996; Ona, 1999; Torgersen and Kaartvedt, 2001; Klevjer and Kaartvedt, 2006), to observe individual behaviour of fishes (Huse and Ona, 1996; Torgersen and Kaartvedt, 2001; Gjelland *et al.*, 2004; Christiansen *et al.*, 2019), measure fish tail-beat frequency(Olav Handegard *et al.*, 2009), track zooplankton (De Robertis *et al.*, 2003; Klevjer and Kaartvedt, 2006; Kaartvedt *et al.*, 2011), to observe feeding behaviour (cech and Kubecka, 2002; Christiansen *et al.*, 2021; II;III)) , and study trawl avoidance (Handegard *et al.*, 2003).Acoustic target tracking is advantageous as it is still effective in turbid and or dark water, unreachable for a camera, and can be measured at a long distance from the transducer (Simmonds and MacLennan, 2007).

Resolving and tracking single targets has been a key motivation for all three studies of this thesis (I,II,III). To ensure this, a lowered observation platform was deployed, to

reduce the pulse volume and thus isolating single targets(Figure 4). For further description of the platform see (I section (2.2)) and for different deployments see materials and methods (I,II,III). Another aim was to track the same organism before measuring additional information such as target strength (I,III), frequency dependent target strength (TS(f))(Figure 6 and 7), and swimming behaviour for pearlside (Figure 5 and 8) (II) and their prey *C.finmarchicus*(III)(Figure 10). To Efficiently track the same target for an extended period, a tracking algorithm using phase deviation estimations from the split beam echosounder, target strength, vertical position, and range was simultaneously used to initiate, and associate the target, (Handegard *et al.*, 2005; Handegard, 2007; Korneliussen, 2010) where specific parameters were set to separate and initiate new tracks from previous tracks as well as assosciate tracks for each ping . For further information see material and methods (I, II and III) and for full description (Handegard, 2007)

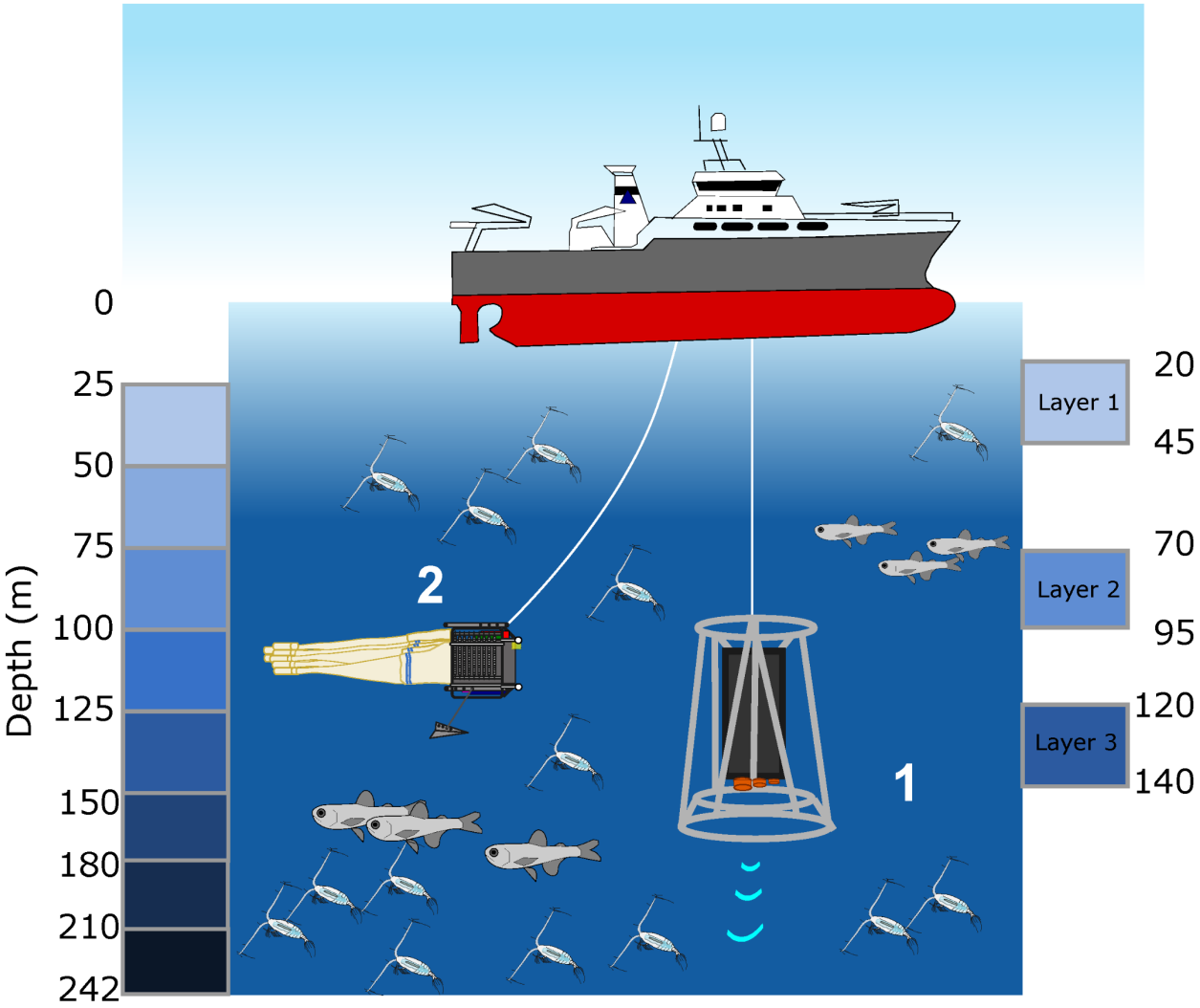

Figure 4: example from a TS-probe deployment where the echosounders mounted on the TS-probe (1) in paper (III), are lowered into several layers before zooplankton are vertically resolved using a mammoth

multinet to ground truth the acoustic targets (2) where deoth bins are marked on the left.

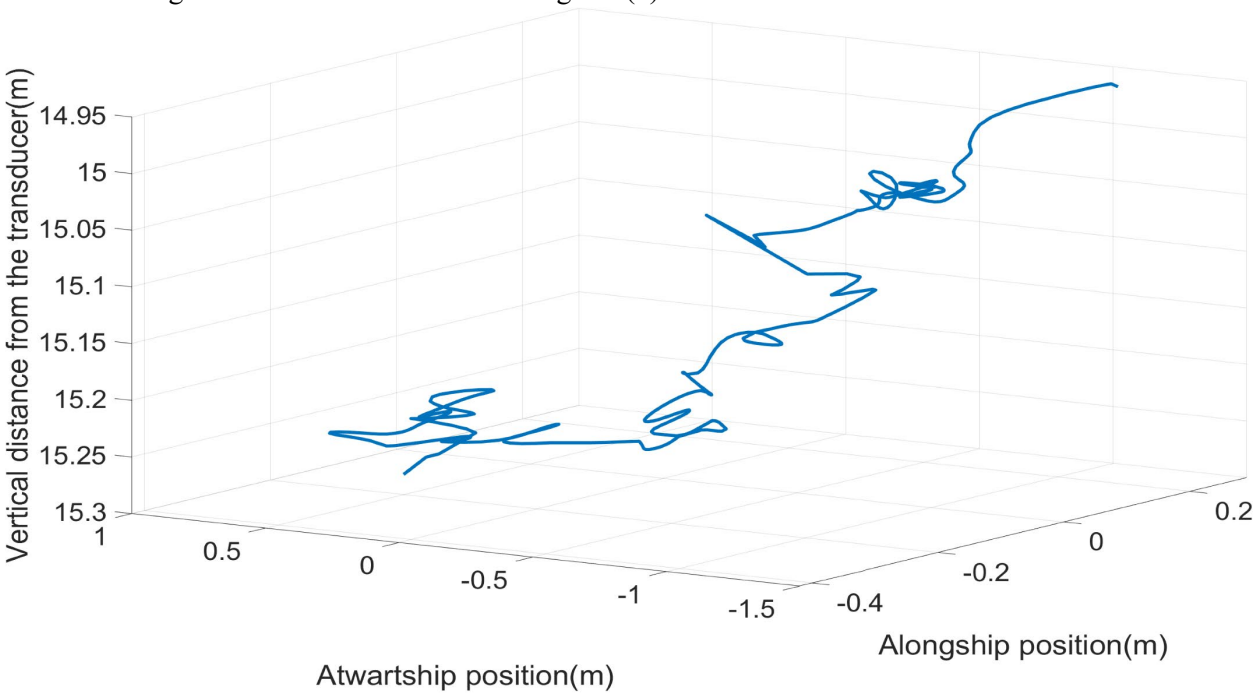

Figure 5. Example of Maurolicus muelleri trajectory obtained by the split beam echosounder at 120 m depth (II), and after using the curve-fitting tool. Presented are the alongship position (x), athwarship position (y) and vertical distance from the transducer (z). This particular trajectory started from the top and swam downwards.

3.3.1 Acoustic properties of pearlside

Swimbladder irregularities are one of the main challenges with acoustic approaches identifying and quantifying mesopelagic fishes(Proud *et al.*, 2019). The swimbladder of pearlside is thin-walled but well developed with a resonance frequency at approximately 10 kHz (Fig 3) , and its gas filled structure remains throughout the life span (Scoulding *et al.*, 2015; Sobradillo *et al.*, 2019). Due to their more "traditional" swimbladder

morphology, competing scatterers might be the most important source of bias for pearlside. Knowledge on scattering properties and resonance peaks can be used to separate pearlside from other scatterers as (I) highlighted in figure 6 where panel b is showing the TS(f) of mesopelagic fish fish track. those seen in the upper 200 meters likely belong to pearlside, while TS(f) spectra seen in 6 a) belong to siphonophores based on ground truthing with a photo camera(figure 7)(I).

3.4 Ground truthing challenges

Ground truthing is an important part of acoustic studies, where acoustic backscatter is allocated to different animal groups to identify spatial distribution and estimate biomass. Traditional ground truthing techniques can be simply separated into net sampling, visual sampling, comparisons with fishery and submersible vehicles and or observation platforms (McClatchie *et al.*, 2000). Net sampling is an often used tool in acoustic surveys to resolve the biological composition, and to obtain the mean length of the fishes to apply the length specific Target strength.

Traditional net samples have a low catch efficiency for pearlside (Kaartvedt *et al.*, 2012) and underestimates total biomass, while almost excludes gelatinous zooplankton completely as they are easily destroyed with mechanical contact(Hosia and Båmstedt, 2008). Pairing acoustics with optical tools can be used to identify elusive gelatinous zooplankton(I)(Figure 7). However, there are challenges with optical tools as usually

densities are low, and penetration ranges in water is up to 7 meters. Furthermore, mesopelagic fish avoid lowered devices up to 10 meters, and are scared by the flash provided by the camera(Dias Bernardes *et al.*, 2020;(I)) . Both swimbladder morphology and gelatinous zooplankton composition will vary spatially and one universal approach in identifying mesopelagic fish is most likely not enough to solve these problems (Proud *et al.*, 2019; (I))(I). Based on previous target strength measurements (Scoulding *et al.*, 2015; Sobradillo *et al.*, 2019), vertical distribution of pearlside(Giske *et al.*, 1990; Giske and Aksnes, 1992; Kaartvedt *et al.*, 1998; Staby and Aksnes, 2011) and increased knowledge of scattering properties of other mesopelagic components (Lavery *et al.*, 2007; Knutsen *et al.*, 2018; Agersted *et al.*, 2021; Khodabandeloo *et al.*, 2021), pearlside appears to be one of the mesopelagic fishes which is possible to identify and quantify.

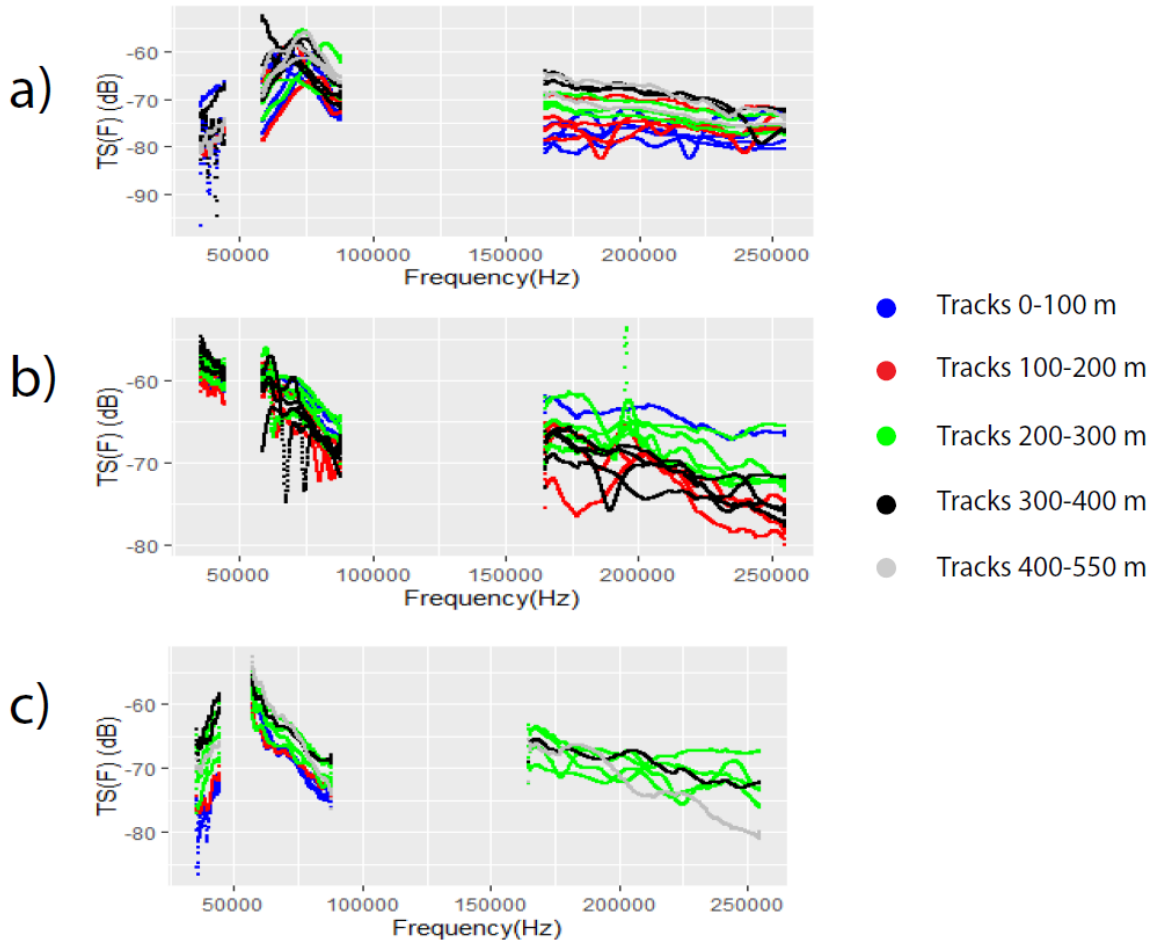

Figure 6: Highlighted in situ TS(F) Measurements during the TS-probe deployments at vøringplatået (I) where frequency (Hz) is plotted at the x-axis and TS (dB re $1m^2$). A) b) and c) represent three different acoustic signatures found during the vertical profile of the water column manually sorted into three categories based on backscatter properties, where a) likely belonged to siphonophores b) likely to mesopelagic fishes, and finally c also likely to siphonophores.

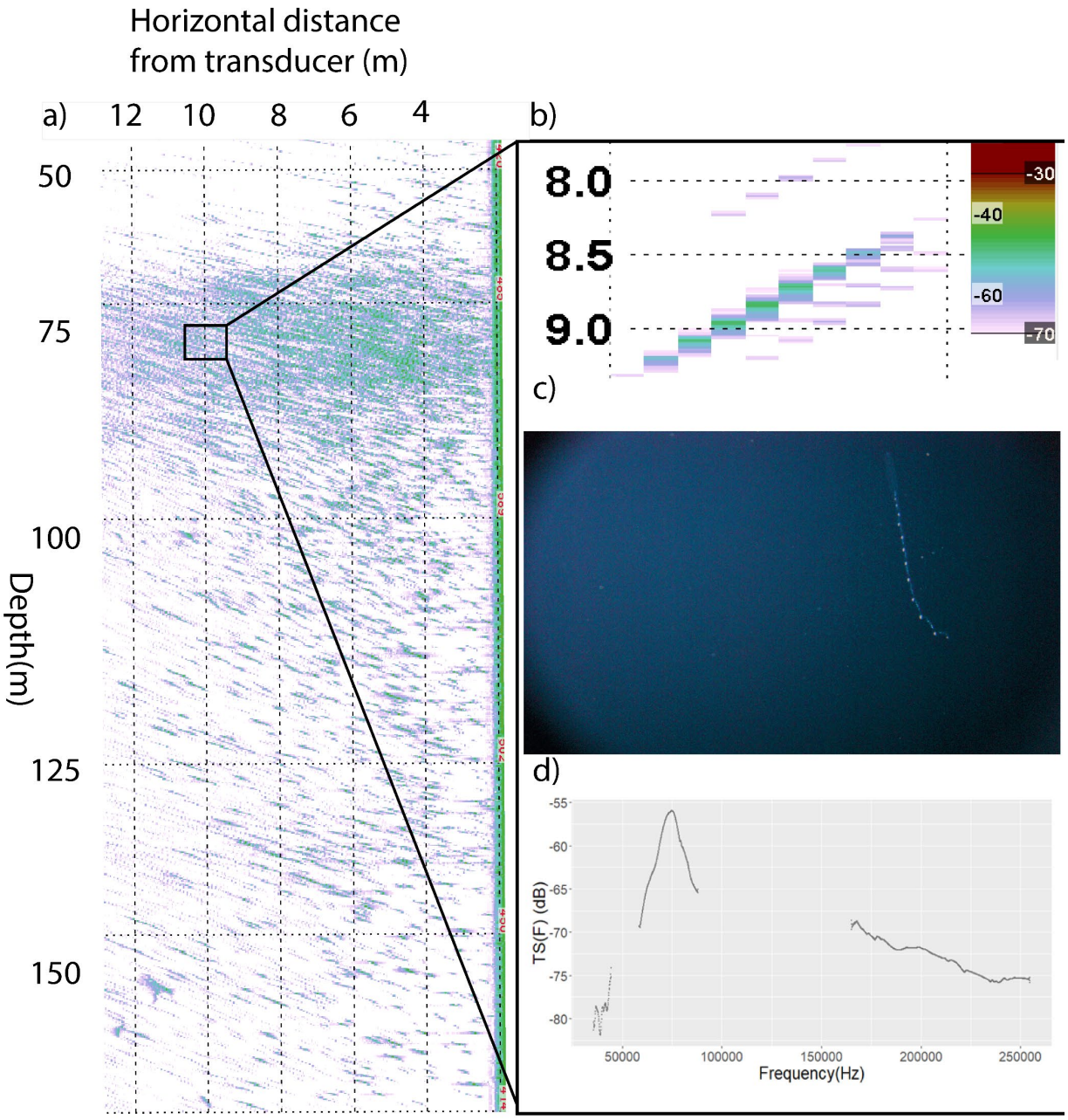

Figure 7. Acoustic identification of single targets(I). Panel a is showing an echogram measured with the TS-probe. The TS-probe were lowered downwards from the surface while the echosounders project laterally. Transducers are mounted on the side of the transducer and the x-axis is the horizontal distance from the echosounder while the y axis is depth. The green traces on the echogram mainly single targets with resonant at 70 kHz. B) is a single target where target tracking were successful and d) is the TS(F) of

that particular target, where the x-axis is frequency (Hz) and the y axis is target strength (dB re 1 m^2). C is a an image of an identified specimen of *Nanomia cara.* This was one of 3 observations in rapid succession, identifying the resonant target to most likely be *Nanomia cara.*

4 Movement ecology

In This chapter I will introduce movement ecology as a scientific field. Furthermore I will review movement ecology studies of mesopelagic fishes, and especially pearlside. Subsequently I will describe path geometry methodologies applied on in situ data of mesopelagic fishes, and their prey *C.finmarchicus*. Finally I discuss trophic interactions between pearlside and its prey *C.finmarchicus.*

4.1 A new emerging scientific field

Movement leads to many ecological processes, and it is crucial for evolution, dispersal, migrations, invasions and forming home ranges and habitats. Movement leads to encounters which shape the life history of the animal (Nathan *et al.*, 2008; Allen *et al.*, 2018). The emergence of movement ecology have led to increased efforts in applying telemetric measures terrestrial and aquatic environments to quantify movement (Hussey *et al.*, 2015; Kays *et al.*, 2015).

Swimming is a nearly universal feature of fishes and many other marine organisms, but swimming capacities, and the nature of swimming is highly variable. Swimming leads to multiple biological processes such as foraging, predation, mating and distribution. Swimming can be influenced by internal and external factors, and can be influenced by hydrology, temperature, oxygen salinity, currents light conditions and other factors (Cooke *et al.*, 2022). Marine organisms' movement paths range from a few mm(Visser and Kiørboe, 2006; Chen and Hwang, 2018) to large migrations, spanning thousands of kilometres(Rizzo and Schulte, 2009).

Movement in the mesopelagic zone has crucial ecological impacts. Mesopelagic fishes contribute to the active biological carbon transport and their trophic interactions appear to contribute up to 15-17 percent of the total active carbon export(Davison *et al.*, 2013). There are large holes in our knowledge of trophic interactions in the mesopelagic, and it is even more challenging as they vertically change habitats during DVM (Beamish *et al.*, 1999). Many mesopelagic fishes are both important food for epipelagic predators (Battaglia *et al.*, 2013, 2018; Duffy *et al.*, 2017; Dornan *et al.*, 2019; McMahon *et al.*, 2019; Goulet *et al.*, 2020) and mesopelagic predators(Bjelland, 1995; Kristoffersen and Salvanes, 1998; Eduardo *et al.*, 2020), and the knowledge on how different types of predators contribute to the carbon transport is lacking.

As the mesopelagic zone is challenging to reach both with regards to depth and visibility, mesopelagic movement behaviour is not simple to quantify. Most mesopelagic organisms are small and fragile, which complicates tagging studies, makes them challenging to capture alive, and their light sensitivity leads to migration attempts where they are usually damaged and killed hitting the walls of the aquarium (Salvanes and Kristoffersen, 2001).

4.11 quantifying 3d behaviour, the self overlap model

A non-invasive approach to observe fish behaviour is tracking the animals directly, either by video (Voesenek *et al.*, 2020; Lucas *et al.*, 2021; Burns *et al.*, 2022; Gong *et al.*, 2022)) with a high frequency acoustic camera (Handegard and Williams, 2008; Handegard *et al.*, 2012; Rieucau *et al.*, 2016; Kandimalla *et al.*, 2022) or with the split beam echosounder mentioned in chapter 3.3. The mesopelagic habitat is challenging to reach as mesopelagic fish actively avoid lowered observation platforms to such a degree that they become challenging to resolve with a photo camera (Dias Bernarde*s et al*., 2020; (I)) or the effective range of an acoustic camera. Mesopelagic fish have been successfully tracked using split beam echosounders where parameters such as target strength have been directly (Kloser *et al.*, 2016; Agersted *et al.*, 2021; Khodabandeloo *et al.*, 2021; (I)) and swimming patterns (Torgersen and Kaartvedt, 2001; Kaartvedt *et al.*, 2008; Christiansen *et al.*, 2019;II;III))

At some stages of the daily or annual cycle, mesopelagic fish, piscivorous fish, and zooplankton share the same volume of water, and it is assumed that all trophic levels have strategies to facilitate or eliminate encounters (II;III). Path geometry describes the motion patterns of an organism and can be used to quantify search efficiency and encounters(Bianco *et al.*, 2014). .Famous examples to describe path geometry are the levy flight(Viswanathan *et al.*, 1996), random walks (Berg, 1993; Niwa, 2007) the

diffusion/ballistic model seen in mesozooplankton (Miyazaki, 2006; Visser and Kiørboe, 2006; Kiørboe, 2008), as well as spiral helixes and wiener sausages (Levandowsky *et al.*, 1988; Berezhkovskii *et al.*, 1989; Bartumeus *et al.*, 2003; Visser, 2007). The behaviour of mesopelagic fish are very likely relying on path geometry, prevailing in the mid trophic layers, and having an extremely successful global distribution.

While highly variable, all organisms have a detective radius. The detective radius of marine organisms can be seen as a volume and can be expressed as V(r). This value will differ from the detection ranges of 144 meters in a sperm whale (Tønnesen *et al.*, 2020)to detection radiuses at millimetre scales in copepods (Visser and Kiørboe, 2006; Bianco *et al.*, 2014). V(r) will be highly variable interspecifically within an ecosystem and heavily influenced by environmental factors(Aksnes and Utne, 1997). Typically this value is increasing with trophic level as increased detective radius is advantageous when prey increases in size (Aksnes and Utne, 1997). Mesopelagic fish can use this to their advantage since their prey are small and can only be observed by close range, enabling foraging in a way leading to encounters at their own V(r) (II) while staying hidden at ranges of higher (V(r)). This is also called self-overlap(Bianco *et al.*, 2014). Self-overlap as the name implies describes how much a trajectory is intersecting itself. The degree of self-intersection or overlap is further determined by the detective radius of the organism (r).

Self-overlap is expressed as

$$\psi(r) = 1 - \frac{V(r)}{V_{max}(r)} \qquad (3)$$

Where V(r) is the scanned volume within a visual range, while $V_{max}(r)$ is the maximum swept volume if the trajectory would be considered a straight line. For calculations of see material and methods (II;III). All values of self overlap are between 0 and 1, and self overlap of 0 means that there are no overlap at that detective radius, while a self overlap-value of 1 means there is full overlap, and in practicality means that the organism have not moved within the detective radius.

Triangulated positions with short cycles are needed for analysing self-overlap, and this can be for acquired with for example video (Bianco *et al.*, 2014) or high ping-rate hydro acoustics(II,III). The split beam derived triangular positions were used in a monte-carlo approach where 9 billion points are thrown into a bounding box. For further calculations of the bounding box see material and methods (II;III). The detective volume for a range of detective radiuses are calculated as:

$$(4)\ V(r) = \frac{n(r)}{NP} V_{box}. \qquad (4)$$

Where n(r) is the number of the randomly distributed points for each detective radius and NP is the total number of random points. The self-overlap model was applied on both trajectories of pearlside and their prey *C.finmarchicus.*

4.2 Movement ecology of maurolicus muelleri

Living their entire life in the free water masses, movement is a crucial part of the life history of pearlside. By staying in a specific isolume or light comfort zone(Staby and Aksnes, 2011; Kaartvedt *et al.*, 2019; Langbehn *et al.*, 2019), pearlside are using the anti-predator window (Clark and Levy, 1988) taking advantage of the dim light during dusk and dawn to allow foraging with lower risk of predation.

The specific nature of DVM of pearlside is well documented, and deviations from traditional DVM-behaviour have been coupled to seasonal patterns (Prihartato *et al.*, 2015), extreme light regimes(Kaartvedt *et al.*, 1998; Christiansen *et al.*, 2019) ontogenetic differences(Giske and Aksnes, 1992; Prihartato *et al.*, 2015; Folkvord *et al.*, 2016)(II), and individual deviations from the main scattering layer (Christiansen *et al.*, 2021). Pearlside often swim upwards and downwards in a step wise pattern (figure 5 and 8). as an antipredator measure as to their counter illumination properties (Mensinger and Case, 1990) reduce their silhouette seen from below. This behaviour is most likely efficient when the fish is tilted horizontally (Kaartvedt *et al.*, 2008; Christiansen *et al.*, 2019, 2021)(II) There is less mechanistic knowledge on antipredator measures when all trophic levels are foraging within the same volume. During summer, all pearlside migrate towards the surface, visually feeding on copepods(Rasmussen and Giske, 1994), while during the fall and winter, juvenile pearlside distribute at shallower water, and continue to migrate and forage(Giske and Aksnes, 1992; Staby *et al.*, 2013; Prihartato *et al.*, 2015; Thorvaldsen *et*

al., II;III)) . During this period, juvenile pearlside is assumed to be the only size group benefiting from foraging as they are harder to detect by predators while the adults overwinter, discarding foraging to reduce natural mortality(Giske and Aksnes, 1992).

4.2.1 Self overlap with maurolicus muelleri

Applying the self-overlap model (equation x) to triangular trajectories for juvenile and adult mesopelagic fish in December, gave insight on the 3D behaviours for both ontogenetic stages (II)(Figure 8). For detective radiuses from 1-100 cm, the calculated self-overlap were never larger than 0.6 at a visual range for about one meter, and usually lower (Figure 9). Self overlap of 1 means the trajectory always intersect itself at the give detection radius, while a self overlap of 0 means the trajectory never intersect itself. The degree of self overlap are thus highly dependent on the detective radius of both predator and prey. The swimming trajectories were mostly ballistic at a small scale, and in some cases more protective at larger ranges. The juvenile fish swum both faster, and longer with lower degree of self-overlap (Figure 9) in the surface layer, and it could be explained by internal and external factors leading to a vast range of behaviours. Some of the trajectories showed properties of anti-predator behaviour at the larger scale. A large detective radius for prey

might mitigate the movement patterns, explaining the higher risks also seen in other studies(Christiansen *et al.*, 2021),

SSL1 (20m transducer depth)

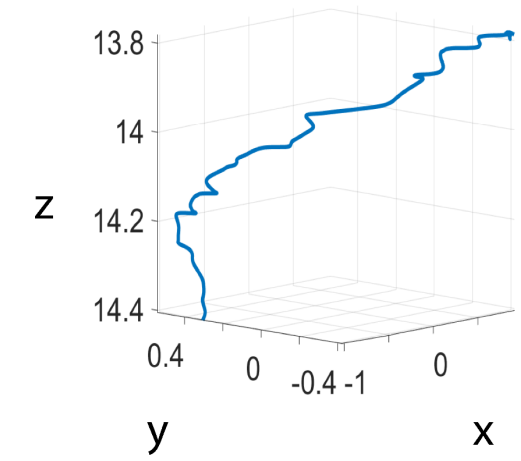

SSL2 (120 m transducer depth)

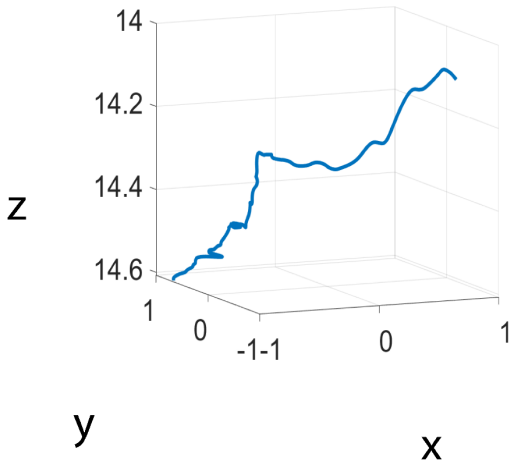

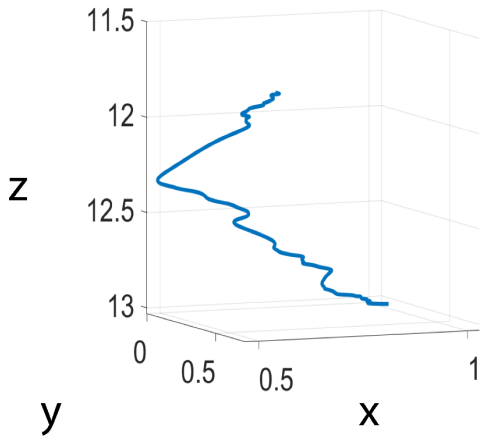

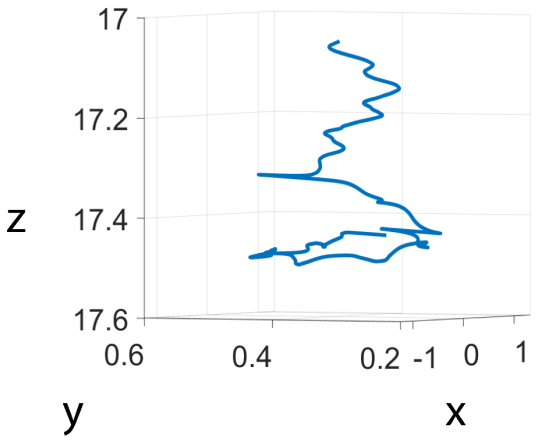

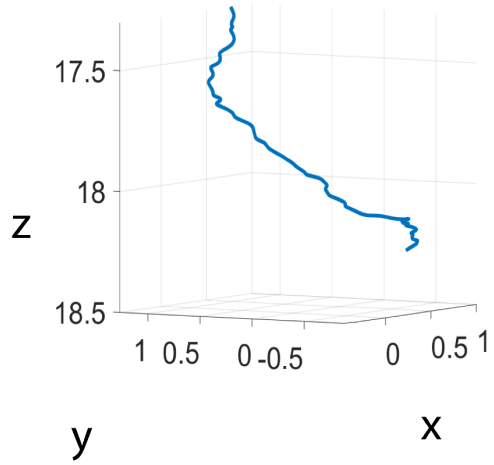

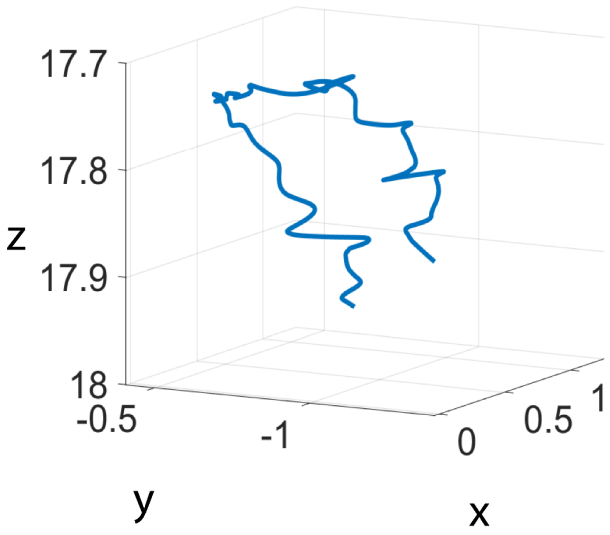

Figure 8. Trajectories of juvenile and adult pearlside. Juvenile pearlside are found in sound scattering layer 1 or SSL1(tracks in left column, while adults are found in SSL2 (right column)(II). Smoothed Angular positions are plotted against alongship position (x), athwartship position (y), and vertical range from the transducer (z).

Increased pearlside swimming at the surface will come with an increased risk of predation. However, prey densities were also low(III), and might influence the effective search volume of the fishes(II). It was expected that the behaviours of pearlside were found in a range instead of them all being similar, as behaviour usually are highly diverse (Figure9). More information on visual range for both *C.finmarchicus* detection and for avoiding predators is needed together with knowledge on turbulence and currents to fully understand the trajectories.

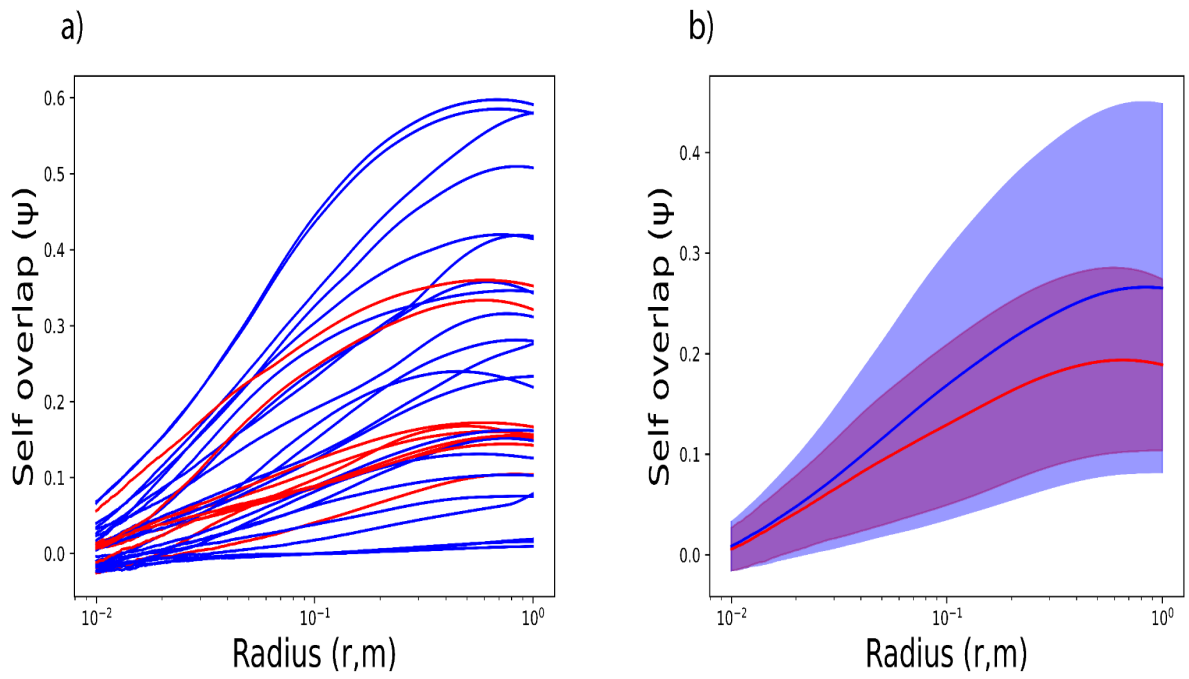

Figure 9. Self-overlapping behaviour of pearlside in the SSL1 (red lines) and SSL2 (blue lines, where panel a shows self-overlap behaviour for all trajectories, while panel b show averaged self-overlap with standard deviation(II).

4.2.2 Trophic interactions with prey

In Sørfjorden (II, III) and generally along the Norwegian coast, *Cfinmarchicus* is the main prey for pearlside (Giske and Aksnes, 1992; Rasmussen and Giske, 1994; Bagøien *et al.*, 2001). In our studies, light and movement seem more important in facilitating encounters than individual density(II,III).Our observations show that juvenile pearlside migrate vertically to a lower density of *C.finmarchicus*, implying that the visual range at the day-

time depths are not sufficient for efficient foraging. During the feeding period at dusk, both juvenile pearlside (II)(Figure 9 red lines), and *C.finmarchicus* (III) (figure 11 red lines) are taking higher risks in the surface. The movement of the *C.finmarchicus* in the surface were highly ballistic, covering a large horizontal and vertical range (III)(figure 10 track 1-4, figure 11 red lines). However, all trajectories showed very low compared to what is seen in laboratory data both with regard to self-overlap (Bianco *et al.*, 2014), orthe ballistic/diffuse component seen in copepods (Visser and Kiørboe, 2006). In the intermediate depth of 70-95 meters was a higher degree of self-overlap for the prey *C.finmarchicus* (Figure 11 blue lines), which might have possible ecological explanations as they are mostly foraging in the surface(Bagøien *et al.*, 2001; Ringelberg, 2010; Rabindranath *et al.*, 2011). The *C.finmarchicus* might be vertically migrating, or sensing migrating fishes and behaving with a higher degree of protection as the mere presence of the predator might change the behaviour of the prey (Brown *et al.*, 1999; Zanette and Clinchy, 2019). Turbidity likely played a large role in especially forming the *C.finmarchicus* trajectories, and there is discussions on how turbidity and currents affect the efficiency of the 3D-behaviour (Michalec *et al.*, 2015). Finally, the escape reactions of *C.finmarchicus* are challenging to track as swimming speeds increase to ~50 cm s^{-1}(Yen *et al.*, 2015), which will eventually lead to challenges in the target tracking process, as a pingrate of 4 Hz will not resolve the behaviour completely.

Trajetories 20 meters	Trajectories 70 meters	Trajectories 120 meters
1 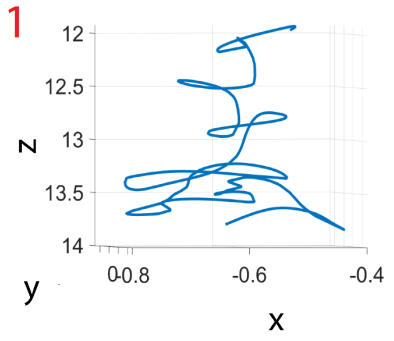	5 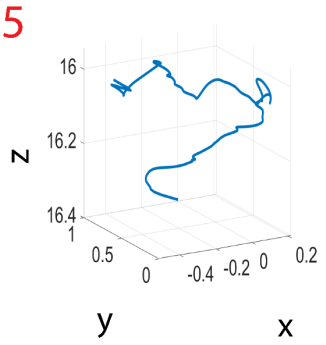	9 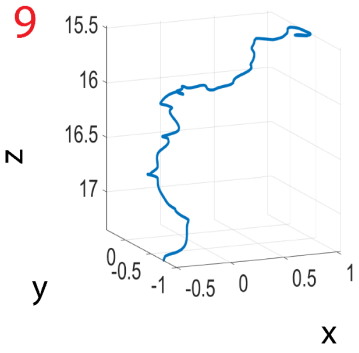
2 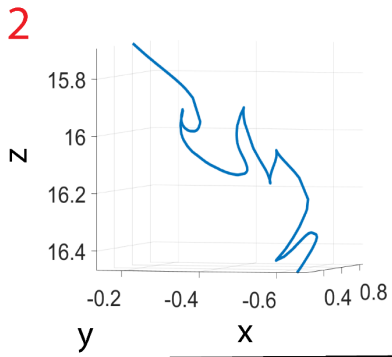	6 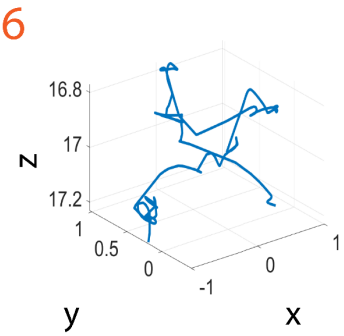	10 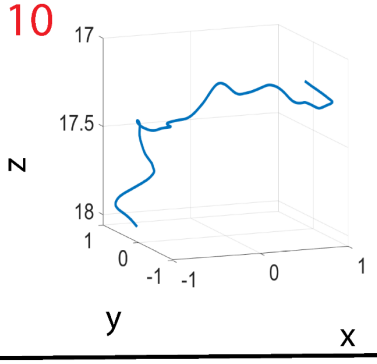
3 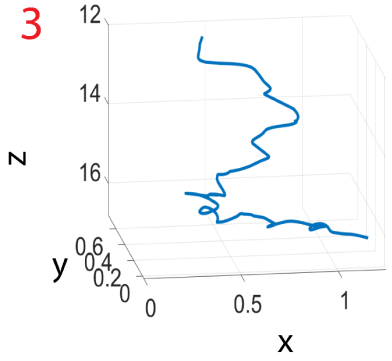	7 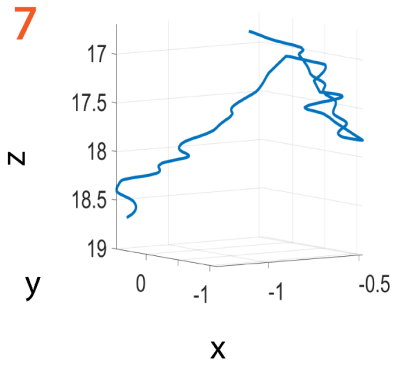	11 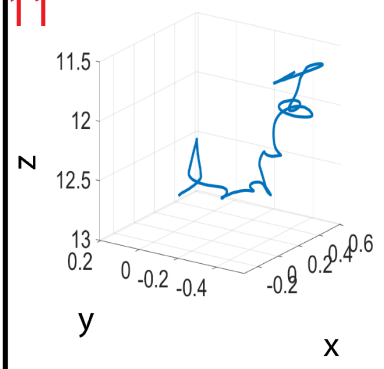
4 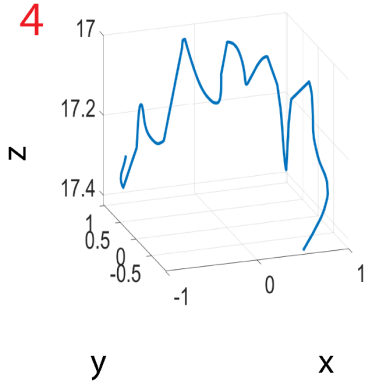	8 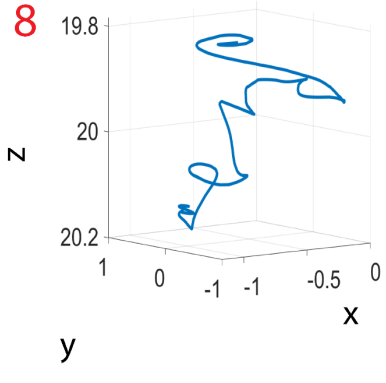	12 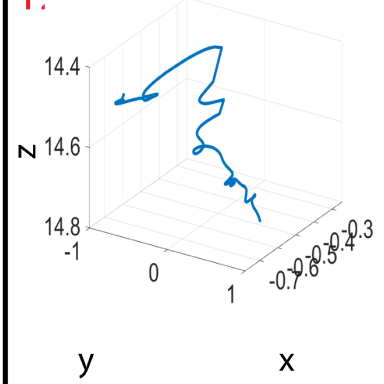

Figure 10. Selected trajectories(III). The columns show 4 tracks from each depth layer of the TS-probe (20-45 m tracks 1-4, 70-95 m tracks 5-9 and 120-145 m tracks 9-12). The x-axis is alongship position (m), y is athwartship position (m) and z is the vertical distance from transducer (m) with the transducer depth listed on the top of the figure panels.

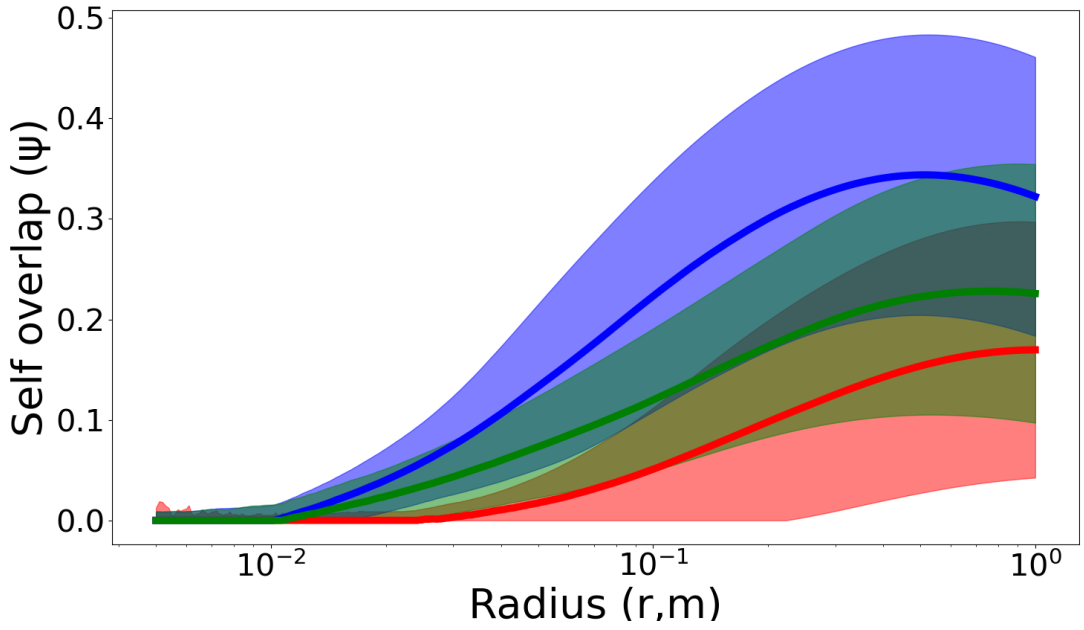

Figure 11. Self overlap for *C.Finmarchicus (III)* On the x-axis visual range (Radius) is displayed on a logarithmic scale and on the y-axis the self-overlap (psi) is shown where 1 is full self-overlap and 0 is no self-overlap. Red, blue and green color lines represent the mean self overlap for each detective readius of depth layers 1, 2 and 3, respectively. The shading represent the standard deviation calculated from the trajectories.

5 Future aspects

In this chapter I will review potential solutions to improve species identifications using broadband acoustic and alternative ground-truthing methodologies, before discussing how to proceed with movement data and analyse the performance of the self-overlap model, comparing previous studies with the in situ results. Furthermore I discuss potential future use of trajectory data in an ecological context.

5.1 Improving observation methodologies in the mesopelagic

The unique backscattering spectra of different targets can provide insight on both acoustic classes(Martin *et al.*, 1996; Lavery *et al.*, 2007; Stanton *et al.*, 2010), and potential species (Lundgren and Nielsen, 2008; Kubilius *et al.*, 2020; Agersted *et al.*, 2021; Khodabandeloo *et al.*, 2021; (I)) there are possibilities to create a library of acoustic "signatures", especially with the applications of deep learning (Handegard *et al.*, 2021). However, ground-truthing are still one of the large challenges in acoustic studies of the mesopelagic, and there is an urge to invent cost efficient, noninvasive ground-truthing methodologies. Environmental DNA has been successfully tested on mesopelagic organisms, and has been used to map biodiversity observing different species compositions than the net samples(Govindarajan *et al.*, 2021). Using a lowered observation platform with broadband echosounders to

observe in situ acoustic signatures can be useful both in off-setting resonance challenges, and to identify acoustic classes based on their frequency dependent backscattering properties(Agersted *et al.*, 2021; Khodabandeloo *et al.*, 2021)(I)(Figure 6 and 7). Cameras and optical tools are useful to identify gelatinous zooplankton and (Hosia and Båmstedt, 2008)(I)(Figure 7), and can be compared with catch data to offset some of the bias. The deep vision system has been successfully implemented as a "photo booth" of fish moving through the trawl(Underwood *et al.*, 2014), and with application of deep learning have automatized this process(Allken *et al.*, 2021). This is a good tool to ground truth the species that can handle the mechanic stress of entering the trawl. However siphonophores would still pose as a challenge as any mechanical contact are problematic(Hosia and Båmstedt, 2008). Analyzing movement patterns from triangular data, might be a useful ground truthing tool for the future. Taxa-specific movement patterns were used in (III)(Figure 12) to identify tracks of *C. finmarchicus*. The approaches to map behaviour of different taxa will vary with availability of the animal in question. Copepods are generally easy to observe in a laboratory setup (Fields and Yen, 1997; Visser, 2007; Kiørboe, 2008; Abrahamsen *et al.*, 2010; Michalec *et al.*, 2015), while mesopelagic fish still needs to be observed *in situ.* Many taxa found in the mesopelagic have unique movement patterns (II, III)(Klevjer and Kaartvedt, 2003; Kaartvedt *et al.*, 2008; Christiansen *et al.*, 2019), and acoustic tracking studies with the appropriate ground truthing methodology could provide insight in the specific behaviour patterns of specific animals.

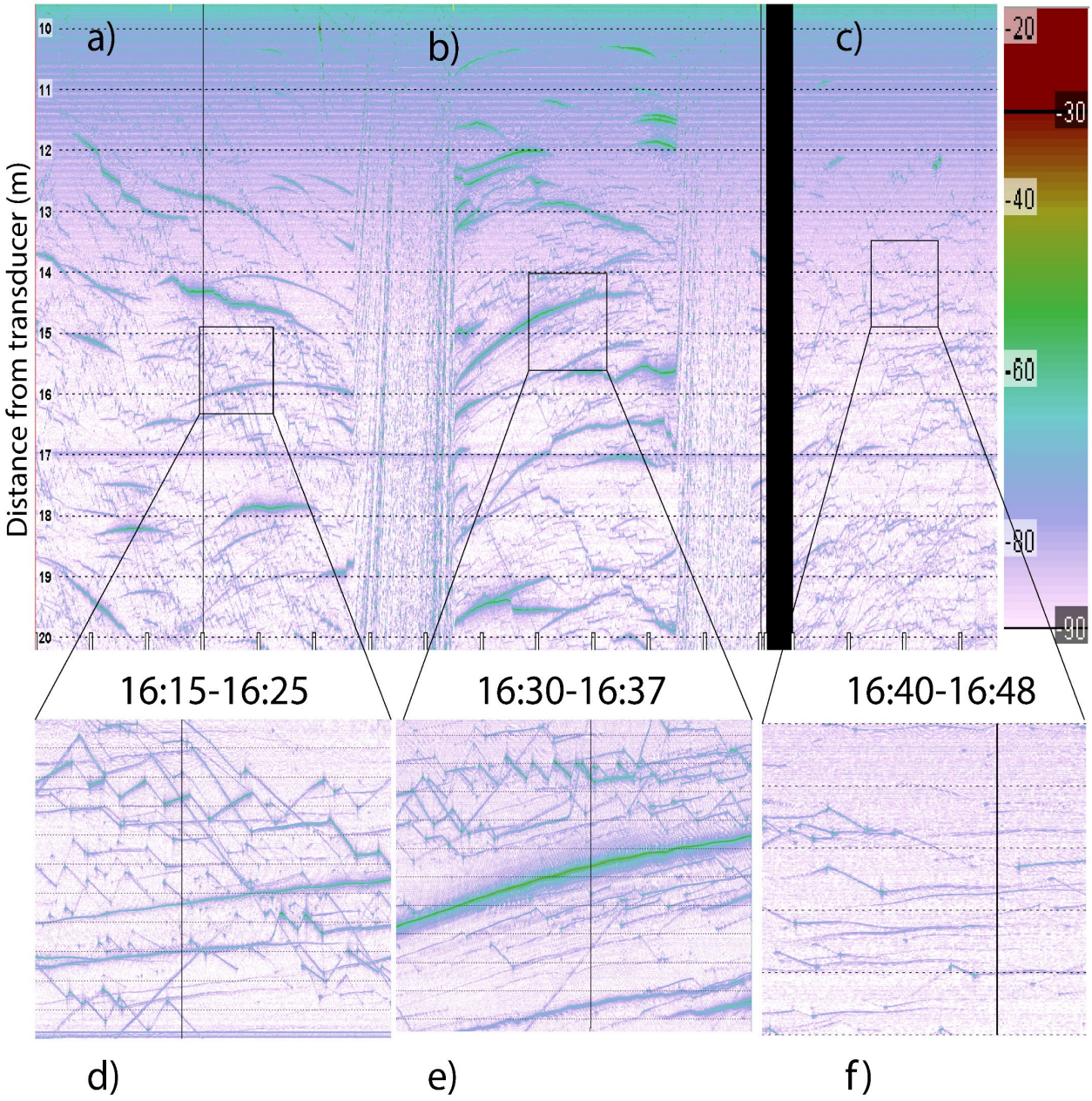

Figure 12 Echogram recorded by the TS-probe(III) in this particular study, transducers were mounted below the probe, and the probe were lowered into layers, while recording standing completely still. The x-axis of the echogram shows time in hours and minutes and the y-axis the vertical distance from the transducer. The large traces were depicted to be pearlside while the small trajectories with the vertical zig-zag movement were allocated to C. finmarchicus Panels a), b) and c) are showing echograms from 30-40 m, 80-90 m, and 130-140 m total water depth, respectively. Panels d) and e) and f) are selected parts of each echogram

showing CFtrajectories as thin lines seen in d), e) and f), and fish targets in e) with thicker lines. The parts of the echogram between a), b) and c), where trajectories appear to move simultaneously upwards is just due to the Probe being lowered to the next depth layer.

5.2 Following the life-stages of mesopelagic fish ping by ping

”Lifetime paths” is identified one of the aims of the movement ecology paradigm (Nathan, 2008). Obtaining enough tracking data to observe the life-time path would be challenging with pearlside and other micro nekton as both tagging studies, and laboratory setups appear to be very difficult (Salvanes and Kristoffersen, 2001). However, to understand the biological pump, and the fish mediated carbon transport, we need better knowledge on trophic interactions in the mesopelagic. Our studies, and others suggest that movement is important to facilitate encounters, and as anti-predatory measures (Nathan, 2008; Bianco *et al.*, 2014; Cooke *et al.*, 2022; II;III)). Understanding interactions with lower and higher trophic layers gives us an insight in both growth, mortality and possibly spawning. Even if not observed in our acoustic data on, there should be possibilities to see their direct interactions by observing trajectories of predator and prey where the trajectory of the predator might merge with the prey trajectory before it disappears. However to observe predation events on C.finmarchicus from pearlside would require high ping rate as C.finmarchicus escape responses can be mistaken as predation due to the high speed escape(Yen *et al.*, 2015) and would either require high ping rate, or a large range gate in the target tracking algorithm. Trajectories can be combined with tagging data from species such as Bluefin tuna and stomach data from mesopelagic predators. More knowledge of

where predation of mesopelagic fish occur could be combined in future studies, as different trophic levels movement ecology require different telemetry. However, one of the advantages is that several trophic layers can be observed directly (II;III)(Figure 12)

There is still a lot of work to be done on trajectories of small acoustic targets as the angular positions of the split beam echosounders are prone to error(Ehrenberg and Torkelson, 1996; Klevjer and Kaartvedt, 2003; Simmonds and MacLennan, 2007). However, some of these challenges can be overcome by adding a smoothing spline through the raw measurements (II;III) as the residuals of the raw data seemed to distribute evenly for the data derived from phase deviation (x and y).

The bioluminescent properties of mesopelagic fish is completely neglected in acoustics-derived behaviour studies. Mesopelagic fishes including pearlside are known to use bioluminescence for communication, protection and luring prey(Edward Young *et al.*, 1973; Barnes and Case, 1974; Mensinger and Case, 1990; Warrant and Locket, 2004; Haddock *et al.*, 2010). Bioluminescence might modulate ambient light levels, and thus increase or reduce encounter rates. Mesopelagic organisms have been measured to increase bioluminescence when attacked by an elephant seal(Goulet *et al.*, 2020). I suggest that future studies should overcome the current optical challenges to observe behaviour combined with bioluminescence.

5.2.1 Challenges in using the self-overlap model.

All path geometry models are simplified to understand complex phenomena such as encounter rates and evolution(Bianco *et al.*, 2014). The increased number of high resolution animal movement stueis is promising, and has been compared in importance to the mapping of the genome and its role in genetics (Nathan *et al.*, 2008). Many factors influence aquatic life, as turbulence, currents, hydrographical properties and light influence movement in many ways, and to gain accurate movement models, many of these parameters need to be measured simultaneously. The observed in situ self-overlap of both fish and zooplankton were low (II,III)(Figure 9 and 11), and can be explained by turbulence and currents and potentially patchy food distribution(III), scenarios not usually applied in laboratory studies. However, it is also crucially important to observe if and how these other factors influence motion strategies to fully understand the observations done *ex situ.*

Ideally, ambient hydrographical conditions could be measured simultaneously, similar to how wind has been included in movement studies of birds (Richardson *et al.*, 2018). If theoretically all animal groups were influenced similarly by turbulence, motion strategies would still be effective. However, there are many taxa capable of resisting and swimming against currents, including micro nekton, and copepods (Wilson and Boehlert, 2004; Weidberg *et al.*, 2021). Furthermore, the increased swimming behaviour of *C.finmarchicus* (III), might be a different and unknown anti-predator strategy, as detective radius of both predator and prey are unknown (III), and visual capability are extremely important for planktivorous fishes.

5.3 Further use of trajectories

In traditional encounter models(Lotka, 1920; Volterra, 1926; Holling, 1959, 1966; Rothschild *et al.*, 1988), all organisms are assumed to follow the law of mass action where encounters are proportional with the observed densities as all components moves in a Brownian way, and density is usually the crucial parameters as seen in functional response models (Holling, 1959, 1966). However most animals do not follow the law of mass action (Martinez-Garcia *et al.*, 2020). Both pearlside and C.finmarchicus behaved in specific ways where light seemed to be the main factor, not density (III). Improving the knowledge on individual motion of the trophic layers in the mesopelagic will further lead to better understanding of habitat-structure, migration, growth and mortality. Trajectories can further be used in agent based models which have been successfully used for human trajectories (Bonabeau, 2002; Alsaleh and Sayed, 2020)fish (Zielinski *et al.*, 2018) marine mammals (Chudzinska *et al.*, 2021), and dispersal of mussels(Pastor *et al.*, 2021), and there

are potential to use these models to observe trophic interactions in the mesopelagic and predict spatial structure under different scenarios. This would require effort obtaining trajectories and learning the specific behaviour for each species over a longer time span, as it is crucial to understand behaviour mechanistically in order to learn more about mesopelagic fishes ecological role as well as carbon sequestering.

6 References

Abrahamsen, M. B., Browman, H. I., Fields, D. M., and Skiftesvik, A. B. 2010. The three-dimensional prey field of the northern krill, Meganyctiphanes norvegica, and the escape responses of their copepod prey. Marine Biology, 157: 1251–1258.

Agersted, M. D., Khodabandeloo, B., Liu, Y., Melle, W., and Klevjer, T. A. 2021. Application of an unsupervised clustering algorithm on in situ broadband acoustic data to identify different mesopelagic target types. ICES Journal of Marine Science, 78: 2907–2921.

Aksnes, D. L., and Utne, A. C. W. 1997. A revised model of visual range in fish. Sarsia, 82: 137–147.

Aksnes, D. L., Nejstgaard, J., Sædberg, E., and Sørnes, T. 2004. Optical control of fish and zooplankton populations. Limnology and Oceanography, 49: 233–238.

Allen, R. M., Metaxas, A., and Snelgrove, P. V. R. 2018. Applying movement ecology to marine animals with complex life cycles. Annual Review of Marine Science, 10: 19–42.

Allken, V., Rosen, S., Handegard, N. O., and Malde, K. 2021. A deep learning-based method to identify and count pelagic and mesopelagic fishes from trawl camera images. ICES Journal of Marine Science, 78: 3780–3792.

Alsaleh, R., and Sayed, T. 2020. Modeling pedestrian-cyclist interactions in shared space using inverse reinforcement learning. Transportation Research Part F: Traffic Psychology and Behaviour.

Alvheim, A. R., Kjellevold, M., Strand, E., Sanden, M., and Wiech, M. 2020. Mesopelagic species and their potential contribution to food and feed security—a case study from Norway. Foods, 9: 344.

Bagøien, E., Kaartvedt, S., Aksnes, D. L., and Eiane, K. 2001. Vertical distribution and mortality of overwintering Calanus. Limnology and Oceanography, 46: 1494–1510.

Barham, E. G. 1963. Siphonophores and the deep scattering layer. Science, 140: 826–828.

Barham, E. G. 1966. Deep scattering layer migration and composition: Observations from a diving saucer. Science, 151: 1399–1403.

Barnes, A. T., and Case, J. F. 1974. The luminescence of lanternfish (myctophidae): Spontaneous activity and responses to mechanical, electrical, and chemical

stimulation. Journal of Experimental Marine Biology and Ecology, 15: 203–221.

Bartumeus, F., Peters, F., Pueyo, S., Marrasé, C., and Catalan, J. 2003. Helical Lévy walks: Adjusting searching statistics to resource availability in microzooplankton. Proceedings of the National Academy of Sciences of the United States of America, 100: 12771–12775.

Battaglia, P., Andaloro, F., Consoli, P., Esposito, V., Malara, D., Musolino, S., Pedà, C., *et al.* 2013. Feeding habits of the Atlantic bluefin tuna, Thunnus thynnus (L. 1758), in the central Mediterranean Sea (Strait of Messina). Helgoland Marine Research.

Battaglia, P., Ammendolia, G., Esposito, V., Romeo, T., and Andaloro, F. 2018. Few But Relatively Large Prey: Trophic Ecology of Chauliodus sloani (Pisces: Stomiidae) in Deep Waters of the Central Mediterranean Sea. Journal of Ichthyology, 58: 8–16.

Beamish, R. J., Leask, K. D., Ivanov, O. A., Balanov, A. A., Orlov, A. M., and Sinclair, B. 1999. The ecology, distribution, and abundance of midwater fishes of the Subarctic Pacific gyres. Progress in Oceanography, 43: 399–442.

Berezhkovskii, A. M., Makhnovskii, Y. A., and Suris, R. A. 1989. Wiener sausage volume moments. Journal of Statistical Physics, 57: 333–346.

Berg, H. C. 1993. Random Walks in Biology: New and Expanded Edition: 152.

Bestley, S., Jonsen, I. D., Hindell, M. A., Harcourt, R. G., and Gales, N. J. 2015. Taking animal tracking to new depths: Synthesizing horizontal - vertical movement relationships for four marine predators. Ecology, 96: 417–427.

Bianco, G., Mariani, P., Visser, A. W., Mazzocchi, M. G., and Pigolotti, S. 2014. Analysis of self-overlap reveals trade-offs in plankton swimming trajectories. Journal of the Royal Society Interface, 11.

Bjelland. 1995. Life-history tactics of two fjord populations of Maurolicus muelleri. Cand. scient. thesis, Univ. Bergen, Department of Fisheries and Marine Biology.

Bonabeau, E. 2002. Agent-based modeling: Methods and techniques for simulating human systems. Proceedings of the National Academy of Sciences of the United States of America, 99: 7280–7287.

Brown, J. S., Laundré, J. W., and Gurung, M. 1999. The ecology of fear: Optimal foraging, game theory, and trophic interactions. Journal of Mammalogy, 80: 385–399.

Burns, A. L., Schaerf, T. M., Lizier, J., Kawaguchi, S., Cox, M., King, R., Krause, J., *et al.* 2022. Self-organization and information transfer in Antarctic krill swarms. Proceedings of the Royal Society B, 289.

cech, M., and Kubecka, J. 2002. Sinusoidal cycling swimming pattern of reservoir fishes. Journal of Fish Biology, 61: 456–471.

Chen, M. R., and Hwang, J. S. 2018. The Swimming Behavior of the Calanoid Copepod Calanus sinicusUnder Different Food Concentrations. Zoological Studies, 57.

Christiansen, S., Titelman, J., and Kaartvedt, S. 2019. Nighttime Swimming Behavior of a Mesopelagic Fish. Frontiers in Marine Science, 6.

Christiansen, S., Klevjer, T. A., Røstad, A., Aksnes, D. L., and Kaartvedt, S. 2021. Flexible behaviour in a mesopelagic fish (Maurolicus muelleri). ICES Journal of Marine Science.

Chudzinska, M., Nabe-Nielsen, J., Smout, S., Aarts, G., Brasseur, S., Graham, I., Thompson, P., *et al.* 2021. AgentSeal: Agent-based model describing movement of marine central-place foragers. Ecological Modelling.

Clark, C. W., and Levy, D. A. 1988. Diel vertical migrations by juvenile sockeye salmon and the antipredation window. American Naturalist, 131: 271–289.

Cooke, S. J., Bergman, J. N., Twardek, W. M., Piczak, M. L., Casselberry, G. A., Keegan Lutek, |, Dahlmo, L. S., *et al.* 2022. The movement ecology of fishes. Journal of Fish Biology.

Davison, P. C., Checkley, D. M., Koslow, J. A., and Barlow, J. 2013. Carbon export mediated by mesopelagic fishes in the northeast Pacific Ocean. Progress in Oceanography, 116: 14–30.

Davison, P. C., Koslow, J. A., and Kloser, R. J. 2015. Acoustic biomass estimation of mesopelagic fish: Backscattering from individuals, populations, and communities. ICES Journal of Marine Science, 72: 1413–1424.

De Robertis, A., Schell, C., and Jaffe, J. S. 2003. Acoustic observations of the swimming behavior of the euphausiid Euphausia pacifica Hansen. ICES Journal of Marine Science.

Dias Bernardes, I., Ona, E., and Gjøsæter, H. 2020. Study of the Arctic mesopelagic layer with vessel and profiling multifrequency acoustics. Progress in Oceanography, 182: 102260.

Dornan, T., Fielding, S., Saunders, R. A., and Genner, M. J. 2019. Swimbladder morphology masks Southern Ocean mesopelagic fish biomass. Proceedings of the Royal Society B: Biological Sciences, 286.

Duffy, L. M., Kuhnert, P. M., Pethybridge, H. R., Young, J. W., Olson, R. J., Logan, J. M., Goñi, N., *et al.* 2017. Global trophic ecology of yellowfin, bigeye, and albacore tunas: Understanding predation on micronekton communities at ocean-basin scales. Deep Sea Research Part II: Topical Studies in Oceanography, 140: 55–73.

Duvall, G. E., and Christensen, R. J. 1946. Stratification of Sound Scatterers in the Ocean. The Journal of the Acoustical Society of America, 18: 254–254.

Eduardo, L. N., Lucena-Frédou, F., Mincarone, M. M., Soares, A., Le Loc'h, F., Frédou, T., Ménard, F., *et al.* 2020. Trophic ecology, habitat, and migratory behaviour of the viperfish Chauliodus sloani reveal a key mesopelagic player. Scientific Reports, 10: 1–13.

Edward Young, R., E Roper, C. F., Backus, R. H., Craddock, E., Haedrich, R. L., Shores, D. L., Teal, M., *et al.* 1973. Nature (Lon-don). P. Foxlon, J. Mar. Biol. Assoc. U.K, 11: 20.

Ehrenberg, J. E., and Torkelson, T. C. 1996. Application of dual-beam and split-beam

target tracking in fisheries acoustics. ICES Journal of Marine Science, 53: 329–334.

Eiane, K., Aksnes, D. L., Bagøien, E., and Kaartvedt, S. 1999. Fish or jellies - A question of visibility? Limnology and Oceanography, 44: 1352–1357.

FaO. 2020. The State of World Fisheries and Aquaculture 2020. In brief.

Fields, D. M., and Yen, J. 1997. The escape behavior of marine copepods in response to a quantifiable fluid mechanical disturbance. Journal of Plankton Research, 19: 1289–1304.

Folkvord, A., Gundersen, G., Albretsen, J., Asplin, L., Kaartvedt, S., and Giske, J. 2016. Impact of hatch date on early life growth and survival of Mueller's pearlside (Maurolicus muelleri) larvae and life-history consequences. Canadian Journal of Fisheries and Aquatic Sciences, 73: 163–176.

Giske, J., Aksnes, D. L., Baliño, B. M., Kaartvedt, S., Lie, U., Nordeide, J. T., Salvanes, A. G. V., *et al.* 1990. Vertical distribution and trophic interactions of zooplankton and fish in Masfjorden, Norway. Sarsia, 75: 65–81.

Giske, J., and Aksnes, D. L. 1992. Ontogeny, season and trade-offs: Vertical distribution of the mesopelagic fish maurolicus muelleri. Sarsia, 77: 253–261.

Gjelland, K. Ø., Bøhn, T., Knudsen, F. R., and Amundsen, P. A. 2004. Influence of light on the swimming speed of coregonids in subarctic lakes. *In* Annales Zoologici Fennici.

Gjøsaeter, J., and Kawaguchi, K. 1980. A review of the world resources of mesopelagic

fish. FAO Fisheries Technical Paper, 193: 123–134.

Gjøsæter, J., and Kawaguchi, K. 1980. A Review of the World Resources of Mesopelagic Fish - J. Gjøsaeter, K. Kawaguchi, Food and Agriculture Organization of the United Nations - Google Bøker.

Gjøsæter, J. 1981. Variation in Growth Rate and Age at First Maturation in Rainbow Trout; Growth, Production and Reproduction of the Myctophid Fish Benthosema Glaciale From Western Norway and Adjacent Seas; Life History and Ecology of Maurolicus Muelleri (Gonostomatidae) i. 109–131 pp.

Godø, O. R., Patel, R., and Pedersen, G. 2009. Diel migration and swimbladder resonance of small fish: Some implications for analyses of multifrequency echo data. *In* ICES Journal of Marine Science, pp. 1143–1148.

Gong, L., Hu, Z., and Zhou, X. 2022. A real time video object tracking method for fish. *In* ACM International Conference Proceeding Series, pp. 78–84.

Goulet, P., Guinet, C., Campagna, C., Campagna, J., Tyack, P. L., and Johnson, M. 2020. Flash and grab: Deep-diving southern elephant seals trigger anti-predator flashes in bioluminescent prey. Journal of Experimental Biology, 223.

Govindarajan, A. F., Francolini, R. D., Jech, J. M., Lavery, A. C., Llopiz, J. K., Wiebe, P. H., and Zhang, W. 2021. Exploring the Use of Environmental DNA (eDNA) to Detect Animal Taxa in the Mesopelagic Zone. Frontiers in Ecology and Evolution, 9: 146.

Grimaldo, E., Grimsmo, L., Alvarez, P., Herrmann, B., Møen Tveit, G., Tiller, R., Slizyte, R., *et al.* 2020. Investigating the potential for a commercial fishery in the Northeast Atlantic utilizing mesopelagic species. ICES Journal of Marine Science.

Haddock, S. H. D., Moline, M. A., and Case, J. F. 2010. Bioluminescence in the sea. Annual Review of Marine Science, 2: 443–493.

Handegard, N. O., Michalsen, K., and Tjøstheim, D. 2003. Avoidance behaviour in cod (Gadus morhua) to a bottom-trawling vessel. *In* Aquatic Living Resources.

Handegard, N. O., Patel, R., and Hjellvik, V. 2005. Tracking individual fish from a moving platform using a split-beam transducer. The Journal of the Acoustical Society of America, 118: 2210–2223.

Handegard, N. O. 2007. Observing individual fish behavior in fish aggregations: Tracking in dense fish aggregations using a split-beam echosounder. The Journal of the Acoustical Society of America, 122: 177–187.

Handegard, N. O., and Williams, K. 2008. Automated tracking of fish in trawls using the DIDSON (Dual frequency IDentification SONar). ICES Journal of Marine Science.

Handegard, N. O., Boswell, K. M., Ioannou, C. C., Leblanc, S. P., Tjostheim, D. B., and Couzin, I. D. 2012. The Dynamics of Coordinated Group Hunting and Collective Information Transfer among Schooling Prey. Current Biology, 22: 1213–1217.

Handegard, N. O., Buisson, L. Du, Brehmer, P., Chalmers, S. J., De Robertis, A., Huse, G., Kloser, R., *et al.* 2013. Towards an acoustic-based coupled observation and

modelling system for monitoring and predicting ecosystem dynamics of the open ocean. Fish and Fisheries, 14: 605–615.

Handegard, N. O., Tonje, F. N., Johnsen, E., Pedersen, G., Tenningen, M., Korneliussen, R., and Ona, E. 2021. Fisheries acoustics in Norway—Wide band data, autonomous platforms and deep learning. The Journal of the Acoustical Society of America, 150: A254.

Hidaka, K., Kawaguchi, K., Murakami, M., and Takahashi, M. 2001. Downward transport of organic carbon by diel migratory micronekton in the western equatorial pacific: Its quantitative and qualitative importance. Deep-Sea Research Part I: Oceanographic Research Papers, 48: 1923–1939.

Holling, C. S. 1959. Some Characteristics of Simple Types of Predation and Parasitism. The Canadian Entomologist, 91: 385–398.

Holling, C. S. 1966. The Functional Response of Invertebrate Predators to Prey Density. The Memoirs of the Entomological Society of Canada, 98: 5–86.

Hosia, A., and Båmstedt, U. 2008. Seasonal abundance and vertical distribution of siphonophores in western Norwegian fjords. Journal of Plankton Research, 30: 951–962.

Huse, I., and Ona, E. 1996. Tilt angle distribution and swimming speed of overwintering Norwegian spring spawning herring. ICES Journal of Marine Science, 53: 863–873.

Hussey, N. E., Kessel, S. T., Aarestrup, K., Cooke, S. J., Cowley, P. D., Fisk, A. T.,

Harcourt, R. G., *et al.* 2015. Aquatic animal telemetry: A panoramic window into the underwater world. Science, 348: 1255642.

Ikeda, T. 1994. Growth and life cycle of the mesopelagic fish Maurolicus muelleri (Sternoptychidae) in Toyama Bay, southern Japan Sea. Bulletin of Plankton Society of Japan, 40: 127–138.

Ikeda, T. 1996. Metabolism, body composition, and energy budget of the mesopelagic fish Maurolicus muelleri in the Sea of Japan. Fishery Bulletin.

Irigoien, X., Klevjer, T. A., Røstad, A., Martinez, U., Boyra, G., Acuña, J. L., Bode, A., *et al.* 2014. Large mesopelagic fishes biomass and trophic efficiency in the open ocean. Nature communications, 5: 3271.

Jech, J. M., Lawson, G. L., and Lavery, A. C. 2017. Wideband (15-260 kHz) acoustic volume backscattering spectra of Northern krill (Meganyctiphanes norvegica) and butterfish (Peprilus triacanthus). ICES Journal of Marine Science, 74: 2249–2261.

Kaartvedt, S., Knutsen, T., and Holst, J. C. 1998. Schooling of the vertically migrating mesopelagic fish Maurolicus muelleri in light summer nights. Marine Ecology Progress Series, 170: 287–290.

Kaartvedt, S., Torgersen, T., Klevjer, T. A., Røstad, A., and Devine, J. A. 2008. Behavior of individual mesopelagic fish in acoustic scattering layers of Norwegian fjords. Marine Ecology Progress Series, 360: 201–209.

Kaartvedt, S., Titelman, J., Røstad, A., and Klevjer, T. A. 2011. Beyond the average:

Diverse individual migration patterns in a population of mesopelagic jellyfish. Limnology and Oceanography, 56: 2189–2199.

Kaartvedt, S., Staby, A., and Aksnes, D. L. 2012. Efficient trawl avoidance by mesopelagic fishes causes large underestimation of their biomass. Marine Ecology Progress Series, 456: 1–6.

Kaartvedt, S., Langbehn, T. J., and Aksnes, D. L. 2019. Enlightening the ocean's twilight zone. ICES Journal of Marine Science, 76: 803–812.

Kandimalla, V., Richard, M., Smith, F., Quirion, J., Torgo, L., and Whidden, C. 2022. Automated Detection, Classification and Counting of Fish in Fish Passages With Deep Learning. Frontiers in Marine Science, 8: 2049.

Kays, R., Crofoot, M. C., Jetz, W., and Wikelski, M. 2015. Terrestrial animal tracking as an eye on life and planet. Science, 348: aaa2478.

Kelly, T. B., Davison, P. C., Goericke, R., Landry, M. R., Ohman, M. D., and Stukel, M. R. 2019. The Importance of Mesozooplankton Diel Vertical Migration for Sustaining a Mesopelagic Food Web. Frontiers in Marine Science, 6.

Khodabandeloo, B., Agersted, M. D., Klevjer, T., Macaulay, G. J., and Melle, W. 2021. Estimating target strength and physical characteristics of gas-bearing mesopelagic fish from wideband in situ echoes using a viscous-elastic scattering model . The Journal of the Acoustical Society of America, 149: 673–691.

Kiørboe, T. 2008. Optimal swimming strategies in mate-searching pelagic copepods.

Oecologia, 155: 179–192.

Klevjer, T. A., and Kaartvedt, S. 2003. Split-beam target tracking can be used to study the swimming behaviour of deep-living plankton in situ. Aquatic Living Resources, 16: 293–298.

Klevjer, T. A., and Kaartvedt, S. 2006. In situ target strength and behaviour of northern krill (Meganyctiphanes norvegica). ICES Journal of Marine Science, 63: 1726–1735.

Klevjer, T. A., Irigoien, X., Røstad, A., Fraile-Nuez, E., Benítez-Barrios, V. M., and Kaartvedt., S. 2016. Large scale patterns in vertical distribution and behaviour of mesopelagic scattering layers. Scientific Reports, 6.

Kloser, R. J., Ryan, T., Sakov, P., Williams, A., and Koslow, J. A. 2002. Species identification in deep water using multiple acoustic frequencies. Canadian Journal of Fisheries and Aquatic Sciences, 59: 1065–1077.

Kloser, R. J., Ryan, T. E., Keith, G., and Gershwin, L. 2016. Deep-scattering layer, gas-bladder density, and size estimates using a two-frequency acoustic and optical probe. *In* ICES Journal of Marine Science, pp. 2037–2048.

Knutsen, T., Wiebe, P. H., Gjøsæter, H., Ingvaldsen, R. B., and Lien, G. 2017. High Latitude Epipelagic and mesopelagic scattering layers-a reference for future Arctic ecosystem change. Frontiers in Marine Science, 4.

Knutsen, T., Hosia, A., Falkenhaug, T., Skern-Mauritzen, R., Wiebe, P. H., Larsen, R. B., Aglen, A., *et al.* 2018. Coincident mass occurrence of gelatinous zooplankton in

Northern Norway. Frontiers in Marine Science, 5.

Korneliussen, R. J., and Ona, E. 2002. An operational system for processing and visualizing multi-frequency acoustic data. ICES Journal of Marine Science, 59: 293–313.

Korneliussen, R. J., and Ona, E. 2003. Synthetic echograms generated from the relative frequency response. *In* ICES Journal of Marine Science, pp. 636–640.

Korneliussen, R. J. 2010. Large Scale Survey System – LSSS. Database.

Korneliussen, R. J., Heggelund, Y., Macaulay, G. J., Patel, D., Johnsen, E., and Eliassen, I. K. 2016. Acoustic identification of marine species using a feature library. Methods in Oceanography, 17: 187–205.

Kristoffersen, J. B., and Salvanes, A. G. V. 1998. Life history of Maurolicus muelleri in fjordic and oceanic environments. Journal of Fish Biology, 53: 1324–1341.

Kristoffersen, J. B., and Salvanes, A. G. V. 2001. Sexual size dimorphism and sex ratio in Müller's pearlside (Maurolicus muelleri). Marine Biology, 138: 1087–1092.

Kubilius, R., Macaulay, G. J., and Ona, E. 2020. Remote sizing of fish-like targets using broadband acoustics. Fisheries Research, 228: 105568.

Lam, V. W. M., and Pauly, D. 2005. Mapping the global biomass of mesopelagic fishes. 4 pp.

Langbehn, T. J., Aksnes, D. L., Kaartvedt, S., Fiksen, Ø., and Jørgensen, C. 2019. Light

comfort zone in a mesopelagic fish emerges from adaptive behaviour along a latitudinal gradient. Marine Ecology Progress Series, 623: 161–174.

Lavery, A. C., Wiebe, P. H., Stanton, T. K., Lawson, G. L., Benfield, M. C., and Copley, N. 2007. Determining dominant scatterers of sound in mixed zooplankton populations. The Journal of the Acoustical Society of America, 122: 3304–3326.

Levandowsky, M., Klafter, J., and White, B. S. 1988. Feeding and Swimming Behavior in Grazing Microzooplankton,. The Journal of Protozoology, 35: 243–246.

Lotka, A. J. 1920. Analytical Note on Certain Rhythmic Relations in Organic Systems. Proceedings of the National Academy of Sciences.

Lucas, J., Ros, A., Gugele, S., Dunst, J., Geist, J., and Brinker, A. 2021. The hunter and the hunted—A 3D analysis of predator-prey interactions between three-spined sticklebacks (Gasterosteus aculeatus) and larvae of different prey fishes. PLOS ONE, 16: e0256427.

Lundgren, B., and Nielsen, J. R. 2002. Experiments for possible hydroacoustic discrimination of free-swimming juvenile gadoid fish by analysis of broadband pulse spectra as well as 3d fish position from video images and split beam acoustics. Bioacoustics.

Lundgren, B., and Nielsen, J. R. 2008. A method for the possible species discrimination of juvenile gadoids by broad-bandwidth backscattering spectra vs. angle of incidence. ICES Journal of Marine Science.

Marshall, N. 1951. Bathypelagic fishes as sound scatterers in the ocean. Journal of Marine Research, 10: 1–17.

Marshall, N. B. 1960. Swimbladder structure of deep-sea fishes in relation to their systematics and biology. 1–121 pp.

Martin, A., Boyd, P., Buesseler, K., Cetinic, I., Claustre, H., Giering, S., Henson, S., *et al.* 2020. The oceans' twilight zone must be studied now, before it is too late. Nature 2021 580:7801, 580: 26–28.

Martin, L. V., Stanton, T. K., Wiebe, P. H., and Lynch, J. F. 1996. Acoustic classification of zooplankton. ICES Journal of Marine Science, 53: 217–224.

Martinez-Garcia, R., Fleming, C. H., Seppelt, R., Fagan, W. F., and Calabrese, J. M. 2020. How range residency and long-range perception change encounter rates. Journal of Theoretical Biology, 498: 110267.

McClatchie, S., Thorne, R. E., Grimes, P., and Hanchet, S. 2000. Ground truth and target identification for fisheries acoustics. Fisheries Research.

McMahon, C. R., Hindell, M. A., Charrassin, J. B., Corney, S., Guinet, C., Harcourt, R., Jonsen, I., *et al.* 2019. Finding mesopelagic prey in a changing Southern Ocean. Scientific Reports, 9.

Medwin, H., and Clay, C. S. 1998. Sources and Receivers. *In* Fundamentals of Acoustical Oceanography, pp. 127–152.

Mensinger, A. F., and Case, J. F. 1990. Luminescent properties of deep sea fish. Journal

of Experimental Marine Biology and Ecology, 144: 1–15.

Michalec, F. G., Souissi, S., and Holzner, M. 2015. Turbulence triggers vigorous swimming but hinders motion strategy in planktonic copepods. Journal of the Royal Society Interface, 12.

Miyazaki, S. 2006. Crossover between Ballistic and Normal Diffusion. Progress of Theoretical Physics Supplement.

Naito, Y., Costa, D. P., Adachi, T., Robinson, P. W., Fowler, M., and Takahashi, A. 2013. Unravelling the mysteries of a mesopelagic diet: A large apex predator specializes on small prey. Functional Ecology, 27: 710–717.

Nakken, O., and Olsen, K. (Institute of M. R. B. (Norway)). 1977. Target strength measurements of fish. Rapports et Proces-Verbaux des Reunions (ICES).

Nathan, R., Getz, W. M., Revilla, E., Holyoak, M., Kadmon, R., Saltz, D., and Smouse, P. E. 2008. A movement ecology paradigm for unifying organismal movement research. Proceedings of the National Academy of Sciences of the United States of America, 105: 19052–19059.

Nathan, R. 2008, December 9. An emerging movement ecology paradigm.

Niwa, H. S. 2007. Random-walk dynamics of exploited fish populations. ICES Journal of Marine Science, 64: 496–502.

Olav Handegard, N., Pedersen, G., Brix Handegard, O., Handegard, N. O., and Pedersen, G. 2009. Estimating tail-beat frequency using split-beam echosounders. ICES

Journal of Marine Science, 66: 1252–1258.

Olson, R. J., Duffy, L. M., Kuhnert, P. M., Galván-Magaña, F., Bocanegra-Castillo, N., and Alatorre-Ramírez, V. 2014. Decadal diet shift in yellowfin tuna Thunnus albacares suggests broad-scale food web changes in the eastern tropical Pacific Ocean. Marine Ecology Progress Series, 497: 157–178.

Ona, E. 1999. ICES COOPERATIVE RESEARCH REPORT Methodology for Target Strength Measurements (With special reference to in situ techniques for fish and mikro-nekton) International Council for the Exploration of the Sea Conseil International pour 1'Exploration de la Mer.

Paoletti, S. ;, Rasmus Nielsen, J. ; R., Sparrevohn, R. ;, Bastardie, C. ;, and Vastenhoud, M. J. 2021. Potential for Mesopelagic Fishery Compared to Economy and Fisheries Dynamics in Current Large Scale Danish Pelagic Fishery. Citation.

Pastor, A., Larsen, J., Hansen, F. T., Simon, A., Bierne, N., and Maar, M. 2021. Agent-based modeling and genetics reveal the Limfjorden, Denmark, as a well-connected system for mussel larvae. Marine Ecology Progress Series, 680: 193–205.

Pauly, D., Christensen, V., Guénette, S., Pitcher, T. J., Sumaila, U. R., Walters, C. J., Watson, R., *et al.* 2002. Towards sustainability in world fisheries. Nature 2002 418:6898, 418: 689–695.

Prihartato, P. K., Aksnes, D. L., and Kaartvedt, S. 2015. Seasonal patterns in the nocturnal distributionand behavior of the mesopelagic fish Maurolicus muelleri at

high latitudes. Marine Ecology Progress Series, 521: 189–200.

Proud, R., Handegard, N. O., Kloser, R. J., Cox, M. J., Brierley, A. S., and Demer, D. 2019. From siphonophores to deep scattering layers: Uncertainty ranges for the estimation of global mesopelagic fish biomass. ICES Journal of Marine Science, 76: 718–733.

Pugh, P. R. 1984. The diel migrations and distributions within a mesopelagic community in the North East Atlantic. 7. Siphonophores.

Rabindranath, A., Daase, M., Falk-Petersen, S., Wold, A., Wallace, M. I., Berge, J., and Brierley, A. S. 2011. Seasonal and diel vertical migration of zooplankton in the High Arctic during the autumn midnight sun of 2008. Marine Biodiversity, 41: 365–382.

Rasmussen, O. I., and Giske, J. 1994. Life-history parameters and vertical distribution of Maurolicus muelleri in Masfjorden in summer. Marine Biology, 120: 649–664.

Rees, D. J., Poulsen, J. Y., Sutton, T. T., Costa, P. A. S., and Landaeta, M. F. 2020. Global phylogeography suggests extensive eucosmopolitanism in Mesopelagic Fishes (Maurolicus: Sternoptychidae). Scientific Reports, 10.

Richardson, P. L., Wakefield, E. D., and Phillips, R. A. 2018. Flight speed and performance of the wandering albatross with respect to wind. Movement Ecology, 6: 1–15.

Rieucau, G., Holmin, A. J., Castillo, J. C., Couzin, I. D., and Handegard, N. O. 2016. School level structural and dynamic adjustments to risk promote information transfer

and collective evasion in herring. Animal Behaviour, 117: 69–78.

Ringelberg, J. 2010. Diel vertical migration of zooplankton in lakes and oceans: Causal explanations and adaptive significances. Diel Vertical Migration of Zooplankton in Lakes and Oceans: Causal Explanations and Adaptive Significances: 1–356.

Rizzo, L. Y., and Schulte, D. 2009. A review of humpback whales' migration patterns worldwide and their consequences to gene flow. Journal of the Marine Biological Association of the United Kingdom, 89: 995–1002.

Rothschild, B., Research, T. O.-J. of plankton, and 1988, undefined. 1988. Small-scale turbulence and plankton contact rates. academic.oup.com, 10: 465–474.

Sakinan, S., Lawson, G. L., Wiebe, P. H., Chu, D., and Copley, N. J. 2019. Accounting for seasonal and composition-related variability in acoustic material properties in estimating copepod and krill target strength. Limnology and Oceanography: Methods, 17: 607–625.

Salvanes, A. G. V., and Kristoffersen, J. B. 2001. Mesopelagic Fishes. *In* Encyclopedia of Ocean Sciences.

Scoulding, B., Chu, D., Ona, E., and Fernandes, P. G. 2015. Target strengths of two abundant mesopelagic fish species. The Journal of the Acoustical Society of America, 137: 989–1000.

Simmonds, J., and MacLennan, D. 2007. Fisheries acoustics: Theory and practice: Second edition. 1–252 pp.

Sobradillo, B., Boyra, G., Martinez, U., Carrera, P., Peña, M., and Irigoien, X. 2019. Target Strength and swimbladder morphology of Mueller's pearlside (Maurolicus muelleri). Scientific Reports, 9.

St.John, M. A. S., Borja, A., Chust, G., Heath, M., Grigorov, I., Mariani, P., Martin, A. P., *et al.* 2016. A dark hole in our understanding of marine ecosystems and their services: Perspectives from the mesopelagic community. Frontiers in Marine Science, 3.

Staby, A., and Aksnes, D. L. 2011. Follow the light-diurnal and seasonal variations in vertical distribution of the mesopelagic fish Maurolicus muelleri. Marine Ecology Progress Series, 422: 265–273.

Staby, A., Srisomwong, J., and Rosland, R. 2013. Variation in DVM behaviour of juvenile and adult pearlside (Maurolicus muelleri) linked to feeding strategies and related predation risk. Fisheries Oceanography, 22: 90–101.

Standal, D., and Grimaldo, E. 2020. Institutional nuts and bolts for a mesopelagic fishery in Norway. Marine Policy, 119: 104043.

Stanton, T. K., Chu, D., and Wiebe, P. H. 1998. Sound scattering by several zooplankton groups. II. Scattering models. The Journal of the Acoustical Society of America, 103: 236–253.

Stanton, T. K., Chu, D., Jech, J. M., and Irish, J. D. 2010. New broadband methods for resonance classification and high-resolution imagery of fish with swimbladders

using a modified commercial broadband echosounder. ICES Journal of Marine Science, 67: 365–378.

Sundnes, G., and Sand, O. 1975. Studies of a physostome swimbladder by resonance frequency analyses. ICES Journal of Marine Science, 36: 176–182.

Thorvaldsen, K. G., Neuenfeldt, S., Kubilius, R., and Ona, E. 2022a. Towards identifying broadband signatures of the Norwegian shelf's sound scattering layers.

Thorvaldsen, K. G., Neuenfeldt, S., Mariani, P., and Nielsen, J. R. 2022b. Hiding in plain sight: Predator avoidance behaviour of mesopelagic Maurolicus muelleri during foraging.

Thorvaldsen, K. G., Neuenfeldt, S., Mariani, P., Hauss, H., and Nielsen, J. R. 2022c. Deviations from functional predation responses Light and anti-predator behaviour are more important than density in encounters between the mesopelagic fish and its prey.

Tønnesen, P., Oliveira, C., Johnson, M., and Madsen, P. T. 2020. The long-range echo scene of the sperm whale biosonar. Biology Letters, 16: 20200134.

Torgersen, T., and Kaartvedt, S. 2001. In situ swimming behaviour of individual mesopelagic fish studied by split-beam echo target tracking. ICES Journal of Marine Science, 58: 346–354.

Toyokawa, M., Inagaki, T., and Terazaki, M. 1997. Distribution of Aurelia Aurita (Linnaeus, 1758) in Tokyo Bay. *In* Proceedings of the 6th International Conference

on coelenterate Biology, pp. 483–490.

Underwood, M. J., Rosen, S., Engas, A., and Eriksen, E. 2014. Deep vision: An in-trawl stereo camera makes a step forward in monitoring the pelagic community. PLoS ONE.

Visser, A. W., and Kiørboe, T. 2006. Plankton motility patterns and encounter rates. Oecologia, 148: 538–546.

Visser, A. W. 2007. Motility of zooplankton: fitness, foraging and predation. Journal of Plankton Research, 29: 447–461.

Viswanathan, G. M., Afanasyev, V., Buldyrev, S. V., Murphy, E. J., Prince, P. A., and Stanley, H. E. 1996. Lévy flight search patterns of wandering albatrosses. Nature, 381: 413–415.

Voesenek, C. J., Li, G., Muijres, F. T., and van Leeuwen, J. L. 2020. Experimental-numerical method for calculating bending moments in swimming fish shows that fish larvae control undulatory swimming with simple actuation. PLoS Biology, 18.

Volterra, V. 1926. Variazioni e fluttuazioni del numero d'individui in specie animali conviventi. Memoria della regia accademia nazionale del lincei ser.

Warrant, E. J., and Locket, N. A. 2004, August. Vision in the deep sea.

Warren, J. D., Stanton, T. K., Benfield, M. C., Wiebe, P. H., Chu, D., and Sutor, M. 2001. In situ measurements of acoustic target strengths of gas-bearing siphonophores. ICES Journal of Marine Science, 58: 740–749.

Warren, J. D., and Wiebe, P. H. 2008. Accounting for biological and physical sources of acoustic backscatter improves estimates of zooplankton biomass. Canadian Journal of Fisheries and Aquatic Sciences, 65: 1321–1333.

Webb, T. J., vanden Berghe, E., and O'Dor, R. 2010. Biodiversity's big wet secret: The global distribution of marine biological records reveals chronic under-exploration of the deep pelagic ocean. PLoS ONE, 5.

Weidberg, N., DiBacco, C., Pezzola, C., Rebiffe, E., and Basedow, S. 2021. Swimming performance of subarctic Calanus spp. facing downward currents. Marine Ecology Progress Series.

Wilson, C. D., and Boehlert, G. W. 2004. Interaction of ocean currents and resident micronekton at a seamount in the central North Pacific. *In* Journal of Marine Systems, pp. 39–60.

Yen, J., Murphy, D. W., Fan, L., and Webster, D. R. 2015. Sensory-Motor Systems of Copepods involved in their Escape from Suction Feeding. *In* Integrative and Comparative Biology, pp. 121–133.

Youngbluth, M., Sørnes, T., Hosia, A., and Stemmann, L. 2008. Vertical distribution and relative abundance of gelatinous zooplankton, in situ observations near the Mid-Atlantic Ridge. Deep-Sea Research Part II: Topical Studies in Oceanography, 55: 119–125.

Zanette, L. Y., and Clinchy, M. 2019. Ecology of fear. Current Biology, 29: R309–R313.

Zielinski, D. P., Voller, V. R., and Sorensen, P. W. 2018. A physiologically inspired agent-based approach to model upstream passage of invasive fish at a lock-and-dam. Ecological Modelling, 382: 18–32.

7 Appendix paper (I,II and III)

8 Paper I

Towards identifying broadband signatures of the Norwegian shelf's sound scattering layers

Kjetil Gjeitsund Thorvaldsen[1], Stefan Neuenfeldt[1], Rokas Kubilius[2] & Egil Ona[2]

[1]National Institute of Aquatic Resources, Technical University of Denmark, 2800 Kongens Lyngby, Denmark

[2] Institute of Marine Research, P.O. Box 1870 Nordnes, NO-5817 Bergen, Norway

*Corresponding author tel: +4526864697; email: kjgth@aqua.dtu.dk

Keywords

Mesopelagic, Broadband acoustics, siphonophores, density estimation, Target strength

Abstract

Mesopelagic fish might become an important source for protein, oils, and feeds in aquaculture, and play a role in regulating climate. Better knowledge about the composition of the mesopelagic layers is needed. A pre-requisite is efficient acoustic separation of

organism groups for acoustics-based density estimation. Mesopelagic fishes are difficult to distinguish acoustically from physonect siphonophores. This is an important source of bias. We used a lowered acoustic probe equipped with split aperture broadband echosounders and a photo-camera to study the mesopelagic layer at close range. Physonect siphonophores were found to be resonant at frequencies close to 70 kHz, resulting in a *c.* 400% overestimate of mesopelagic fish density for this operating frequency. We could separate three distinct broadband backscatter acoustic signatures, out of which two likely belong to siphonophores, while one likely belongs to mesopelagic fish. This way, we demonstrate that single target acoustic broadband signatures can be used to separate fish from siphonophores, when combined with optical ground truthing.

1 Introduction

With a growing human population, and increasing demand for food, the lightly exploited (Gjøsaeter and Kawaguchi, 1980), but presumed abundant (Lam and Pauly, 2005; Irigoien *et al.*, 2014; Proud *et al.*, 2019) mesopelagic fish have gained increased attention. Mesopelagic organisms usually live at daytime depths of 200 - 1000 meters, and form one or several sound scattering layers (Andreeva *et al.*, 2000). The scatterers are often swim-bladdered fishes (Marshall, 1951). These layers are present in all world oceans (Gjøsaeter and Kawaguchi, 1980; Knutsen *et al.*, 2017).

Even though the diversity of mesopelagic fishes is high, there are usually only a few species dominating local biomass (Gjøsaeter and Kawaguchi, 1980). The most abundant

species in Norwegian waters is Mueller's pearlside *Maurolicus muelleri* (Gmelin 1789). This is a short lived, vertically migrating planktivorous fish with a gas-filled swimbladder(Gjøsæter, 1973, 1981). The pearlside's preferred habitats are continental slopes, sea mounts, and fjords(Okiyama, 1971; Bañon *et al.*, 2016). Pearlside is often found in a distinct layer above the deep sound scattering layer (Giske and Aksnes, 1992). Their vertical distribution depends on ambient light levels (Staby and Aksnes, 2011), ontogeny (Folkvord *et al.*, 2016), and geographical location (Kaartvedt *et al.*, 1998).

Pearlside have recently been targeted by commercial fisheries, because the nutrient composition of mesopelagic layers off the Norwegian coast has shown promise for fish meal production (Alvheim *et al.*, 2020; Grimaldo *et al.*, 2020), and potential for substantial commercial catches (Standal and Grimaldo, 2020). However, there are large knowledge gaps on the different populations of mesopelagic fish, their role in the oceanic food web, and how commercial fishing would impact local populations as well as the carbon cycling process (St.John *et al.*, 2016). The global biomass of mesopelagic fish including pearlside is currently estimated to 11 billion tons, using 38 kHz echosounder data (Irigoien *et al.*, 2014).

However, there are major potential sources of bias when quantifying mesopelagic fish abundance using echosounders (Kloser *et al.*, 2002; Davison *et al.*, 2015). In some regions mesopelagic fishes show swimbladder resonance where the pressure wave is similar to the natural oscillation of the swimbladder, which amplifies the backscatter several times (Simmonds and MacLennan, 2007). Swimbladder resonance can lead to

overestimation when resonance peaks occur at operating frequencies.(Kloser *et al.*, 2002, 2016; Godø *et al.*, 2009; Davison *et al.*, 2015; Proud *et al.*, 2019). However, resonance can also be used in species identification(Simmonds and MacLennan, 2007; Agersted *et al.*, 2021; Khodabandeloo *et al.*, 2021) In some regions an important source of error is the misinterpretation of gelatinous zooplankton as fish. Several types of gelatinous zooplankton are capable of producing strong acoustic backscatter at low echosounder frequencies (Barham, 1963; Toyokawa *et al.*, 1997; Brierley *et al.*, 2001; Mianzan *et al.*, 2001).

Physonect siphonophores are a group of organisms, which have been observed to have similar acoustic backscattering properties as mesopelagic fish, due to a gas filled pneumatophore (Mackie *et al.*, 1988). The siphonophores are predatory, with diets including copepods, crustaceans, and small fishes (Mackie *et al.*, 1988). Siphonophores are often found in the mesopelagic zone (Barham, 1966; Robison *et al.*, 1998; Youngbluth *et al.*, 2008), and they are known to perform diel vertical migrations (Pugh, 1984; Mackie, 1985; Mackie *et al.*, 1988; Mills, 1995; Youngbluth *et al.*, 1996; Robison *et al.*, 1998), and can become very numerous during mass blooms. These blooms have been reported to produce strong sound scattering layers in the water column (Warren *et al.*, 2001; Benfield *et al.*, 2003; Knutsen *et al.*, 2018). However, it has been reported that siphonophore density declines in the open ocean (Kloser *et al.*, 2016). Due to their fragile body structure, siphonophores are shredded trough the meshes of trawls, and hence not well caught by traditional net samples (Hosia and Båmstedt, 2008). Recent mesopelagic fish biomass

estimates have large error bounds, partially due to potential misinterpretation of siphonophores as fish, ranging from 1.8 to 16 billion tons (Proud *et al.*, 2019).

In this study, we recorded mesopelagic layers at close range with an acoustic probe equipped with 4 split aperture broadband echosounders and a photo-camera. We observed mesopelagic layers *in situ*, resolved and tracked their constituents as single acoustic targets, optically identified some of the acoustic scatterers within the layers, and investigated their specific acoustic backscattering properties with broadband and narrowband acoustic pulses. The main objective of this work was to observe co-occurring mesopelagic fish and siphonophores at close range *in situ* to identify characteristic acoustic backscattering signatures that would enable the separation of these two animal groups in acoustic data.

2 Material and methods

2.1 Sampling region

Data were collected with the research vessel G.O. Sars from 19th of November to the 4th of December 2017. Mesopelagic sound scattering layers, herring schools and blue whiting layers were observed with different acoustic observation platforms. Mesopelagic layers were investigated at the edge of Vøringplatået (Figure 1). Photo images taken *in situ* by the acoustically and optically equipped probe ('TS-Probe' onwards), were collected from all the TS-probe deployment stations (3 in total). One of these sample sites (Figure 1, blue dot) was chosen for further in-depth investigation of the acoustic targets with narrow- and

broadband echosounders (two consecutive profiles in the same water column performed in narrowband mode and broadband mode respectively)(Table 1). To investigate how representative one TS-probe deployment station is for a horizontally layered system, the acoustic backscattering recorded by the ship-mounted echosounders was studied for about 25 nautical miles of sailed distance (Figure 1, green line) on each side of the selected TS-probe deployment station.

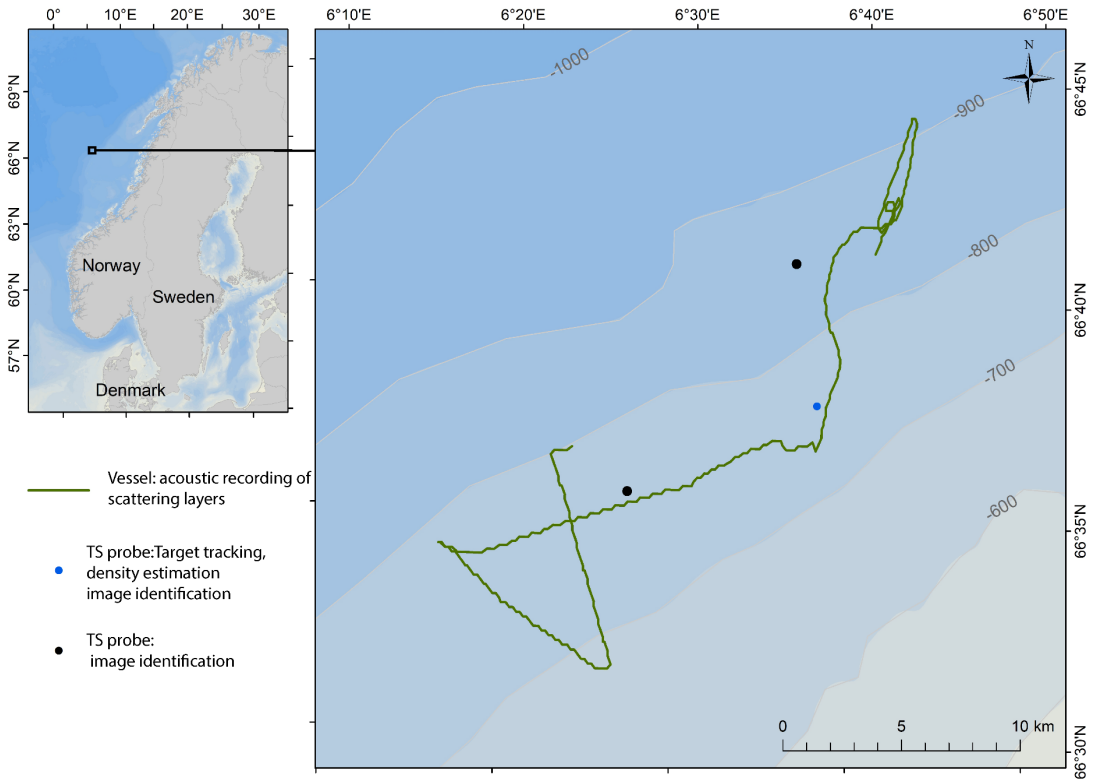

Figure 1. Map of the geographic area with marked 50 nmi long ship track for backscattering inspection, TS-probe deployment stations sites.

2.2 TS-Probe description

The TS-Probe was developed by IMR (Institute of Marine Research, Bergen, Norway) to resolve single acoustic targets at close range at depths less than 1500 m (Ona and Pedersen, 2006). The probe is composed of three elements: an outer protective metal frame, a movable motorized transducer platform and a water-tight cylinder (500 mm diameter, 1400 mm tall) containing the power supplies, broadband transceivers (Simrad EK80), camera interface, and other sensors, communicating to the surface vessel via fibre optical cable. The TS-probe was used to perform vertical profiles of the water column (Table 1), while the vessel position was maintained using dynamic positioning. Both acoustic volume backscattering (S_V, dB re 1 m^{-1}) and acoustic target strength (TS, dB re 1 m^2), were extracted by use of the acoustic post-processing software LSSS version 2.7.0 (Korneliussen *et al.*, 2016). Real time observations of echograms, depth, and pressure as well as photographs were available at surface via a steel reinforced fibre electric cable, which was used to deploy the probe from the vessel. The TS-probe's pressure sensor (Scansense AS, PS30) was used to record the probe depth as it was moved in the water column.

During the TS-probe deployment station on November 29th, the 38 (35-45), 70 (55-90), and 200 (160-260) kHz transducers were mounted to project sideways, while the 120 kHz transducer was mounted to project downwards to track height above the bottom.

Echosounder calibrations took place one-week prior to the acoustic data collection. Both the ship and TS-probe mounted echosounders were calibrated using standard methods and a spherical target (Demer *et al.*, 2015; Ona *et al.*, 2020). A 57.2 mm diameter tungsten carbide calibration sphere with 6 % cobalt binder was used as the reference target. The echosounders were calibrated and acoustic data collected with two pulse forms, the narrowband (continuous wave, 'CW') and broadband (frequency modulated, 'FM') (Table 2). The tapering of the linear up-sweep frequency modulated pulses (Table 2) was chosen and set in the acoustic data collection software (Simrad EK80 version 1.11.1.0). Taper indicates the proportion of the pulse duration (in percent) over which the transmit amplitude went from zero to maximum and maximum to zero at the beginning and end of the acoustic pulse, respectively. The 'linear up-sweep' conveys the linear progression in acoustic frequency change from lower to higher within the given bandwidth of the frequency modulated acoustic pulse.

Table 1. Deployments of the TS-Probe.

Operation	Target tracking/TS(f) measurements	Density estimation narrowband
Location (longitude/latitude)	N 66.613/E 6.59	N 66.613/E 6.59
Date	29.11.2017	29.11.2017
Time (UTC)	14:06	12:38

Depth (m)	0-550	0-550
Frequencies used (kHz)	35-45, 55-90 and 160-260	38, 70, 120 and 200
Ping rate (Hz)	2	2
Ground truthing	Photo camera	Photo camera
Deployment	Profiling wat er column at 0.3 (m s^{-1})	Profiling water column at 0.5 (m s^{-1})
Range from transducer used in post-processing (m)	7-20	10-30
Beam projection direction	Lateral	Lateral (120 kHz dorsal)

Table 2. Echosounder settings and calibration results for Simrad EK80 system installed on the vessel and the TS-probe. CW - means narrowband and FM refers to broadband.

Simrad EK80 vessel, CW pulses						
Transducer type	ES18	ES38-7	ES70-7C	ES120-7C	ES200-7CD	ES333-7C
Frequency (kHz)	18	38	70	120	200	333
Power (W)	2000	2000	600	200	105	40

Gain (dB)	22.01	26.8	28.02	26.89	26.95	26.1
Equivalent beam angle (dB)	-17.0	-20.7	-20.7	-20.7	-20.7	-20.7
Taper (%)	25.7	10.28	2.79	1.63	0.98	0.77
Absorption coefficient (dB km^{-1})	0.0025	0.009	0.022	0.036	0.051	0.77
Pulse duration (ms)	1.024	1.024	1.024	1.024	1.024	1.024
Half power beam widths (along/athwart ship) (deg)	10.29/10.3 6	6.51/6.48	6.94/6.92	6.35/6.27	6.39/6.15	5.04/5.52
Transducer angle sensitivity (deg) (along ship and athwart ship)	15.5	18	23.0	23.0	23.0	23.0
Sound speed (measured) (m s^{-1})	1472	1472	1472	1472	1472	1472

Simrad EK80 TS-Probe, CW pulses

Transducer type	ES38D	ES38-18DK	ES70-7CD	ES120-7CD	ES200-7CD
Frequency (kHz)	38	38	70	120	200
Power (W)	400	100	500	400	150
Gain (dB)	25.27	19.17	26.98	27.1	26.66
Equivalent beam angle (dB)	-20.7	-12.5	-20.7	-20.7	-20.7
Taper (%)	25.7	10.28	2.79	1.63	0.98
Absorption coefficient (dB km^{-1})	9.36	9.36	21.87	36.10	51.14
Pulse duration (ms)	1.024	1.024	1.024	1.024	1.024
Half power beam widths (along/athwart ship) (deg)	7.06/7.04	17.02/17.11	7.26/7.11	6.91/6.76	6.64/6.1
Transducer angle sensitivity (deg) (along ship and athwart ship)	23.0	10.0	23.0	23.0	23.0
Sound speed (measured) (m s^{-1})	1479	1479	1479	1479	1479

Simrad EK80 TS-Probe, FM pulses					
Transducer type	-	ES38-18DK	ES70-7CD	ES120-7CD	ES200-7CD
Power (W)		100	500	400	120
Frequency (kHz)	-	35-45	55-90	90-170	160-260
Taper (%)	-	5.58	2.17	1.08	0.61
Pulse duration (ms)		2.048	2.048	2.048	2.048

2.3 Analysis of photographs

For visual target identification, the camera system consisting of two 12.1 Mpx Imenco SDS 1210 underwater photo cameras, mounted laterally in the opposite direction of the transducers (Kubilius *et al.*, 2015), was used to take images of the water column during both probe descent and ascent phases. No constant light was used but a photo camera flash that was triggered by a manual remote controller, between 7 and 14 times per minute depending on TS-probe deployment station. Photographs from all TS-probe deployment stations were used to identify the vertical distributions and potential overlap of mesopelagic fish and siphonophores from the surface down to 800 meters. Only photos with targets in sufficient focus for identification were analysed. Afterwards, a specialist in siphonophore taxonomy identified specimens to closest family: Dr Aino Hosia, Department of Natural History, University of Bergen, Norway. The camera was not used to size objects.

2.4 Deployment of the TS-Probe and ground truthing

Multi frequency acoustic target identification methods and photo camera data were used to identify parts of the scattering layers. Both narrowband and broadband echograms were processed to identify different types of acoustic target classes by using previous work on zooplankton, micro nekton, and the local mesopelagic fishes(Martin *et al.*, 1996; Lavery *et al.*, 2007; Scoulding *et al.*, 2015). The imagery and acoustic frequency responses of the single targets that had been accepted by the target tracking algorithm were used to identify some of the components of the scattering layers that TS-Probe descended or ascended through. The scattering from 7 to 30 meters (7-20 for target tracking, 10-30 m for biomass estimation) lateral range from the probe was chosen for detailed interpretation and target density estimation. This choice was motivated by the acoustic signal to noise ratio, resolution, target tracking capability, and transducer near field considerations(Medwin and Clay, 1998).

2.5 Tracking single targets in broadband acoustic data to obtain TS(f) signatures

Individual targets recorded by the vertically profiling probe were tracked using the TS-probe's echosounder split aperture functionality, and broadband backscatter data was extracted for analysis. The goal was to isolate acoustic target strength as function of frequency (TS(f)) signatures over the operating bandwidth of the broadband system . The set range for target tracking was between 7-20 meters from the laterally projecting

transducer. Tracks were automatically detected and created, using the single echo detection algorithm, as implemented in target tracking module of the LSSS acoustic data post processing software (Handegard *et al.*, 2005; Handegard, 2007; Korneliussen *et al.*, 2016) (SED filters for broad band see table 3). The minimum TS was set to -80 dB, and the maximum to –45 dB (these refer echo amplitude after pulse compression). Maximum one-way gain compensation was set to 6 dB (Table 3). The track association settings were set with α_G = 2.8 (deg), β_G = 2.8 (deg), r_G = 0.44 (m), I_G = 20 (dB), and track initiation settings of α_0 = 2.8(deg), β_0 = 2.8 (deg), r_0 = 0.44 (m), I_0 = 20 (dB). The α and β represent the maximum accepted along-ship and athwart-ship angle values within the acoustic beam for each subsequent acoustic target detection within a track (αG, βG), or for accepting a new target detection as first detection of a new track close to the end of a previously terminated track (α0, β0). The parameter *r* is range, and r_G is the maximum deviation in range from the transducer, between the subsequent detections within a track. Similarly, the parameter r_0 is the maximum deviation in range between the last detection in a terminated track and the first detection in a newly initiated track. I_G is the maximum deviation in TS between the subsequent detections within the track, while I_0, similarly, is the maximum difference in TS between the last target detection within a terminated track, and the first target detection in a newly initiated track. The minimum track length was set to eight detections. For detailed target tracking algorithm description, see Handegard (2007). The tracking settings had to be adjusted and evaluated in trials on the recorded material and conditions. The maximum number of missing detections within the track were set to 8, the number of missing samples were set to 8, and the ratio of missing detections to the total number of

detections in a track (track 'length') were set to 0.8. In some cases, tracking targets of interest was only possible at the mid frequencies (55-90 kHz), due to poor signal to noise ratio at the low frequencies channel (35-45 kHz) or difficulties to separate tracks allocated to smaller targets like zooplankton at 160-260 kHz. Each track was also manually interpreted before further post processing. TS values were exported as a function of the acoustic frequency within the three available acoustic bands at 0.1 kHz increments. TS was averaged for each 0.1 kHz increment in the linear domain, before conversion to dB. Resolved tracks relevant for mesopelagic fish were manually counted from 7 to 20 meters away from the TS-probe.

Table 3. Single echo detection (SED) filters applied for single target measurements with narrowband (38, and 70 kHz) and broadband (35-45, 45-90, and 160-260 kHz) pulses.

SED-Filters for target tracking using broadband pulses	
Min TS (dB)	-80
Pulse length determination level (dB)	6
Max one-way gain compensation (dB)	6
SED-Filters for TS-measurements using narrowband pulses	
Min TS (dB)	-70
Pulse length determination level (dB)	6
Min echo length	0.8 (Relative to pulse duration)

Max echo length	1.8 (Relative to pulse duration)
Max one-way gain compensation (dB)	3
Do phase deviation check	yes
Max phase deviation (phase steps)	8

2.6 Target density estimation at 38 and 70 kHz

During the probe deployment, echo-integration derived density estimates over the water column were performed. For the acoustic echo integrator data recorded by the TS-probe, the TS of the targets were measured directly within the scattering layers with depth bins of 100 meters tall as probe descend or ascend in water column (Table 3). Targets with TS above -50 dB were assumed not to be mesopelagic fish and were manually removed from the TS measurements data. TS were converted to acoustic backscattering cross-section (σ_{bs}), and averaged for each 100-meter depth cell of the TS-probe profile. TS-probe echo integration values were converted from the Nautical Area Scattering Coefficient ($s_{A,}$ or NASC) to area density (ρ_a):

$$\rho_a = \frac{s_A}{\sigma_{bs}} \qquad (1)$$

Area density was converted to volume density per cubic meter (ρ_v) by using the following equation where Δz is the 10-meter depth cell (Simmonds & MacLennan (2007)):

$$\rho_v = \frac{\rho_a}{((1852^2)\cdot\Delta z)} \qquad (2)$$

3 Results

Two sound scattering layers were observed in the area, namely, one Deep Scattering Layer (DSL) between 300 and 500 meters depth and one Shallow Scattering Layer (SSL) at about 150 meters depth (Figure 2a,b). There were clear circadian patterns of both scattering layers (Figure 2a). The shallow scattering layer at 150 meters became dense during the very short daylight hours, before migrating from 150 to 75 meters for ~ 3,5 hours during dusk , then migrating back to 150 meters. Approximately 1/5 of the backscatter from the DSL migrated to join the upper scattering layer. However, a large proportion of the DSL was stationary (Figure 2a). There was a zooplankton layer in the upper 200 meters clearly visible at 200 kHz. The TS-probe was deployed during the period where the SSL was located between 50 and 100 meters, hence also monitoring the migrating fraction of the DSL .

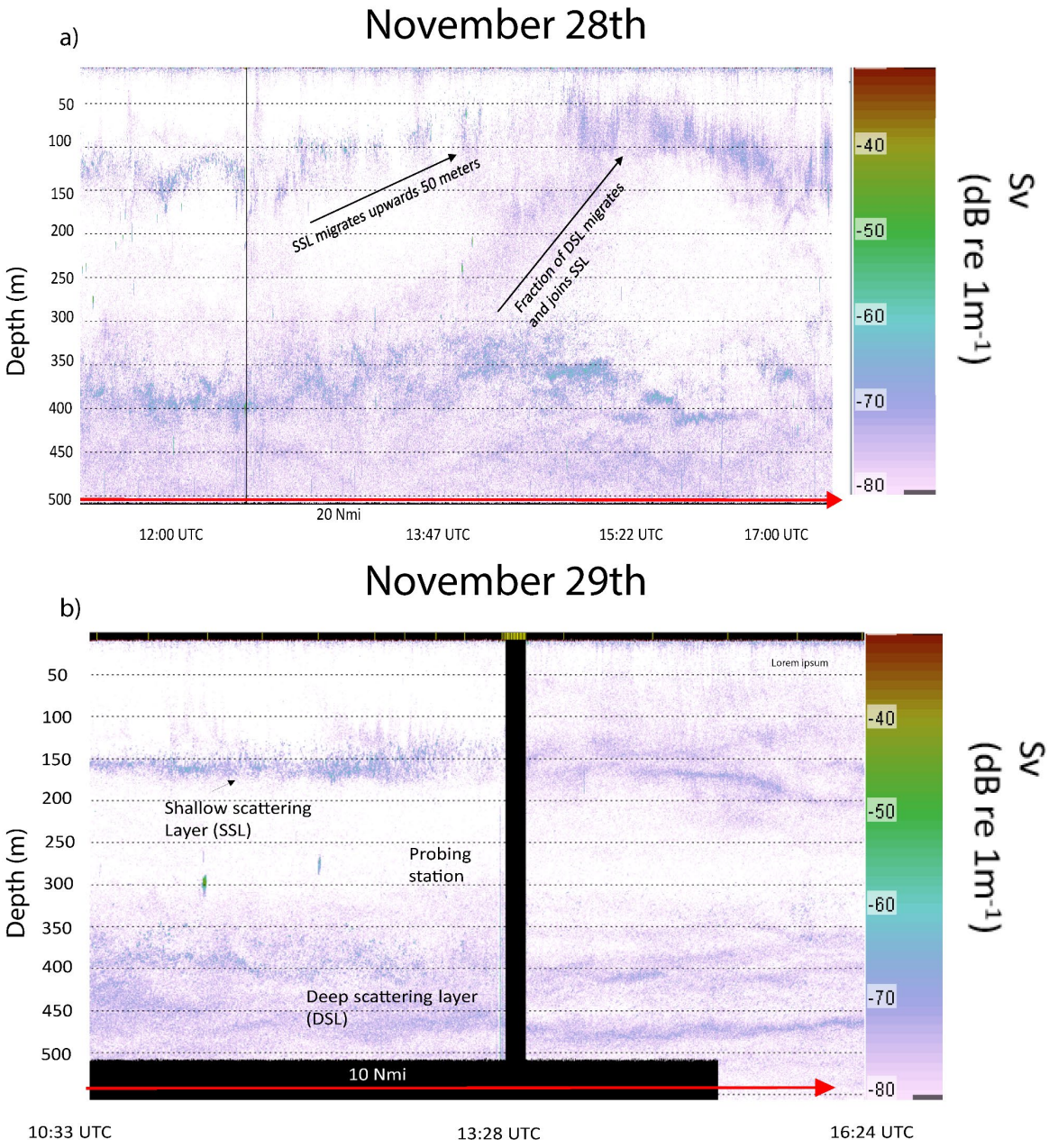

Figure 2. (a) Echogram recorded by the ship mounted 70 kHz echosounder (1.024ms narrowband pulses) on the day prior to TS-probe deployment, evening time around dusk is shown. (b) Echogram recorded by the ship mounted 70 kHz echosounder (1.024 ms narrowband pulses). It shows ~ 10 nmi (2 h) of sailing

distance prior and posterior to the TS-Probe deployment station (profiling duration 2 h). There are two prominent layers, one layer at approximately 150 meters depth and a thicker layer between 300-500 meters.

3.1 Acoustic and optical data analysis

The photo image data contained mostly sightings of siphonophores. Mesopelagic fish were seen only twice in sufficient resolution for identification (at about 450 meters depth), while siphonophores were observed at all TS-probe deployment stations (Table 4). The pooled camera images over 3 days showed that siphonophores were present in both scattering layers as well as throughout the water column. Their total number was highest below the first scattering layer. Still, absolute density was low and the average probability of taking a siphonophore picture was 0.01 (11 siphonophores in 1000 pictures taken). However, there were 3 consecutive images of siphonophores in the upper layer (at about 75 meters depth) during the migrant period at November 29th , indicating that they were a significant component of this particular layer, because assuming Poisson distribution over the whole water column, this event would have had a probability <0.000001.

The vertical profile data at 35-45 kHz and 55-90 kHz showed two main layers, one between 20-200 meters and a deep scattering layer between 400-500 meters. The upper scattering layer contained a mix of several types of scatterers. Weak acoustic targets detected only at 160-260kHz frequency band, strong targets at 55-90 kHz (>-65 dB) and some strong echo fish-like targets (->60 dB) at 35-45 kHz that are excepted to be pearlside,

based on previous work on pearlside in fjords and oceanic areas in these latitudes (Rasmussen and Giske, 1994; Kristoffersen and Salvanes, 1998).

There were strong scatterers (>-60 dB) observed at 20-200m depth in the mid frequency band data (55-90 kHz). These targets stood out and were especially dense at about 75 meters depth (Figure 3a, b). The relatively strong TS at -60 dB or higher is at least one order of magnitude stronger backscatter than one expected for krill or copepods; a clear resonance peak was also evident indicating a possible presence of a gas inclusion (Figure 3d). The only micro-nekton group identified in this layer were siphonophores with 3 consecutive observations at about 75 meters depth (Figure 3c). The deep scattering layers were dominated by targets that have strongest backscatter at the low frequencies (34-45kHz), co-occuring with some weaker targets.

Table 4. Observations of siphonophores by photo camera. Pooled counts of observations for all four TS-probe deployments

Depth (m)	Number of observations
0-100	4
100-200	2
200-300	5
300-400	1
400-500	5

500-600	1
600-700	0
700-800	4

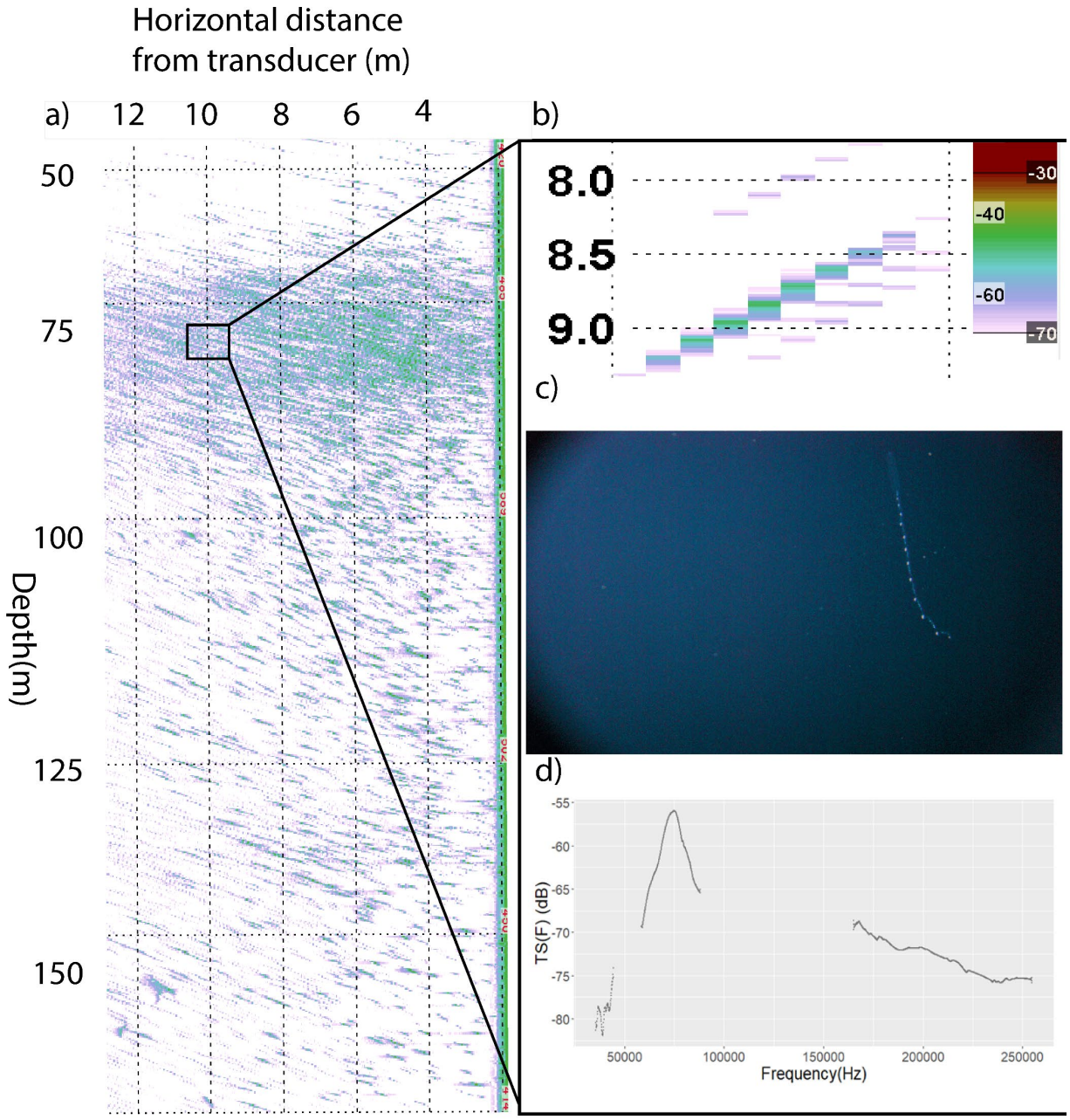

Figure 3. (a) The epipelagic layer observed by the TS-probe laterally projecting echosounder (55-90 kHz) that is descending at a constant speed from the surface to 500 meters depth. The vertical axis is water depth while the horizontal axis is the lateral distance from the transducer. The echogram (a) shows targets

between 50-200 m depth where backscatter is especially strong at about 75 meters depth. (b) one single track of a target resonant close to 70 kHz. (c) is one of the three consecutive images taken of the siphonophore *Nanomia Cara* by the TS-probe mounted photo camera within the layer at 75 meters depth. (d) is the extracted TS(f) of one representative track from this layer. Such TS(f) pattern was dominating in this layer.

3.2 Acoustic backscatter signatures

Three types of TS(f)-signatures were common among the individually tracked targets: Signature 1 showed resonance close to 70 kHz (Figure 4a), Signature 2 was within the geometric scattering region (Figure 4b), and Signature 3 displayed TS(f) ascending at 35-45 kHz and descending from 55-90 kHz (Figure 4c). Signature 1 displayed a comparatively low TS of -70 to -85 dB at 35-45 kHz, while at the mid range frequencies (55-90 kHz), the TS peaked between -55 to -65 dB. Signature 2) appeared to be within the geometric scattering region (Figure 4b). It displayed, with some variation, declining TS(f) for all frequency bands from -55 dB at 34-45 kHz to -80 dB at 260 kHz. Some of the targets had a 3-7 dB local increase in TS(f) close 50-55 kHz, but did not show signs of resonance (a relatively narrow, localised peak in TS(f)). Other targets displayed sudden drops at 60-70 kHz where TS(f) changed from –57 to –75 dB at some specific acoustic frequencies. Signature 3) increased in TS(f) and appeared to have a peak that falls between the two operational frequency bands, 34-45 and 55-90 kHz.

Signature 1) was the most common signature, and co-occuring with optical identification of siphonophores in the epipelagic layer recorded during dusk. Signature 3)

are very similar to signature 1) and could also belong to siphonophores, signature 2) was allocated to mesopelagic fish, with the gas-filled swimbladder resonance frequency lower than the applied echosounder frequencies in this study.

Signature 1) dominated the layer in the upper 200 m with 119 tracks, where signature 2) and 3) had 33 and 18 tracks, respectively. Between the scattering layers (200 - 400 meters) signature 3) was most numerous with 38 observations compared to signature 1 (26) and 2 (14). In the deep scattering layer at 400-500 m, signature 2) was most numerous (15 tracks), with 8 tracks for signature 1), and 2 tracks for signature 3).

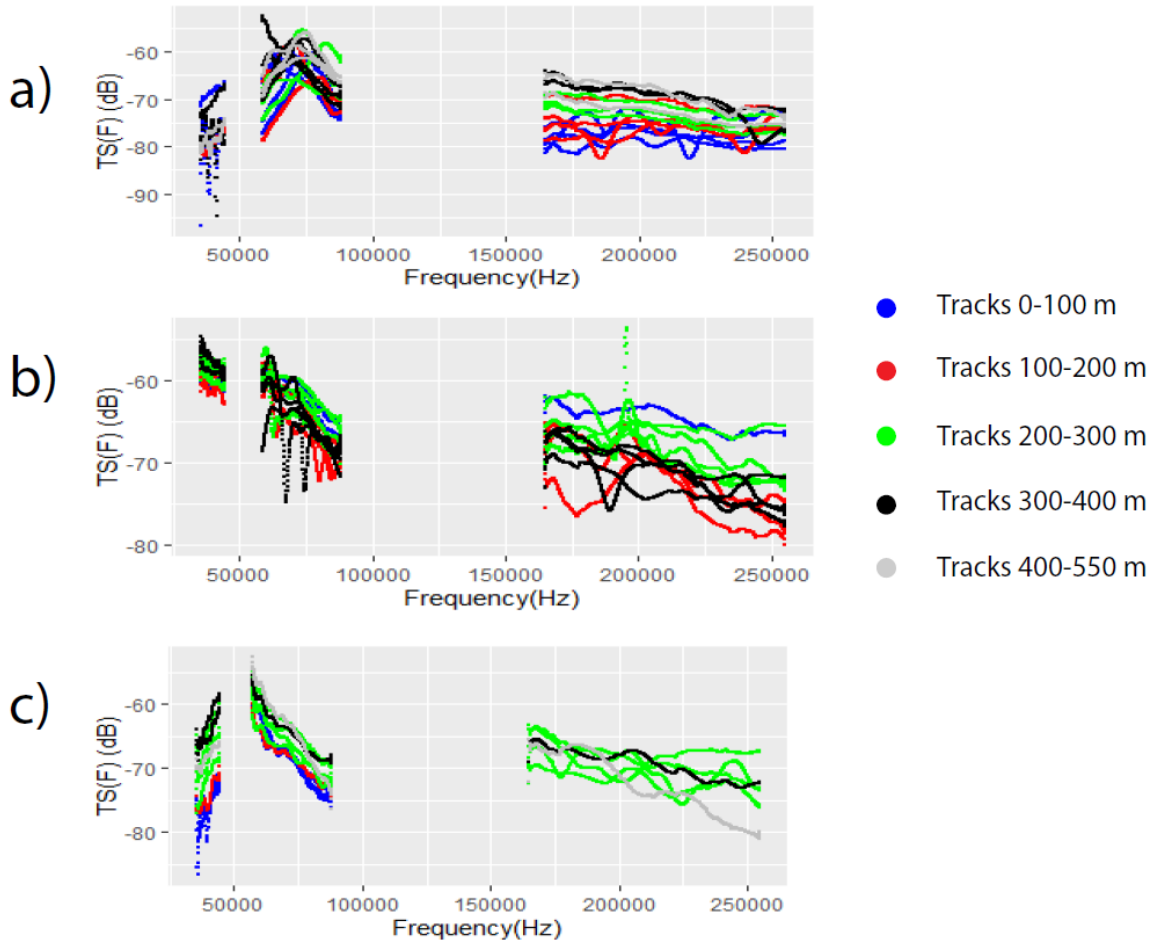

Figure 4. Indivudually tracked target broadband acoustic target strength spectrum TS(f) examples (~20 targets for each signature), extracted from the acoustic data of one vertical water volume profile by the TS-Probe. TS (dB) is plotted against the acoustic frequency for 35-45 kHz, 55-90 kHz, and 160-260 kHz bands. Each line represents the mean TS(f) for one individually tracked target. Each color represents a 100 meter depth cell. (a), (b), and (c) show signatures 1, 2, and 3, respectively (see text for signature description).

3.3 Acoustic target density estimates narrowband

Acoustic target density estimates were derived from narrowband data of 38 kHz and 70 kHz (TS-Probe, laterally sideways oriented, see Table 5 for target strength measurements, and table 1 and 3 for details).

Narrowband-derived volume density of targets/m^3 were several orders of magnitude higher at 70 kHz, compared to 38 kHz in the shallow layer peaking at 75 m depth (0.06/m^3 70 kHz and 0.0004/mat 38 kHz) (Figure 5a). Averaging over the whole water column, density estimates were 4.07 times higher for the 70 kHz frequency with average target densities of 0.0169/^{3} for 70 kHz and 0.004/m^3 for 38 kHz (Fig. 5a). Removing signatures 1) and 3) observed from the broadband data some tracks will disappear completely at 38 kHz, but remain visible at 70 kHz and might hence be wrongly interpreted as mesopelagic fish in the narrowband data, if 70 kHz were the only frequency used (exemplified in Fig. 5b to 5e).

Table 5. A summary of TS measurements obtained with 38 and 70 kHz narrowband pulses by the laterally sideways observing TS-Probe transducers.

Depth (m)	Mean (dB)	Median (dB)	Max (dB)	Min (dB)	Q25 (dB)	Q75 (dB)	N
38 kHz							

0-100	-58.6	-60.0	-53.37	-64.8	-61.7	-57	28
100-200	-61.4	-64.1	-52.2	-69.8	-67.7	-61.6	69
200-300	-59.4	-60.2	-52.3	-69.9	-64.3	--57.3	64
300-400	-59.3	-60.7	-51.7	-69.9	-65.4	-57.8	137
400-500	-54.8	-55.2	-50.5	-69.8	-56.0	-54.3	610
500-550	-53.8	-54.3	-50.0	-69.7	-54.9	-53.5	279
			70 kHz				
0-100	-60.5	-64.0	-57.4	-65.9	-64.095	-59.355	767
100-200	-63.0	-65.0	-58.0	-69.7	-68.0	-61.7	36
200-300	-64.0	-66.4	-58.1	-69.5	-67.5	-63.5	16
300-400	-62.2	-65.0	-53.5	-70.0	-66.6	-63.4	22

400-500	-62.5	-65.0	-52.6	-70.0	-67.5	-62.4	345
500-550	-61.8	-63.8	-55.7	-69.9	-67.0	-59.1	283

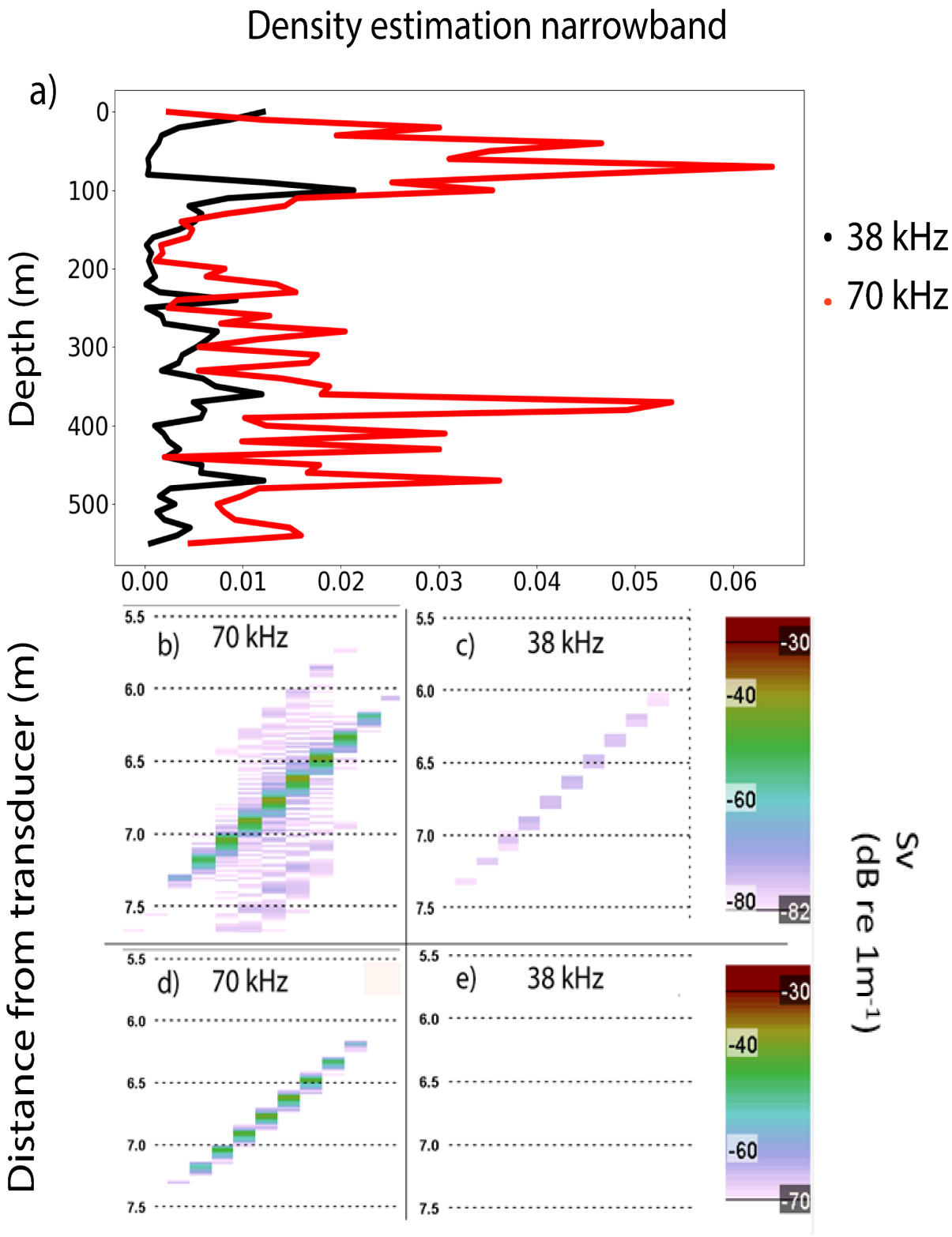
Density estimation narrowband
a)
Depth (m)
0
100
200
300
400
500
0.00
0.01
0.02
0.03
0.04
0.05
0.06
• 38 kHz
• 70 kHz
Distance from transducer (m)
b) 70 kHz
c) 38 kHz
d) 70 kHz
e) 38 kHz
5.5
6.0
6.5
7.0
7.5
-30
-40
-60
-80
-82
-70
Sv
(dB re 1m-1)

Figure 5. A) Target density estimates obtained using the TS-probe. 38 kHz (black curve) and 70 kHz were compared. The measured density was 4 times higher using the 70 kHz transducer. B, c , d ,e Track at 38 (c, e) and 70 kHz (b, d) (narrowband pulses) that we interpret to be a siphonophore. (b) and (c) show the single target at 38 and 70 kHz, respectively, with the lower amplitude threshold value of –82 dB. These settings are commonly applied during conventional acoustic surveys in Norway to remove zooplankton backscattering from the sample. (d) and (e) show the same track at a higher threshold of -70 dB commonly applied to remove separate fish-backscatter from plankton-backscatter.

4 Discussion

4.1 Inspecting different acoustic signatures

This study provided a promising methodology to separate swim-bladdered mesopelagic fish from physonect siphonophores in acoustic backscatter data. The key feature is to resolve single acoustic targets *in situ* and to further investigate optically, and to utilize broadband acoustic backscatter features for target classification. This way, a well-known potential bias in acoustics-based methods for estimating mesopelagic fish abundance can be resolved or at least mitigated.

In our case study situation, the bias in density estimates for swim-bladdered mesopelagic fish were up to +400%, if gas-bearing gelatinous zooplankton is erroneously included at the mid frequency band of 55-90 kHz. With a future library of acoustic broadband backscatter “signatures” from different optically identified species of mesopelagic fish and

physonect siphonophores, mesopelagic fishes could be identified using exclusively acoustics.

The decomposition of the deep scattering layer into exploitable and unexploitable species is a key challenge for estimating the size of this very important protein and oil resource. Pearlsides, lanternfish (Gjøsaeter and Kawaguchi, 1980; Scoulding *et al.*, 2015), and in some cases siphonophores (Knutsen *et al.*, 2018) are the most abundant acoustic targets in the mesopelagic layers, at least in our area of investigation. Combining photo camera images, observed individual target acoustic backscatter tracks, together with knowledge on scattering properties of pearlside and lanternfish, the signature 1) (Figure 4a) likely represented siphonophores, while signature 2) (Figure 4b) likely belonged to swim bladdered (gas-filled) mesopelagic fish with similar detailed acoustic backscatter features as reported by (Khodabandeloo *et al.*, 2021). This signature 2) was detected 33 times in the upper migratory layer, hence might belong to crepuscular feeding mesopelagic fishes.

There is greater uncertainty about which organism was represented by signature 3) (Figure 4 c), which had no visible acoustic backscatter resonance peak within used acoustic bandwidth. However, there is a possibility for a resonance peak between 45 and 55 kHz. This signature shares similarities with signature 1) and could belong to the siphonophore group. While the narrowband TS of pearlside is measured and currently well-described(Torgersen and Kaartvedt, 2001; Scoulding *et al.*, 2015; Sobradillo *et al.*, 2019), reports on siphonophore *Nanomia cara* acoustic backscatter are few and variable (Warren *et al.*, 2001; Lavery *et al.*, 2007; Knutsen *et al.*, 2018), but generally with lower acoustic

resonance frequency than the two mesopelagic fish species relevant in our investigation area (*M. muelleri (~60 kHz, or lower), and B. glaciale (~50 kHz, or lower*)(Scoulding *et al.*, 2015; Sobradillo *et al.*, 2019).

The numerical dominance of signature 1) among the tracks in the broadband data, co-occurring with images from the photo camera, implies that signature 1) does represent siphonophores. 3 siphonophores were observed in this 75 m layer in rapid succession, despite the observed probability for 11 sightings per 1000 images, we consider this as strongly implying that siphonophores were significant contributors to this scattering layer. In our study, mesopelagic fish were not at all observed by the photo camera system in this layer, likely due to gear avoidance. Furthermore, several of the acoustically observed individual target tracks were present at range coinciding with the effective observation range of the camera, which is why we conclude that signature 1) did not represent mesopelagic fish.

4.2 Ground truthing challenges

Without trawl samples, the knowledge on the species of fish in these scattering layers was based on previous work in similar geographical areas (Gjøsaeter and Kawaguchi, 1980; Kristoffersen and Salvanes, 1998, 2009), as well as two observations of glacier lanternfish in the photo camera data at ~400 m water depth.

Conventional surveys for measuring mesopelagic fish density occur both during day and night. The probing, however, was performed during the crepuscular period. This would have implications on the biomass estimates, because migrants from deeper layers were

probably mixed in the different, more shallow scattering layers. This complicates the process of allocating signature 2 to a specific mesopelagic fish. However, siphonophores were observed frequently in this 75-meter layer (3 observations in quick succession), and signature 1 was by far the most abundant signature numerically in this layer.

Siphonophores and mesopelagic fishes most probably co-occurred both during daytime and at night as siphonophores were observed in the pooled photo camera data at every 100 meter depth bin except for 600-700 m depth. Both siphonophores and fishes migrate vertically during the day, however, the measured DVM in this region was fairly limited. This could be excepted due to high latitude and the low ambient light levels during winter, especially in the deep scattering layer. Siphonophores were observed in all parts of the water column with the highest pooled numbers between 200-300 meters. However, the most observations in short succession were at about 75 meters depth, suggesting that siphonophores also migrate to this layer and are co-occuring with mesopelagic fish, potentially feeding on the same zooplankton.

Though if not present in the photo sampling, we argue that pearlside are present in the shallow scattering layer, based on previous work in fjords and off-shore, representing areas similar to our study area (Rasmussen and Giske, 1994; Kristoffersen and Salvanes, 1998; Godø *et al.*, 2009). Mesopelagic fish have been observed to avoid trawls (Kaartvedt *et al.*, 2012), vessels using dynamic positioning (Penã and Ratilal, 2019). They also avoid the TS-probes up to 10 meters, but not between 10 and 50 meters (Dias Bernardes *et al.*, 2020). The ground- truthing process of this study is highly dependent on the photo camera,

and mesopelagic fish density is hence most likely higher than observed with the camera. Combined with the generally very low densities of fish (Figure 5 A), the probability to take a photo of a mesopelagic fish is further reduced. For future investigations, ground-truthing these layers more precisely would require a camera with longer penetration range in water.

4.3 implications on density estimations

Combining acoustics and video techniques, a possibly important bias in traditional acoustics-based methods for measuring mesopelagic fish density can be resolved. We report a 400% difference between the 38 kHz and 70 kHz probe narrowband data-derived density estimates. Traditionally 18 and 38 kHz are the applied frequencies to measure mesopelagic fish, largely due to the high effective penetration range needed for ship-mounted echosounders. However, basing fish density estimates solely on 18 or 38 kHz acoustic measurements is currently discussed controversially, because of challenges associated with acoustic resonance of gas-filled swimbladder or zooplankton body inclusions (Davison *et al.*, 2015; Proud *et al.*, 2019) . Introducing 70 kHz, especially on lowered devices, would include some previously excluded mesopelagic targets (Agersted *et al.*, 2021). Yet, applying 70 kHz narrowband echosounder as the only solution would produce new challenges as we report here (Figure 5 b-e).

Even with several potential error sources and difficulties in the ground-truthing process, combining lowered acoustic devices like the TS-probe and optics provide a framework for solving some of the difficult questions regarding monitoring the increasingly important mesopelagic micro-nekton communities. A promising solution is to

use multifrequency (Greenlaw and Johnson, 1983; Lavery *et al.*, 2007), or even better, broadband acoustics to resolve, group, and quantify targets of interest at close range (such as on probes) and couple this with improved optic tools for ground-truthing.

Acknowledgements

The survey was supported by the Norwegian Research Council via CRISP project (203477, CRISP—Centre of Research-based Innovation in Sustainable fish capture and Processing technology), and we thank the crew of G.O Sars for the help in data collection, and Ronald Pedersen for making sure the TS-probe was working smoothly. The production of the manuscript was funded by the H2020 PANDORA project grant agreement No. 773713, and by the project H2020-MEESO ("Ecologically and economically sustainable mesopelagic fisheries" grant agreement No. 817669, and contributes to the working package 2 of MEESO "survey and sampling technology development").

Data availability

The data in this article will be shared on request to the corresponding author.

References:

Agersted, M. D., Khodabandeloo, B., Liu, Y., Melle, W., and Klevjer, T. A. 2021. Application of an unsupervised clustering algorithm on in situ broadband acoustic data to identify different mesopelagic target types. ICES Journal of Marine Science, 78: 2907–2921.

Alvheim, A. R., Kjellevold, M., Strand, E., Sanden, M., and Wiech, M. 2020. Mesopelagic species and their potential contribution to food and feed security—a case study from Norway. Foods, 9: 344.

Andreeva, I. B., Galybin, N. N., and Tarasov, L. L. 2000. Vertical structure of the acoustic characteristics of deep scattering layers in the ocean. Acoustical Physics, 46: 505–510.

Bañon, R., Arronte, J. C., Rodriguez-Cabello, C., Piñeiro, C. G., Punzon, A., and Serrano, A. 2016. Commented checklist of marine fishes from the Galicia Bank seamount (NW Spain). Zootaxa, 4067: 293–333.

Barham, E. G. 1963. Siphonophores and the deep scattering layer. Science, 140: 826–828.

Barham, E. G. 1966. Deep scattering layer migration and composition: Observations from a diving saucer. Science, 151: 1399–1403.

Benfield, M. C., Lavery, A. C., Wiebe, P. H., Greene, C. H., Stanton, T. K., and Copley, N. J. 2003.

Distributions of physonect siphonulae in the Gulf of Maine and their potential as important sources of acoustic scattering. Canadian Journal of Fisheries and Aquatic Sciences, 60: 759–772.

Brierley, A. S., Axelsen, B. E., Buecher, E., Sparks, C. A. J., Boyer, H., and Gibbons, M. J. 2001. Acoustic observations of jellyfish in the Namibian Benguela. Marine Ecology Progress Series, 210: 55–66.

Davison, P. C., Koslow, J. A., and Kloser, R. J. 2015. Acoustic biomass estimation of mesopelagic fish: Backscattering from individuals, populations, and communities. ICES Journal of Marine Science, 72: 1413–1424.

Demer, D. A., Berger, L., Bernasconi, M., Bethke, E., Boswell, K., Chu, D., and Domokos, R. 2015. Calibration of acoustic instruments. ICES CRR: 133.

Dias Bernardes, I., Ona, E., and Gjøsæter, H. 2020. Study of the Arctic mesopelagic layer with vessel and profiling multifrequency acoustics. Progress in Oceanography, 182: 102260.

Folkvord, A., Gundersen, G., Albretsen, J., Asplin, L., Kaartvedt, S., and Giske, J. 2016. Impact of hatch date on early life growth and survival of Mueller's pearlside (Maurolicus muelleri) larvae and life-history consequences. Canadian Journal of Fisheries and Aquatic Sciences, 73: 163–176.

Giske, J., and Aksnes, D. L. 1992. Ontogeny, season and trade-offs: Vertical distribution of the mesopelagic fish maurolicus muelleri. Sarsia, 77: 253–261.

Gjøsaeter, J., and Kawaguchi, K. 1980. A review of the world resources of mesopelagic fish. FAO Fisheries Technical Paper, 193: 123–134.

Gjøsæter, J. 1973. The food of the mygtophid fish, benthosema glaciale (reinhardt), from Western Norway. Sarsia, 52: 53–58.

Gjøsæter, J. 1981. Variation in Growth Rate and Age at First Maturation in Rainbow Trout; Growth, Production and Reproduction of the Myctophid Fish Benthosema Glaciale From Western Norway

and Adjacent Seas; Life History and Ecology of Maurolicus Muelleri (Gonostomatidae) i. 109–131 pp.

Godø, O. R., Patel, R., and Pedersen, G. 2009. Diel migration and swimbladder resonance of small fish: Some implications for analyses of multifrequency echo data. *In* ICES Journal of Marine Science, pp. 1143–1148.

Greenlaw, C. F., and Johnson, R. K. 1983. Biological Oceanography Multiple-frequency Acoustical Estimation.

Grimaldo, E., Grimsmo, L., Alvarez, P., Herrmann, B., Møen Tveit, G., Tiller, R., Slizyte, R., *et al.* 2020. Investigating the potential for a commercial fishery in the Northeast Atlantic utilizing mesopelagic species. ICES Journal of Marine Science.

Handegard, N. O., Patel, R., and Hjellvik, V. 2005. Tracking individual fish from a moving platform using a split-beam transducer. The Journal of the Acoustical Society of America, 118: 2210–2223.

Handegard, N. O. 2007. Observing individual fish behavior in fish aggregations: Tracking in dense fish aggregations using a split-beam echosounder. The Journal of the Acoustical Society of America, 122: 177–187.

Hosia, A., and Båmstedt, U. 2008. Seasonal abundance and vertical distribution of siphonophores in western Norwegian fjords. Journal of Plankton Research, 30: 951–962.

Irigoien, X., Klevjer, T. A., Røstad, A., Martinez, U., Boyra, G., Acuña, J. L., Bode, A., *et al.* 2014. Large mesopelagic fishes biomass and trophic efficiency in the open ocean. Nature communications, 5: 3271.

Kaartvedt, S., Knutsen, T., and Holst, J. C. 1998. Schooling of the vertically migrating mesopelagic fish Maurolicus muelleri in light summer nights. Marine Ecology Progress Series, 170: 287–290.

Kaartvedt, S., Staby, A., and Aksnes, D. L. 2012. Efficient trawl avoidance by mesopelagic fishes causes

large underestimation of their biomass. Marine Ecology Progress Series, 456: 1–6.

Khodabandeloo, B., Agersted, M. D., Klevjer, T., Macaulay, G. J., and Melle, W. 2021. Estimating target strength and physical characteristics of gas-bearing mesopelagic fish from wideband in situ echoes using a viscous-elastic scattering model . The Journal of the Acoustical Society of America, 149: 673–691.

Kloser, R. J., Ryan, T., Sakov, P., Williams, A., and Koslow, J. A. 2002. Species identification in deep water using multiple acoustic frequencies. Canadian Journal of Fisheries and Aquatic Sciences, 59: 1065–1077.

Kloser, R. J., Ryan, T. E., Keith, G., and Gershwin, L. 2016. Deep-scattering layer, gas-bladder density, and size estimates using a two-frequency acoustic and optical probe. *In* ICES Journal of Marine Science, pp. 2037–2048.

Knutsen, T., Wiebe, P. H., Gjøsæter, H., Ingvaldsen, R. B., and Lien, G. 2017. High Latitude Epipelagic and mesopelagic scattering layers-a reference for future Arctic ecosystem change. Frontiers in Marine Science, 4.

Knutsen, T., Hosia, A., Falkenhaug, T., Skern-Mauritzen, R., Wiebe, P. H., Larsen, R. B., Aglen, A., *et al.* 2018. Coincident mass occurrence of gelatinous zooplankton in Northern Norway. Frontiers in Marine Science, 5.

Korneliussen, R. J., Heggelund, Y., Macaulay, G. J., Patel, D., Johnsen, E., and Eliassen, I. K. 2016. Acoustic identification of marine species using a feature library. Methods in Oceanography, 17: 187–205.

Kristoffersen, J. B., and Salvanes, A. G. V. 1998. Life history of Maurolicus muelleri in fjordic and oceanic environments. Journal of Fish Biology, 53: 1324–1341.

Kristoffersen, J. B., and Salvanes, A. G. V. 2009. Distribution, growth, and population genetics of the

glacier lanternfish (Benthosema glaciale) in Norwegian waters: Contrasting patterns in fjords and the ocean. Marine Biology Research, 5: 596–604.

Kubilius, R., Ona, E., and Calise, L. 2015. Measuring in situ krill tilt orientation by stereo photogrammetry: Examples for Euphausia superba and Meganyctiphanes norvegica. ICES Journal of Marine Science, 72: 2494–2505.

Lam, V. W. M., and Pauly, D. 2005. Mapping the global biomass of mesopelagic fishes. 4 pp.

Lavery, A. C., Wiebe, P. H., Stanton, T. K., Lawson, G. L., Benfield, M. C., and Copley, N. 2007. Determining dominant scatterers of sound in mixed zooplankton populations. The Journal of the Acoustical Society of America, 122: 3304–3326.

Mackie, G. O. 1985. Midwater macroplankton of British Columbia studied by submersible PISCES IV. Journal of Plankton Research, 7: 753–777.

Mackie, G. O., Pugh, P. R., and Purcell, J. E. 1988. Siphonophore Biology. Advances in Marine Biology, 24: 97–262.

Marshall, N. 1951. Bathypelagic fishes as sound scatterers in the ocean. Journal of Marine Research, 10: 1–17.

Martin, L. V., Stanton, T. K., Wiebe, P. H., and Lynch, J. F. 1996. Acoustic classification of zooplankton. ICES Journal of Marine Science, 53: 217–224.

Medwin, H., and Clay, C. S. 1998. Sources and Receivers. *In* Fundamentals of Acoustical Oceanography, pp. 127–152.

Mianzan, H., Pájaro, M., Alvarez Colombo, G., and Madirolas, A. 2001. Feeding on survival-food: Gelatinous plankton as a source of food for anchovies. *In* Hydrobiologia, pp. 45–53.

Mills, C. E. 1995. Medusae, siphonophores, and ctenophores as planktivorous predators in changing

global ecosystems. ICES Journal of Marine Science, 52: 575–581.

Okiyama, M. 1971. Early life history of the gonostomatd fish, Maurolicus muelleri (Gmelin), in the Japan Sea. Bull. Jap. Sea Reg. Fish. Lab., 23: 21–53.

Ona, E., and Pedersen, G. 2006. Calibrating split beam transducers at depth. The Journal of the Acoustical Society of America, 120: 3017–3017.

Ona, E., Zhang, G., Pedersen, G., and Johnsen, E. 2020. In situ calibration of observatory broadband echosounders. ICES Journal of Marine Science, 77: 2954–2959.

Penã, M., and Ratilal, P. 2019. Mesopelagic fish avoidance from the vessel dynamic positioning system. ICES Journal of Marine Science, 76: 734–742.

Proud, R., Handegard, N. O., Kloser, R. J., Cox, M. J., Brierley, A. S., and Demer, D. 2019. From siphonophores to deep scattering layers: Uncertainty ranges for the estimation of global mesopelagic fish biomass. ICES Journal of Marine Science, 76: 718–733.

Pugh, P. R. 1984. The diel migrations and distributions within a mesopelagic community in the North East Atlantic. 7. Siphonophores.

Rasmussen, O. I., and Giske, J. 1994. Life-history parameters and vertical distribution of Maurolicus muelleri in Masfjorden in summer. Marine Biology, 120: 649–664.

Robison, B. H., Reisenbichler, K. R., Sherlock, R. E., Silguero, J. M. B., and Chavez, F. P. 1998. Seasonal abundance of the siphonophore, Nanomia bijuga, in Monterey Bay. Deep-Sea Research Part II: Topical Studies in Oceanography, 45: 1741–1751.

Scoulding, B., Chu, D., Ona, E., and Fernandes, P. G. 2015. Target strengths of two abundant mesopelagic fish species. The Journal of the Acoustical Society of America, 137: 989–1000.

Simmonds, J., and MacLennan, D. 2007. Fisheries acoustics: Theory and practice: Second edition. 1–252

pp.

Sobradillo, B., Boyra, G., Martinez, U., Carrera, P., Peña, M., and Irigoien, X. 2019. Target Strength and swimbladder morphology of Mueller's pearlside (Maurolicus muelleri). Scientific Reports, 9.

St.John, M. A. S., Borja, A., Chust, G., Heath, M., Grigorov, I., Mariani, P., Martin, A. P., *et al.* 2016. A dark hole in our understanding of marine ecosystems and their services: Perspectives from the mesopelagic community. Frontiers in Marine Science, 3.

Staby, A., and Aksnes, D. L. 2011. Follow the light-diurnal and seasonal variations in vertical distribution of the mesopelagic fish Maurolicus muelleri. Marine Ecology Progress Series, 422: 265–273.

Standal, D., and Grimaldo, E. 2020. Institutional nuts and bolts for a mesopelagic fishery in Norway. Marine Policy, 119: 104043.

Torgersen, T., and Kaartvedt, S. 2001. In situ swimming behaviour of individual mesopelagic fish studied by split-beam echo target tracking. ICES Journal of Marine Science, 58: 346–354.

Toyokawa, M., Inagaki, T., and Terazaki, M. 1997. Distribution of Aurelia Aurita (Linnaeus, 1758) in Tokyo Bay. *In* Proceedings of the 6th International Conference on coelenterate Biology, pp. 483–490.

Warren, J. D., Stanton, T. K., Benfield, M. C., Wiebe, P. H., Chu, D., and Sutor, M. 2001. In situ measurements of acoustic target strengths of gas-bearing siphonophores. ICES Journal of Marine Science, 58: 740–749.

Youngbluth, M., Owen, G., Robison, B., Reisenbichler, K., Hunt, J., and Bridges, J. 1996. Estimates of diel predation rates by vertically migrating populations of the physonect siphonophore Nanomia cara in the Gulf of Maine. EOS, 76.

Youngbluth, M., Sørnes, T., Hosia, A., and Stemmann, L. 2008. Vertical distribution and relative abundance of gelatinous zooplankton, in situ observations near the Mid-Atlantic Ridge. Deep-Sea

Research Part II: Topical Studies in Oceanography, 55: 119–125.

9 Paper II

Hiding in plain sight: Predator avoidance behaviour of mesopelagic *Maurolicus muelleri* during foraging

Kjetil Gjeitsund Thorvaldsen, Stefan Neuenfeldt, Patrizio Mariani & J. Rasmus Nielsen

Abstract

Mesopelagic fishes are ubiquitous, ecologically important and a potential protein resource. However, how mesopelagic fish maneuver in their 3D environment and facilitate encounters is unknown. We tracked the swimming trajectories of juvenile *M.muelleri* and adult *M. muelleri* and *B. glaciale* acoustically within two distinct vertical layers, measured swimming speed, and used a self-overlap model to analyse the geometry of the trajectories. Our aim was to investigate, if and how the fishes were optimizing their swimming behaviour, maximising prey

encounters while minimizing predator encounters simultaneously. We found that the mesopelagic fishes were moving actively, displaying a range between ballistic and convoluted movements. Some of the fishes were moving in a manner that minimized self-overlap to optimize prey search ($\psi<0.1$), while increasing self-overlap with regards to a piscivorous predator ($\psi>0.6$) with a hypothetical visual range of 1 m. The differences can possibly be explained by different predator and prey surroundings driving the individual mesopelagics.

Introduction

Motion is a key element in the ecology of living organisms, and it is a critical parameter that both drives evolution and ecology (Nathan, 2008). For the individual organism, motion affects interactions with prey, mates and predators (Nathan, 2008; Barraquand and Murrell, 2013; Martinez-Garcia *et al.*, 2020). Motion has large effects on encounter rates. Hence it is regulating encounters with food, predators and con-specifics. This impacts on survival and reproductive success. Behaviours increasing the likelihood for survival by reducing predator encounters while optimizing foraging, are selected by evolution over a range of organisms (Nathan, 2008).

Simple models have historically been successful in describing encounter (Holling, 1959, 1966; Gerritsen and Strickler, 1977; Rothschild *et al.*, 1988). However, the described

motion patterns have been simplified due to lack of observation methods (Nathan, 2008; Martinez-Garcia *et al.*, 2020; O'Dwyer, 2020). Observing animal motion, especially in aquatic environments has been challenging due to the lack of target tracking methodologies. Usually these methodologies have been reserved for large animal groups (Hays *et al.*, 2016)

Improved telemetric methods such as split-beam echosounders (Ehrenberg and Torkelson, 1996; Ona, 1999; Torgersen and Kaartvedt, 2001; Handegard *et al.*, 2005; Klevjer and Kaartvedt, 2006; Handegard, 2007; Christiansen *et al.*, 2019, 2021), acoustic cameras (Handegard *et al.*, 2012; Ashraf *et al.*, 2016; Rieucau *et al.*, 2016; Kandimalla *et al.*, 2022) and video cameras (Gong *et al.*, 2022.; Edgington *et al.*, 2006; Bianco *et al.*, 2014; Tomaru *et al.*, 2016; Qian and Chen, 2017; Lucas *et al.*, 2021; Burns *et al.*, 2022) have created new opportunities to investigate small marine organisms in their natural environments.

Acoustic methods are specifically advantageous to observe organisms that live hundreds to thousands of meters below the ocean surface, i.e. the oceanic twilight zone, covering the mesopelagic marine water layers from 200-1000 meters depth. This region is one of the world's largest in geographical extension and water volume, and probably the most poorly investigated and understood habitat and food web (Webb *et al.*, 2010; Davison *et al.*, 2015; St.John *et al.*, 2016; Proud *et al.*, 2019; Grimaldo *et al.*, 2020). Ensonified on

an echo sounder, mesopelagic organisms form distinct scattering layers covering large geographical ocean regions (Marshall, 1951; Hersey *et al.*, 1961; Klevjer *et al.*, 2016). Especially the fish component of these scattering layers has gained increased commercial and scientific interest as the total fish biomass of these layers potentially is very big with biomass estimates between 1 gigaton (Lam and Pauly, 2005), 11 gigatons (Irigoien *et al.*, 2014) and 2-19 gigatons (Proud *et al.*, 2019). They likely play an important role controlling global carbon sequestering (Hidaka *et al.*, 2001; Hudson *et al.*, 2014; St. John *et al.*, 2016), as well as being a major potential protein source for human consumption (Alvheim *et al.*, 2020; Grimaldo *et al.*, 2020; Standal and Grimaldo, 2020; Paoletti *et al.*, 2021).

A mesopelagic fish species which is considered ecologically and potentially commercially important (Alvheim *et al.*, 2020; Grimaldo *et al.*, 2020; Standal and Grimaldo, 2020) is Mueller's Pearlside (*Maurolicus muelleri*). Pearlside is a small mesopelagic fish common in fjords, shelfs and along offshore sea mounts (Okiyama, 1971; Gjøsaeter and Kawaguchi, 1980; Gjøsæter, 1981; Bañon *et al.*, 2016). During winter, mesopelagic pearlside are separated in two different vertical layers inside Norwegian Fjords. The adults reside in a deeper layer the entire winter to minimize predation risk (~150 m), but also drastically reducing feeding opportunities (Giske and Aksnes, 1992; Staby *et al.*, 2013). The juveniles have been observed to balance the trade-off between predation and growth (Giske and Aksnes, 1992) and do so by performing vertical migrations upwards to visually feed (Giske and Aksnes, 1992; Bjelland, 1995; Bagøien *et*

al., 2001) and sink down to an intermediate depth after feeding to reduce predation risk (Prihartato *et al.*, 2015; Christiansen *et al.*, 2019).

Mesopelagic fishes are known for choosing specific ambient light levels for efficient foraging also known as the anti-predator window (Clark and Levy, 1988; Langbehn *et al.*, 2019). However, there is still limited knowledge on how these mesopelagic fishes move within their isolume to maximise prey encounter rate and reduce predator encounters. For most mesopelagic fishes in the north-east Atlantic, all search for food comes with a risk of predation from piscivorous, visual predators, such as saithe *(Pollachius virens),* blue whiting *(Micromesistius poutassou)* and other gadoids (Giske *et al.*, 1990; Rasmussen and Giske, 1994; Bjelland, 1995). There is no evidence for active predator avoidance by mesopelagic fish in 3D swimming trajectories other than the step-wise upwards migration (Kaartvedt *et al.*, 1998; Torgersen and Kaartvedt, 2001; Christiansen *et al.*, 2019) . There have also been some observations of schooling (Kaartvedt *et al.*, 1998), and group forming (Benoit-Bird *et al.*, 2017). However, in an environment with no natural borders, there are likely existing strong selective pressure on swimming behaviour. It has been shown that swimming patterns in marine organisms can emerge by the optimization of prey encounters while reducing predation risks (Bianco *et al.*, 2014). In earlier studies, the search volume self-overlap was used to describe optimal swimming patterns in zooplankton groups, and it showed that different swimming behaviour can produce large changes in encounter rates with predators and prey (Visser and Kiørboe, 2006; Bianco *et al.* 2014).

For prey encounters, minimizing self-overlap in the movement trajectory is important (Bianco *et al.*, 2014). Self-overlap is explained by $\psi(r) = 1 - \frac{V(r)}{V_{max}(r)}$ where ψ describes how much the moving trajectory and resulting clearance volume overlaps within its own track and is a function of the actually scanned volume (V(r)) and the max scanned volume given for a visual range (Vmax(r)) where values of self overlap are ranging between 0 and 1 depending on the turtousity of the trajectory. Ideally for a foraging prey item, a low degree of self overlap within it's own visual range and a large degree of self overlap with regards to the predators' visual range provides protection for the individual while the search volume is optimal.

In this study, we recorded individual Pearlside and lanternfish abundances and movements in mesopelagic layers in a Norwegian Fjord with five split aperture broadband echo sounders. Using *in situ* acoustic measurements of three-dimensional swimming behaviour, we investigated if and how the fishes were trading prey encounters off against predation risk.

Materials and methods

Hydrographic conditions influencing acoustic measurements

The study area is in Sørfjorden (N 60.43, E 5.62) the southern part of Osterfjorden surrounding the island Osterøy, Norway. The fjord is at maximum 425 meters deep and has a physical threshold of 170 meters at the entrance of the fjord (Dale *et al.*, 2019), and

it is characterised by a vertical hydrographic structure of cold, fresh surface water which is typical for Western Norwegian fjords in December (Giske *et al.*, 1990). Vertical profiles of temperature, salinity, and oxygen were measured from the surface to 210 meters depth with a CTD probe (Supplementary Figure 1). Temperature was lowest at the surface (~5° C) and increasing to 11°C at 20 m depth, where the water was warmer with a following thermocline from 20-70 meters, where the temperature stabilized at ~8 degrees down to 210 meters. The surface-water was relatively fresh (18 psu), with a rapid increase down to 30 meters (33 psu) followed by a moderate increase down to 210 meters (~35 psu) (Supplementary Figure 1).

Acoustic monitoring and coverage of different sound scattering layers

Individual swimming trajectories of mesopelagic fish were collected during an experimental acoustic survey with the Norwegian research vessel G.O Sars. To resolve the biological components of the fjord, acoustic volume scattering strength (Sv, dB re 1 m^{-1}) was measured on 14th and 15th December 2019 with the ship mounted echo sounders (Simmonds and MacLennan, 2007), identifying sound scattering layers from a mesopelagic community that had previously been quantitatively and qualitatively studied with a well-known stock of mesopelagic fishes and zooplankton (Salvanes *et al.*, 1995; Kristoffersen and Salvanes, 1998; Bagøien *et al.*, 2001). The vessel acoustic data identified two pronounced sound scattering layers

Qualitative check of acoustic data and identifying layers of pearlside

Two scattering layers were identified, (from now on referred to as SSL1 and SSL2) at 70-100 meters and from 120 meters and down to the bottom, respectively (Figure 1 and 2). To ground truth this acoustic profile of the fjord, two trawl hauls were performed14th December 2019. SSL1 at 70-100m depth and SSL2 at 150m depth were towed and covered with a 6x6 meters 110 µm mesh size macro zooplankton trawl (Krill trawl). (Figure 1 a and b). The trawl was towed with a speed of 2.5 and 2.2 m/s respectively for 10 minutes (09:09-09:19 and 14:26-14:36 UTC). The first catch was small and not subsampled. The catch on the second haul was subsampled (species, individual length in mm and mean weight to nearest 0.001 g). The catch was only used as a qualitative check to verify the biological components of the acoustic sound scattering layers.

The acoustic single target tracks were collected as raw data by Simrad EK80 echosounders (Version 1.12.2.0; EK80 Scientific wide-band echo sounder - Kongsberg Maritime, 2022) with transducers mounted on a lowered acoustic split aperture probe called the TS-probe (Dias Bernardes *et al.*, 2020) . SSL1 was measured in the epipelagic due to the migration that had taken place prior to TS-probe deployment (Figure 1c). This was done to ensure full overlap between the net-sampling and the acoustic data measured by the TS-probe . SSL 2 was measured at 120m total depth at 15th of December from 15:58-17:46 UTC (Figure 1d) with transducers pointing downwards.

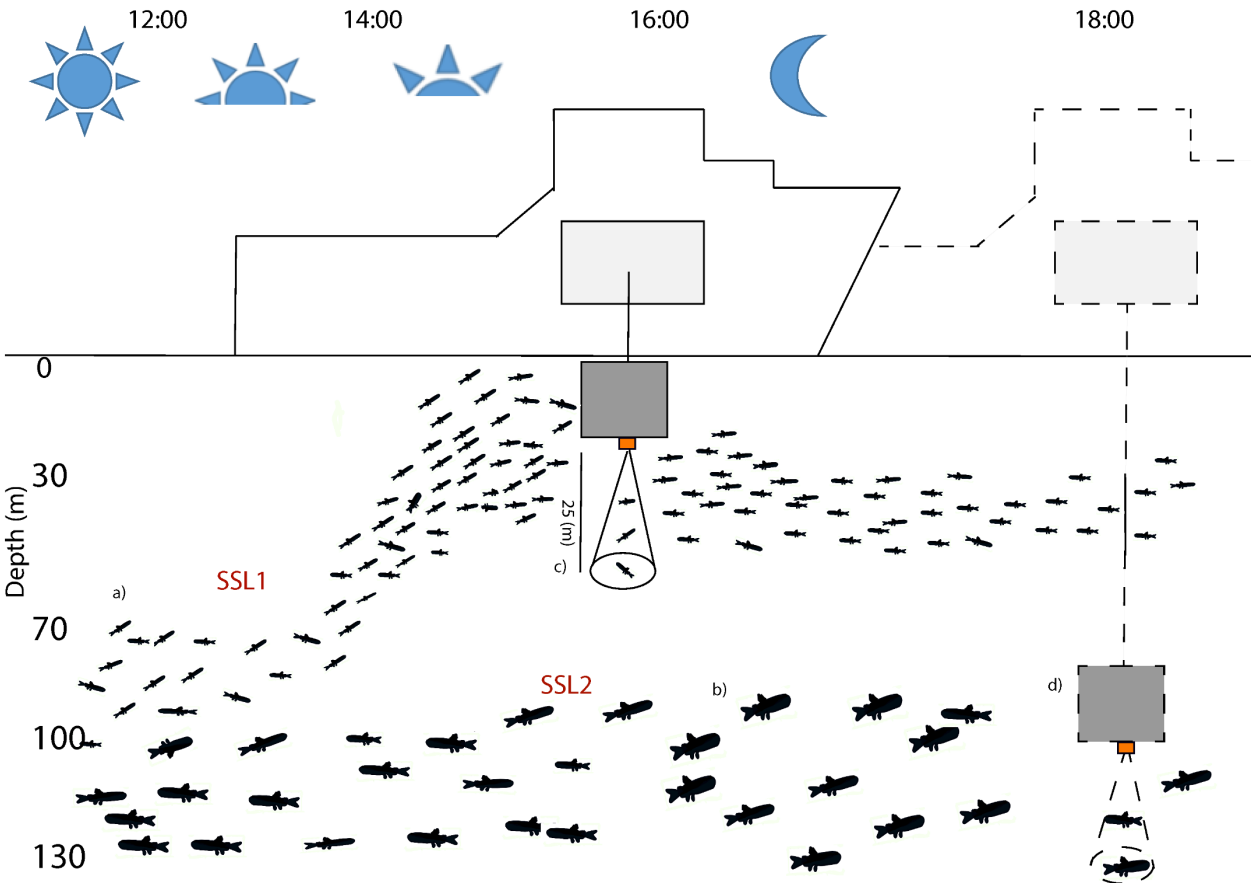

Figure 1. Experimental design for collecting trajectories and biological samples. The two scattering layers (SSL1) and (SSL2) were biologically sampled with the krill-trawl at 70 meters (10:00) UTC and 16:27 UTC (b). While standing in dynamic position, the TS-probe was lowered with a hydraulic winch from the hangar of the ship in to scattering layers SSL (c and SSL2 (d) measuring targets at close range to resolve single targets. The first deployment observed SSL1 during early night (a). During this period SSL1 had migrated towards their daytime depth (70 meters) the surface to feed and were present at 20-45 meters depth. Later the TS-probe was vertically moved down to SSL2 (dashed lines) (d).

Biological components of the fjord system

SSL1 was located at 70-100 m depth during daytime, and migrated towards the surface during dusk and night. The catch composition from the biological sampling with the krill trawl in this layer consisted only of pearlsides with mean lengths of 22.3 ± 3.3 s.d. mm. (Fig 2a, Table 1). SSL2 , was extending from ~120 m depth at daytime and down to the seabed, only moving 20 meters vertically during night (Figure 2b). SSL2 consisted of pearlsides with mean length of 29.8 ± 10.4 s.d. mm and adult glacier lanternfish (*Benthosema glaciale*) as well as krill *(Meganyctiphanes norvegica*) and pelagic shrimps (*Sergestes spp* and *Pasiphacea spp*) (Table 1). As described in previous studies (Giske and Aksnes, 1992; Prihartato *et al.*, 2015) and as also observed in current echograms (Figure 2b), SSL2 does not migrate. Backscatter from larger fish (TS>-40 dB) as observed by the ship mounted transducers in both SSL1 and SSL2 (Figure 2c)was determined to be saithe (*Pollachius virens)* or blue whiting (*Micromesistius poutassou*). SSL1 had fewer recorded tracks of fish compared to the deeper layer, there were also a lower number of zooplankton(Supplementary Figure 2a), compared SSL2(Supplementary Figure 2b).

Table 1. Catch composition from the two trawl hauls of the krill trawl

Haul nr	Time (UTC)	Depth (m)	Towspeed (Knots)	Species	N	Individual Mean length (mm)+- SD	Catch (kg)	Weight

1	10:00	70	2.5	*Maurolicus muelleri*	97	22.8 +-3.33	0.01
2	16:27	152	2.2	*Maurolicus muelleri*	3509	29.9 +-10.4	1.3
2	16:27	152	2.2	*Benthosema glaciale*	1860	34.9 +-16.78	1.2
2	16:27	152	2.2	*Pasiphacea spp*	1583	44.9 +-8.2	6.9
2	16:27	152	2.2	*Sergestes spp*	8761	37 +- 5.9	3.3
2	16:27	152	2.2	*M. Norvegica*	1455	7.24 +-1.55	3.0

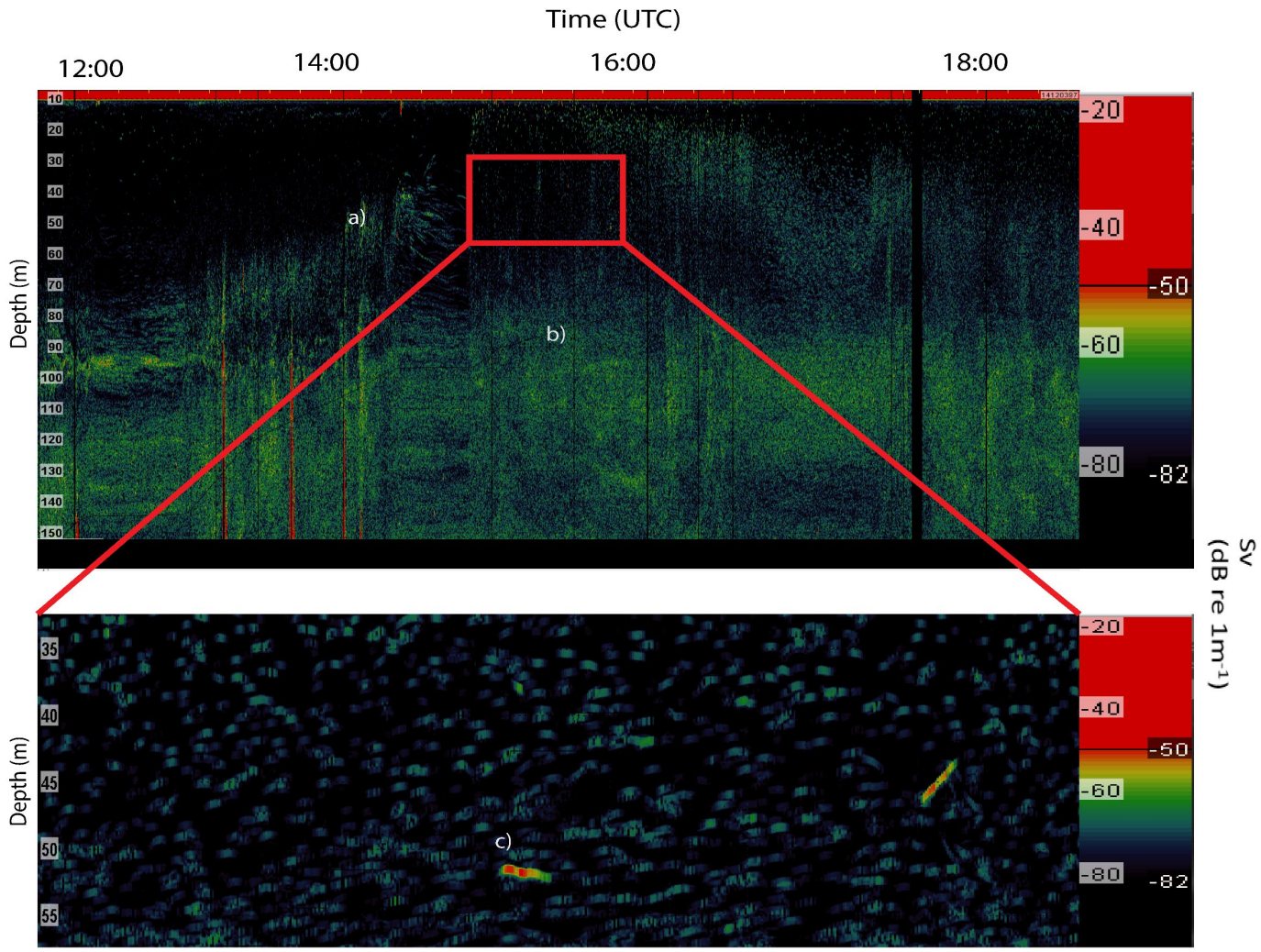

Figure 2. Ship recorded echogram of two the scattering layers. Panel a) is SSL1 consisting of juvenile pearlside migrating towards the surface between ~13-15 UTC. Panel b) is the SSL2 with a mixture of adult pearlside and lanternfish, as well as krill and pelagic shrimps (Table 1). Panel c) is a magnification of the SSL1, showing echoes of larger fish (TS>-40 dB) determined to be saithe and/or blue whiting, together with juvenile pearlside echoes.

TS-probe deployment and compiling acoustic data for target tracking

The TS-probe was equipped with two wide band transducers with 90-170 kHz and 160-260 kHz acoustic beam field and with an opening angle of 7 degrees. Real time data were

collected using the attached fibre optic cable (Figure 1c and d). The use of a high ping rate enabled sampling of high-resolution single target tracks (1-4 Hz). Acoustic data were recorded from 7-25 meters from the TS-probe beyond the transducer near beam field. The TS-probe was hanging motionless for several minutes while the vessel was in Dynamic Position (using the vessel's computer system to maintain a fixed position).

The TS-probe was calibrated with a 57.2 mm in diameter tungsten carbide calibration sphere with 6 % cobalt binder to obtain reference targets for the 38 kHz narrowband, the 56-87 kHz broadband, and the 97-160 kHz broadband transducers, and a 38.1mm in diameter tungsten calibration sphere for the 160-260 kHz and 280-450 kHz broadband transducers. The calibrations were performed within ICES (International Council for Exploration of the Sea) standards (Demer *et al.*, 2015; Ona *et al.*, 2020) (Supplementary table 1)).

Identifying and grouping trajectories

Raw acoustic data were post-processed in LSSS (Large Scale Survey System version 2.7.0), a program used for post processing of raw acoustic data for biomass estimation, TS-measurements and target tracking (Korneliussen and Ona, 2002; 2003; Korneliussen *et al.*, 2016). Acoustic scatterers were identified and grouped to mesopelagic fish or smaller plankton groups based on the difference in their target strengths (TS, dB re 1 m^2) and movement patterns. TS is estimated as a function of frequency, also called TS(f)

(Martin *et al.*, 1996; Scoulding *et al.*, 2015; Sobradillo *et al.*, 2019) and based of the qualitative check performed by the krill trawl (Table 1) . Swimming trajectories were obtained from both SSL1 and SSL2 during dusk and early night. Single target tracks were initially detected and created in LSSS by using a target tracking algorithm developed by (Handegar*d et al*., 2005; Handegard, 2007; Korneliussen, 2010) , following the same single target echo for an extended period with 4 angular position detections per second.

First, the minimum target strength (dB) detection threshold for tracked individuals was set to – 75 dB to include all sizes of pearlside (Supplementary table 2). The tracking distance was set from 5 to 25m distance from the pinging transducer. The settings made for track-initiation were $\alpha_0 = 2.8°$, $\beta_0 = 2.8°$, $r_0 = 0.44$ m, $I_0 = 20$ dB. Here, α_0 and β_0 are the maximum along and atwartship angles within the acoustic beam for tracking individuals, r_0 is the range difference between last terminated track and new initiated track, and I_0 is the minimum difference in target strength (dB) for initiating a new track after a previously measured track. The track association settings were basically the same as for track initiation, namely $\alpha_G = 2.8°$, $\beta_G = 2.8°$, $r_G = 0.44$ (m), $I_G = 20$ (dB), with α_G and β_G again representing maximum alongship and atwarthship cut off angles, r_G the accepted maximum range between the transducer and two following track detections, and I_G is the maximum deviation in TS between two subsequent track detections. Minimum track length was set to 20 detections. The maximum number of missing detections within a track was set to 8, the number of missing samples was set to 8, and the maximum ratio of missing detections to the total number of detections in a track was set to 0.8.

Detection, initiation and processing of tracks to identify mesopelagic fish trajectories

The aim of this study was to observe mesopelagic fish trajectories, but traditional SED-filters used in target tracking often fail in aggregations of fish (Handegard, 2007). To increase the number of initially successful trackings, we allowed a lower mean TS than usual in the more strict protocols for TS-measurement (Ona, 1999). This also ensured the possibility to follow the targets further out in the beam field. Tracks with clear resolution and long duration were post processed (t>60 seconds). Collecting tracks of multiple fish will lead to errors, and thus tracks were visually inspected in LSSS to manually correct for errors done by the target-tracking algorithm both by observing the echogram, and the angular position of the track. To observe behaviour for as long as possible, fragmented tracks were manually re-attached in LSSS. In this process, the x (alongship (m)), y (atwhartship(m)) and z (vertical distance from transducer (m)) positions of the tracks were exported together with time (UTC) and target strength (dB). Erroneous tracks belonging to several individuals were identified due to differences in TS, and large changes in one of the angular positions x, y or z, or radical changes in several of the parameters. The exported x,y and z-data from LSSS were further post processed manually as follows. To reduce the noise in the tracks, erroneous measurements which suggest movements where the measurement of one or two ping do not follow the remaining trajectory (deviations +-30 cm per ping), due to an inclusion of another target for one or two pings in the tracking algorithm, were deleted. To offset any small errors or variations in the movement, the curve

for all the measured points for each ping were smoothed for x, y and z individually, before reused as the trajectory of the fish. Smoothing was done by fitting x, y and z individually over time t with a piece-wise polynomial smoothing spline in MatLab (MathWorks, 2020) with smoothing parameter $p = 0.1$. Since t was unique and equal for x,y and z, predictions for x,y and z at given t could then be merged to three-dimensional trajectories over time. After fitting the curve, the trajectory was reconstructed with the estimated x, y and z values for positions at time t. Using these newly computed positions, average and instantaneous swimming speed were measured by using:

$$(1)\quad W = \sqrt{((x_{t+1} - x_t)^2) + ((y_{t+1} - y_t)^2) + ((z_{t+1} - z_t)^2))l}$$

Where x is the alongship angle, y is the atwarthship angle and z is the depth, between consecutive points in the tracks at time t and t + 1. The mean swimming speed of the whole trajectory is converted into body length per second using average body lengths of pearlside (Eq. l) for each scattering layer.

For the self-overlap measurements we computed the scale dependent self-overlap, $\psi(r)$, for each trajectory using the methodology described in Bianco et al. (2014):

$$(2)\quad \psi(r) = 1 - \frac{V(r)}{V_{max}(r)}$$

where r is the encounter radius, $V(r)$ is the effective scanned volume, and $V_{max}(r)$ is the maximum volume that can be scanned as function of r. The maximum volume is computed as:

$$(3)\ V_{max}(r) = \pi r^2 L + \frac{4}{3}\pi r^3$$

Which considers the trajectory as a straight line also including the start and the end of the path (L).

Generally, we then have that $V(r) \leq V_{max}(r)$ and depending on the tortuosity of the path, and on the encounter radius, a varying portion of the swept volume is self-overlapping providing a scale dependent self-overlap function bounded within zero and one, i.e., $0 \leq \psi(r) \leq 1$. In particular, if $\psi(r) = 0$ then the trajectory never intersects itself for that r and the effective volume is equal to the maximum volume. While, if $\psi(r) = 1$ no new volume is perceived at that r, as for example in the case of a very convoluted path. Additionally, we expect that when $r \to 0$, then $\psi \to 0$ and the self-overlap will increase for larger radius with a maximum at $r < L$. Indeed, at $r \geq L$, V_{max} and V will both roughly scale as the volume of a sphere taking similar values and providing the limit $r \to +\infty$, $\psi \to 0$.

A Monte-Carlo method was used to calculate $V(r)$ (Bianco et al. 2014). We first identified the maximum radius, i.e. the visual range $r\_max = 100\ cm$ and then for each trajectory computed the bounding box $x_{min} - r_{max} < x < x_{max} + r_{max}$ where x_{min},

x_{max} are respectively the minimum and the maximum value of the trajectory along the x coordinate. Similarly, minimum and maximum values are used for the other coordinates on y and z, and finally the volume of the box V_{box} is calculated. We then drawed $NP = 2 \cdot 10^9$ random points uniformly distributed within the bounding box and calculate the histogram of the number of points, i.e., $n(r)$, falling at a distance less than a given radius r from the trajectories with the minim radius at $r_{min} = 1\ cm$, and $r_{min} \leq r < r_{max}$. The distance is measured using the interpolating segment between two consecutive points on the trajectory. Finally, the effective volume is obtained as:

$$(4)\ V(r) = \frac{n(r)}{NP} V_{box}.$$

When applying the method to the dataset, we checked that the trajectories were long enough, so that the results are stationary and not too influenced by the behaviour at the endpoints.

Results:

Classifying individual 3d trajectories and movement patterns

All trajectories were visually inspected, and showed a range of different types of behaviours from ballistic straight lines, to convoluted tracks with higher degree of self-overlap (Figure 3 a-c). Some fish were actively ascending or descending with small bursts adjusting their vertical positions (Figure 4a). There were also tracks that appeared as long spirals with low self-overlap for a large range of distances (Figure 3a). This behaviour was

observed both in the SSL1 and SSL2 layer. In both layers, there were trajectories with low TS (<-90dB) with unique movement patterns. These targets were ascending and descending with ±20 cm up and down with sharp turns. Also, these trajectories were characterized to be zooplankton (Supplementary Figure 2). Due to differences in fish density (Supplementary Figure 2a and b), only ten tracks with sufficient resolution were observed within the SSL1 compared to 22 in the SSL2. The track lengths ranged from 60 to 490 seconds.

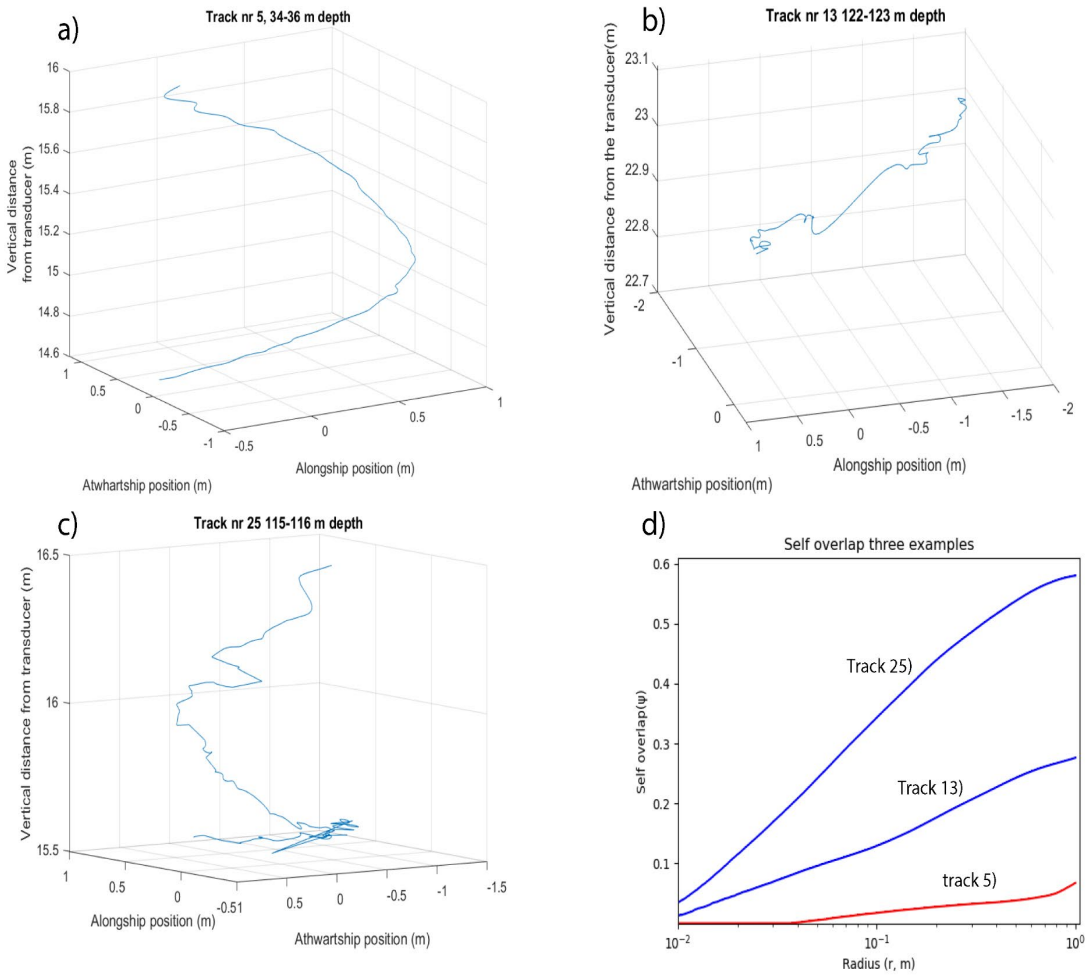

Figure 3: Three examples of tracks of mesopelagic fish and their respective self-overlap. Tracks were taken from SSL1 (a), and SSL2 (b and c), showing the trajectories of the fish in 3D. Panel d) is the measured self-overlap of the three tracks where self-overlap (ψ (r)) is modelled for several visual ranges.

Swimming speed measurements of individual and groups of accepted fish tracks

The calculated instantaneous swimming speeds (Equation 1) were ranging between 0.01 and 9 body lengths/s in SSL1, and 0.1 and 6 body lengths/s in SSL2 (Figure 4). The swimming speeds compared to body length were higher in SSL1 (Figure 4b). Most swimming speeds were measured to be less than 2 body lengths/s (Figure 4b) where the average swimming speed in the SSL1 was 0.984 with SD ±0.55 body lengths/s while the average swimming speed in the SSL2 was 0.73 body lengths/s with s.d. ±0.42 body lengths/s. The instantaneous swimming speeds observed along the tracks were more variable with some individuals moving with a roughly constant speed while others showed variations in swimming speeds (Figure 4a). In some cases, the fishes generated bursts of high speed followed by subsequent slower movements (Figure 4b). In both cases the average speed (Figure 4b), as well as the irregularity of some the individual movements (Figure 4a), suggest active swimming as both swimming speeds are too fast and patterns too complex to represent passive drifting.

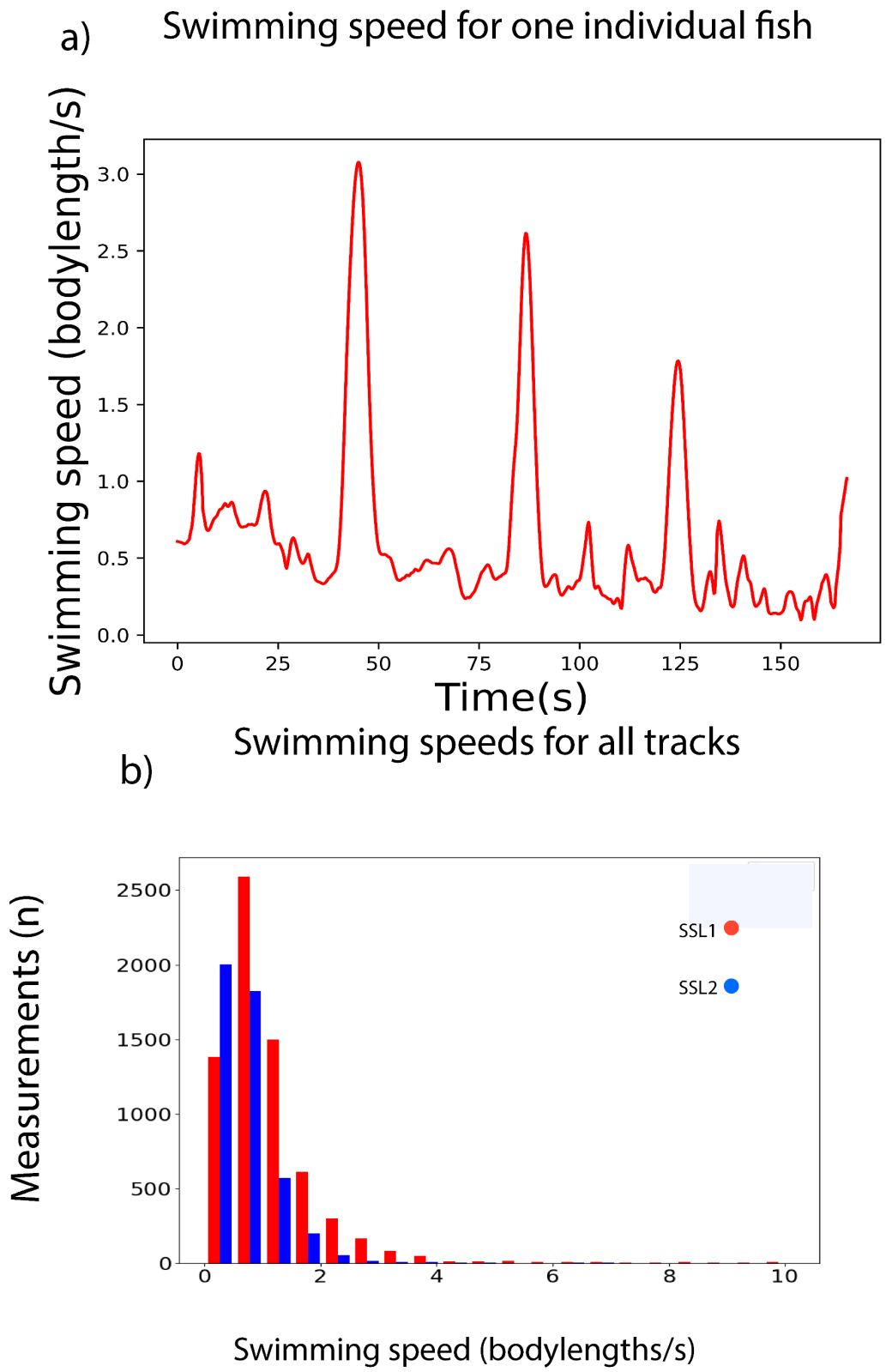
a)
Swimming speed for one individual fish
Swimming speed (bodylength/s)
3.0
2.5
2.0
1.5
1.0
0.5
0.0
0
25
50
75
100
125
150
Time(s)
b)
Swimming speeds for all tracks
Measurements (n)
2500
2000
1500
1000
500
0
0
2
4
6
8
10
SSL1
SSL2
Swimming speed (bodylengths/s)

Figure 4. Panel a) represents the short term swimming speed variability of one pearlside from SSL1 for a period of 160 seconds where the x-axis is showing time, and the y axis is showing swimming speed in bodylengths/s . Panel b) is showing a histogram of the frequency of the measured swimming speeds per ping in bodylengths/s. The histogram is showing all measured swimming speeds from SSL(1) (red), and for SSL2 (blue) from all accepted trajectories.

Analysis of self-overlap measurements for all accepted trajectories

The self-overlap (ψ) measured for the 32 tracks showed values between ψ = 0 and ψ = 0.6 along the range of perception distances from r = 1 cm to r = 1 m. This range of r is used here to describe typical encounter radius for prey and predators. All the tracks show a low degree of self-overlap at the small scale (r =1 cm) and increasing values at higher distances. Hence, tracked individuals had mainly balistic encounters with their prey with values of ψ between 0 and 0.3 for encounter radius between 1 cm to 5 cm, respectively. In some cases balistic encounters were present at both small and large distances. For example for a few tracks values of self-overlap never exceeded ψ=0.1 (Figure 5a), hence indicating swimming behaviours maximizing volume scanning at all scales. On the other hand, more convoluted tracks had values close to ψ =0.6 at r = 1 m (Figure 5a) indicating a substantial reduction of volume scanning at large scales. When grouped together, pronounced differences in self-overlap were evident between the two different sound scattering layers (SSL1 and SSL2) (Figure 5). The average self-overlap in the SSL1 was lower with SD ψ= 0.005 ±0.02, ψ=0.13 ±0.08 and ψ= 0.19± 0.09 at 1 cm, 10 cm and 100 cm respectively (Figure 5b). The average in SSL2 the self-overlap had a mean value of ψ= 0.008 SD±0.03, ψ=0.17 SD±0.14 and ψ=0.27 SD±0.19+- at 0.01, 0.1 and 1 m (Figure 5b) and had a higher

average and higher SD than the SSL1. At visual ranges used in this self-overlap model, no individuals performed full self-overlap (ψ=1).

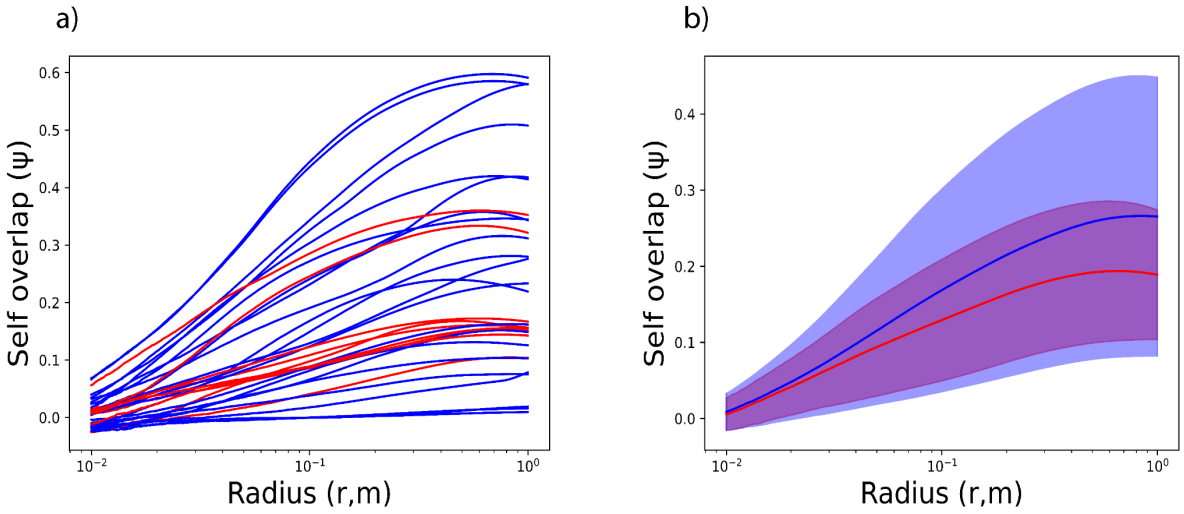

Figure 5. Measured self-overlap for different visual ranges (radius, r). A) is showing the selv overlap for all the tracks from upper layer (Red), and deeper layer (blue), while b) is showing the average self-overlap for the SSL1 (red) and SSL2 blue with their respective error boundaries as the shaded colored areas.

Discussion

Movement patterns of individual fish in a 3D- environment

We observed a spectrum of active swimming behaviours in pearlside individuals (Figure 5a and b). All the tracks recorded showed very low values of self-overlap at characteristic scales for prey encounters (< 5 cm). Some individuals' tracks had large values self-overlap in the visual range of piscivorous fish allowing to reduce encounters with

predators in the absence of natural hideouts in the mesopelagic environment. These tracks generally had a convoluted movement behaviour likely emerging from a compromise between effective foraging and hiding. This behaviour ensures that the fish can forage new volumes within its own visual range, while the movement appears to be convoluted within the visual range of a larger piscivorous predator (Saithe, Blue whiting and haddock)(Giske *et al.*, 1990). This behaviour can also be found in other oceanic animal groups also living in environment without physical and hydrographical borders. (Bianco *et al.*, 2014).

The different degrees of self-overlap found in the 32 trajectories most probably reflect ontogeny, different internal states, different ambient light conditions influencing visual ranges, potential mixing with lanternfish as well as different prey and predator densities in vicinity of the observed individuals. (Supplementary Figure 2a and b) and in some cases gender (Bianco *et al.*, 2014). By observing larger fish in both scattering layers, there is a predation risk in both SSL1 and SSL2 for pearlside. However, it is probably heavily reduced in SSL 2 due to lack of ambient light (Staby *et al.*, 2013). The ballistic shaped trajectories observed in SSL1 represent a bold behaviour, as the search volume is maximal, while self-overlap and hence protection from predation is at minimum. This will theoretically lead to more encounters with prey, especially if prey are located in patches which is typical for zooplankton (Folt and Burns, 1999). This behaviour implies that juvenile pearlside are taking higher risks to efficiently ensure somatic growth throughout the winter as previously reported in Giske and Aksnes,

(1992). However, juvenile pearlside have lower reflection towards the background and can hence afford to migrate higher into the water column where light levels are higher, thus leading to a lower predation risk compared to adult pearlside at the same depth (Giske *et al.*, 1990; Aksnes and Utne, 1997; Utne-Palm, 2002). Pearlside have also been previously described to show different behaviours within themselves where some of the fishes within the layer are leaving the preferred isolume to forage (Christiansen *et al.*, 2021). In these cases the fishes are moving out of a safer light threshold or isolume to maximize foraging.

In SSL2 there were more different behaviours. Low feeding rates and lower natural mortality are assumed in the deeper layers (Staby *et al.*, 2013), and can explain the higher degree of self-overlap seen in some the tracks in SSL2. Some of the variability in SSL2 is likely due to a mixing between pearlside and glacier lanternfish. Hence, some of the tracks could belong to lanternfish and can explain the higher variation in the deeper layer as discrimination between the two species is not easy (Scoulding *et al.*, 2015). (Gjøsaeter and Kawaguchi, 1980; Gjøsæter, 1981; Dypvik *et al.*, 2012; Staby *et al.*, 2013). Hence, it was not to expect that all measured individuals showed the same behaviour in our study.All trajectories were in close proximity to zooplankton individuals (Supplementary Figure 2a and b) based on TS and unique movement patterns, which suggests feeding opportunities within visual range immediately or close by given the measured swimming speeds from the accepted trajectories. Even with a lower total amount of zooplankton, the difference in light level will probably create more encounters

between fish and zooplankton in SSL1 (Staby *et al.*, 2013). Many trajectories were showing complex patterns. Changing direction frequently within both horizontal and vertical axes or in both directions. During these directional changes swimming speeds changed as exemplified in Figure 4a. For these cases, we conclude that the fishes are performing active search or avoidance behaviours. This deviates from total random behaviour, which are often assumed when dealing with encounter rates(Lotka, 1920; Volterra, 1926; Holling, 1959, 1966; Gerritsen and Strickler, 1977; Rothschild *et al.*, 1988)

The lack of vertical migration of individuals from SSL2 observed by the ship mounted transducers, and catch of only juvenile pearlside in the upper layer indicate that there is no vertical migration by adult pearlside, and support that the upper layers actually consists to a large majority of juvenile pearlside. This is supported by previous quantitative and qualitive studies (Giske and Aksnes, 1992; Staby *et al.*, 2013; Prihartato *et al.*, 2015). There was also no evidence of vertical migrations of the lanternfish below 200 meters, even if sporadic migrations have earlier been indicated by trawls (Kaartvedt *et al.*, 1988; Rasmussen and Giske, 1994; Dypvik *et al.*, 2012)

Limitating factors and assumptions

In this study, a narrow acoustic beam was applied at short range. This was needed to resolve single mesopelagic fishes. However, there is a trade-off between separating single targets and beam width (Ona, 1999; Handegard *et al.*, 2005).Targets will eventually move out of the acoustic beam as the observed volumes are usually around $1m^3$, and we acknowledge that behavioural patterns could change if we observe individuals for longer periods.

Tidal currents and or turbulence might influence the movements of the animals, especially zooplankton (Makhlouf Belkahia *et al.*, 2021). However, most trajectories were moving in different horizontal directions across the acoustic beam, and most trajectory shapes were observed to have several directional changes within the horizontal and vertical planes, as well as significant changes in swimming speed (Figure 4a), making it highly unlikely that the observed behaviours are current-driven alone.

There are several factors that impact the visual range for both mesopelagic fish and their piscivourous predators, contributing to the individual variations in observed swimming behaviour. The ambient light level is not constant during this study. The TS-probe deployments were conducted during dusk and early night in SSL1, and during night in SSL2 which provides very different ambient light conditions, and thus the perceptive range i.e. the distance the predator are able to observe prey, would vary to a great extent. This is an crucial factor for individual feeding in fish (Aksnes and Utne, 1997; Aksnes *et al.*, 2004; Langbehn *et al.*, 2019) which influences both feeding and predation rates and could influence individual behaviour accordingly. The visual range of

the predators, both pearlside and piscivorous fish, rely on the ability to distinguish the silhouette of the prey with the background. Turbidity also has a large impact on visual range of fish (Aksnes and Utne, 1997) .

Small transparent fish and zooplankton can highly increase the reaction distance of a visual predator (Aksnes and Utne, 1997). Fishes in the Sternopyctidae family as the pearlsides belong to and, especially the hatchet-fishes here, are known for their counter-illumination photophores which in theory can make the fish almost invisible if the intensity produced by the photophores matches the ambient light levels (Edward Young *et al.*, 1973; Mensinger and Case, 1990)

Conclusions

Use of lowered echosounders and acoustic tracking of several biological trophic levels simultaneously *in situ* in 3D provides a means to study animal ecology, encounters and interactions of undisturbed individuals in their natural environment in the sea. Working with trajectories allows for a more precise measurement of *in situ* clearance volumes as well as behaviours deviating from randomness and probably increasing evolutionary fitness. On this small scale, behaviour is not uniform, but highly depends on several factors that need to be measured *in situ* and understood at the same small spatial and temporal scales in order to understand their effects mechanistically.

Acknowledgements

We thank the crew of G.O Sars for the help in data collection, and Professor Egil Ona for making sure the TS-probe were collecting data properly. The production of the manuscript was funded by the H2020 PANDORA project grant agreement No. 773713, and by the project H2020-MEESO ("Ecologically and economically sustainable mesopelagic fisheries" grant agreement No. 817669).

References

Aksnes, D. L., and Utne, A. C. W. 1997. A revised model of visual range in fish. Sarsia, 82: 137–147.

Aksnes, D. L., Nejstgaard, J., Sædberg, E., and Sørnes, T. 2004. Optical control of fish and zooplankton populations. Limnology and Oceanography, 49: 233–238.

Alvheim, A. R., Kjellevold, M., Strand, E., Sanden, M., and Wiech, M. 2020. Mesopelagic species and their potential contribution to food and feed security—a case study from Norway. Foods, 9: 344.

Ashraf, I., Godoy-Diana, R., Halloy, J., Collignon, B., and Thiria, B. 2016. Synchronization and collective swimming patterns in fish (Hemigrammus bleheri). Journal of the Royal Society Interface, 13.

Bagøien, E., Kaartvedt, S., Aksnes, D. L., and Eiane, K. 2001. Vertical distribution and mortality of overwintering Calanus. Limnology and Oceanography, 46: 1494–1510.

Bañon, R., Arronte, J. C., Rodriguez-Cabello, C., Piñeiro, C. G., Punzon, A., and Serrano, A. 2016. Commented checklist of marine fishes from the Galicia Bank seamount (NW Spain). Zootaxa, 4067: 293–333.

Barraquand, F., and Murrell, D. J. 2013. Scaling up predator-prey dynamics using spatial moment equations. Methods in Ecology and Evolution, 4: 276–289.

Benoit-Bird, K., … M. M.-L. and, and 2017, undefined. 2017. Prey in oceanic sound scattering layers organize to get a little help from their friends. Wiley Online Library, 62: 2788–2798.

Bianco, G., Mariani, P., Visser, A. W., Mazzocchi, M. G., and Pigolotti, S. 2014. Analysis of self-overlap reveals trade-offs in plankton swimming trajectories. Journal of the Royal Society Interface, 11.

Bjelland. 1995. Life-history tactics of two fjord populations of Maurolicus muelleri. Cand. scient. thesis, Univ. Bergen, Department of Fisheries and Marine Biology.

Burns, A. L., Schaerf, T. M., Lizier, J., Kawaguchi, S., Cox, M., King, R., Krause, J., *et al.* 2022. Self-organization and information transfer in Antarctic krill swarms. Proceedings of the Royal Society B, 289.

Christiansen, S., Titelman, J., and Kaartvedt, S. 2019. Nighttime Swimming Behavior of a Mesopelagic Fish. Frontiers in Marine Science, 6.

Christiansen, S., Klevjer, T. A., Røstad, A., Aksnes, D. L., and Kaartvedt, S. 2021. Flexible behaviour in a mesopelagic fish (Maurolicus muelleri). ICES Journal of Marine Science.

Clark, C. W., and Levy, D. A. 1988. Diel vertical migrations by juvenile sockeye salmon and the antipredation window. American Naturalist, 131: 271–289.

Dale, T., Bahr, G., Harendza, A., Velvin, R., Palerud, R., and Szczuciński, W. 2019. Miljøovervåkning i Sørfjorden ved Osterøy. 42.

Davison, P. C., Koslow, J. A., and Kloser, R. J. 2015. Acoustic biomass estimation of mesopelagic fish: Backscattering from individuals, populations, and communities. ICES Journal of Marine Science, 72: 1413–1424.

Demer, D. A., Berger, L., Bernasconi, M., Bethke, E., Boswell, K., Chu, D., and Domokos, R. 2015. Calibration of acoustic instruments. ICES CRR: 133.

Dias Bernardes, I., Ona, E., and Gjøsæter, H. 2020. Study of the Arctic mesopelagic layer with vessel and profiling multifrequency acoustics. Progress in Oceanography, 182: 102260.

Dypvik, E., Røstad, A., and Kaartvedt, S. 2012. Seasonal variations in vertical migration of glacier lanternfish, Benthosema glaciale. Marine Biology, 159: 1673–1683.

Edgington, D. R., Cline, D. E., Davis, D., Kerkez, I., and Mariette, J. 2006. Detecting, tracking and classifying animals in underwater video. OCEANS 2006.

Edward Young, R., E Roper, C. F., Backus, R. H., Craddock, E., Haedrich, R. L., Shores,

D. L., Teal, M., *et al.* 1973. Nature (Lon-don). P. Foxlon, J. Mar. Biol. Assoc. U.K, 11: 20.

Ehrenberg, J. E., and Torkelson, T. C. 1996. Application of dual-beam and split-beam target tracking in fisheries acoustics. ICES Journal of Marine Science, 53: 329–334.

EK80 Scientific wide-band echo sounder - Kongsberg Maritime. 2022. .

Folt, C. L., and Burns, C. W. 1999. Biological drivers of zooplankton patchiness Box 1. Why is scale important?, 14.

Gerritsen, J., and Strickler, J. R. 1977. Encounter Probabilities and Community Structure in Zooplankton: a Mathematical Model. Journal of the Fisheries Research Board of Canada.

Giske, J., Aksnes, D. L., Baliño, B. M., Kaartvedt, S., Lie, U., Nordeide, J. T., Salvanes, A. G. V., *et al.* 1990. Vertical distribution and trophic interactions of zooplankton and fish in Masfjorden, Norway. Sarsia, 75: 65–81.

Giske, J., and Aksnes, D. L. 1992. Ontogeny, season and trade-offs: Vertical distribution of the mesopelagic fish maurolicus muelleri. Sarsia, 77: 253–261.

Gjøsaeter, J., and Kawaguchi, K. 1980. A review of the world resources of mesopelagic fish. FAO Fisheries Technical Paper, 193: 123–134.

Gjøsæter, J. 1981. Variation in Growth Rate and Age at First Maturation in Rainbow Trout; Growth, Production and Reproduction of the Myctophid Fish Benthosema Glaciale From Western Norway and Adjacent Seas; Life History and Ecology of

Maurolicus Muelleri (Gonostomatidae) i. 109–131 pp.

Gong, L., Hu, Z., and Zhou, X. 2022. A real time video object tracking method for fish. *In* ACM International Conference Proceeding Series, pp. 78–84.

Grimaldo, E., Grimsmo, L., Alvarez, P., Herrmann, B., Møen Tveit, G., Tiller, R., Slizyte, R., *et al.* 2020. Investigating the potential for a commercial fishery in the Northeast Atlantic utilizing mesopelagic species. ICES Journal of Marine Science.

Handegard, N. O., Patel, R., and Hjellvik, V. 2005. Tracking individual fish from a moving platform using a split-beam transducer. The Journal of the Acoustical Society of America, 118: 2210–2223.

Handegard, N. O. 2007. Observing individual fish behavior in fish aggregations: Tracking in dense fish aggregations using a split-beam echosounder. The Journal of the Acoustical Society of America, 122: 177–187.

Handegard, N. O., Boswell, K. M., Ioannou, C. C., Leblanc, S. P., Tjostheim, D. B., and Couzin, I. D. 2012. The Dynamics of Coordinated Group Hunting and Collective Information Transfer among Schooling Prey. Current Biology, 22: 1213–1217.

Hays, G. C., Ferreira, L. C., Sequeira, A. M. M., Meekan, M. G., Duarte, C. M., Bailey, H., Bailleul, F., *et al.* 2016. Key Questions in Marine Megafauna Movement Ecology. Trends in Ecology & Evolution, 31: 463–475.

Hersey, J. B., Backus, R. H., and Hellwig, J. 1961. Sound-scattering spectra of deep scattering layers in the western North Atlantic Ocean. Deep Sea Research (1953), 8:

196–210.

Hidaka, K., Kawaguchi, K., Murakami, M., and Takahashi, M. 2001. Downward transport of organic carbon by diel migratory micronekton in the western equatorial pacific: Its quantitative and qualitative importance. Deep-Sea Research Part I: Oceanographic Research Papers, 48: 1923–1939.

Holling, C. S. 1959. Some Characteristics of Simple Types of Predation and Parasitism. The Canadian Entomologist, 91: 385–398.

Holling, C. S. 1966. The Functional Response of Invertebrate Predators to Prey Density. The Memoirs of the Entomological Society of Canada, 98: 5–86.

Hudson, J. M., Steinberg, D. K., Sutton, T. T., Graves, J. E., and Latour, R. J. 2014. Myctophid feeding ecology and carbon transport along the northern Mid-Atlantic Ridge. Deep-Sea Research Part I: Oceanographic Research Papers, 93: 104–116.

Irigoien, X., Klevjer, T. A., Røstad, A., Martinez, U., Boyra, G., Acuña, J. L., Bode, A., *et al.* 2014. Large mesopelagic fishes biomass and trophic efficiency in the open ocean. Nature communications, 5: 3271.

Kaartvedt, S., Aksnes, D., and Aadnesen, A. 1988. Winter distribution of macroplankton and micronekton in Masfjorden, western Norway. Marine Ecology Progress Series, 45: 45–55.

Kaartvedt, S., Knutsen, T., and Holst, J. C. 1998. Schooling of the vertically migrating mesopelagic fish Maurolicus muelleri in light summer nights. Marine Ecology

Progress Series, 170: 287–290.

Kandimalla, V., Richard, M., Smith, F., Quirion, J., Torgo, L., and Whidden, C. 2022. Automated Detection, Classification and Counting of Fish in Fish Passages With Deep Learning. Frontiers in Marine Science, 8: 2049.

Klevjer, T. A., and Kaartvedt, S. 2006. In situ target strength and behaviour of northern krill (Meganyctiphanes norvegica). ICES Journal of Marine Science, 63: 1726–1735.

Klevjer, T. A., Irigoien, X., Røstad, A., Fraile-Nuez, E., Benítez-Barrios, V. M., and Kaartvedt., S. 2016. Large scale patterns in vertical distribution and behaviour of mesopelagic scattering layers. Scientific Reports, 6.

Korneliussen, R. J., Ona, E., Patel, R., Godø, O. R., Giertsen, C., Patel, D., Knudsen, H. P., *et al.* (n.d.). The Large Scale Survey System-LSSS.

Korneliussen, R. J., and Ona, E. 2002. An operational system for processing and visualizing multi-frequency acoustic data. ICES Journal of Marine Science, 59: 293–313.

Korneliussen, R. J., and Ona, E. 2003. Synthetic echograms generated from the relative frequency response. *In* ICES Journal of Marine Science, pp. 636–640.

Korneliussen, R. J. 2010. Large Scale Survey System – LSSS. Database.

Korneliussen, R. J., Heggelund, Y., Macaulay, G. J., Patel, D., Johnsen, E., and Eliassen, I. K. 2016. Acoustic identification of marine species using a feature library. Methods in Oceanography, 17: 187–205.

Kristoffersen, J. B., and Salvanes, A. G. V. 1998. Life history of Maurolicus muelleri in fjordic and oceanic environments. Journal of Fish Biology, 53: 1324–1341.

Lam, V. W. M., and Pauly, D. 2005. Mapping the global biomass of mesopelagic fishes. 4 pp.

Langbehn, T. J., Aksnes, D. L., Kaartvedt, S., Fiksen, Ø., and Jørgensen, C. 2019. Light comfort zone in a mesopelagic fish emerges from adaptive behaviour along a latitudinal gradient. Marine Ecology Progress Series, 623: 161–174.

Lotka, A. J. 1920. Analytical Note on Certain Rhythmic Relations in Organic Systems. Proceedings of the National Academy of Sciences.

Lucas, J., Ros, A., Gugele, S., Dunst, J., Geist, J., and Brinker, A. 2021. The hunter and the hunted—A 3D analysis of predator-prey interactions between three-spined sticklebacks (Gasterosteus aculeatus) and larvae of different prey fishes. PLOS ONE, 16: e0256427.

Makhlouf Belkahia, N., Pagano, M., Chevalier, C., Devenon, J. L., and Daly Yahia, M. N. 2021. Zooplankton abundance and community structure driven by tidal currents in a Mediterranean coastal lagoon (Boughrara, Tunisia, SW Mediterranean Sea). Estuarine, Coastal and Shelf Science, 250: 107101.

Marshall, N. 1951. Bathypelagic fishes as sound scatterers in the ocean. Journal of Marine Research, 10: 1–17.

Martin, L. V., Stanton, T. K., Wiebe, P. H., and Lynch, J. F. 1996. Acoustic classification

of zooplankton. ICES Journal of Marine Science, 53: 217–224.

Martinez-Garcia, R., Fleming, C. H., Seppelt, R., Fagan, W. F., and Calabrese, J. M. 2020. How range residency and long-range perception change encounter rates. Journal of Theoretical Biology, 498: 110267.

MathWorks. 2020. Curve Fitting Toolbox - MATLAB.

Mensinger, A. F., and Case, J. F. 1990. Luminescent properties of deep sea fish. Journal of Experimental Marine Biology and Ecology, 144: 1–15.

Nathan, R. 2008, December 9. An emerging movement ecology paradigm.

O'Dwyer, J. P. 2020. Beyond an ecological ideal gas law. Nature Ecology and Evolution, 4: 14–15.

Okiyama, M. 1971. Early life history of the gonostomatd fish, Maurolicus muelleri (Gmelin), in the Japan Sea. Bull. Jap. Sea Reg. Fish. Lab., 23: 21–53.

Ona, E. 1999. ICES COOPERATIVE RESEARCH REPORT Methodology for Target Strength Measurements (With special reference to in situ techniques for fish and mikro-nekton) International Council for the Exploration of the Sea Conseil International pour 1'Exploration de la Mer.

Ona, E., Zhang, G., Pedersen, G., and Johnsen, E. 2020. In situ calibration of observatory broadband echosounders. ICES Journal of Marine Science, 77: 2954–2959.

Paoletti, S. ;, Rasmus Nielsen, J. ; R., Sparrevohn, R. ;, Bastardie, C. ;, and Vastenhoud,

M. J. 2021. Potential for Mesopelagic Fishery Compared to Economy and Fisheries Dynamics in Current Large Scale Danish Pelagic Fishery. Citation.

Prihartato, P. K., Aksnes, D. L., and Kaartvedt, S. 2015. Seasonal patterns in the nocturnal distributionand behavior of the mesopelagic fish Maurolicus muelleri at high latitudes. Marine Ecology Progress Series, 521: 189–200.

Proud, R., Handegard, N. O., Kloser, R. J., Cox, M. J., Brierley, A. S., and Demer, D. 2019. From siphonophores to deep scattering layers: Uncertainty ranges for the estimation of global mesopelagic fish biomass. ICES Journal of Marine Science, 76: 718–733.

Qian, Z. M., and Chen, Y. Q. 2017. Feature point based 3D tracking of multiple fish from multi-view images. PLOS ONE, 12: e0180254.

Rasmussen, O. I., and Giske, J. 1994. Life-history parameters and vertical distribution of Maurolicus muelleri in Masfjorden in summer. Marine Biology, 120: 649–664.

Rieucau, G., Holmin, A. J., Castillo, J. C., Couzin, I. D., and Handegard, N. O. 2016. School level structural and dynamic adjustments to risk promote information transfer and collective evasion in herring. Animal Behaviour, 117: 69–78.

Rothschild, B., Research, T. O.-J. of plankton, and 1988, undefined. 1988. Small-scale turbulence and plankton contact rates. academic.oup.com, 10: 465–474.

Salvanes, A. G. V., Aksnes, D., Fosså, J. H., and Giske, J. 1995. Simulated carrying capacities of fish in Norwegian fjords. Fisheries Oceanography, 4: 17–32.

Scoulding, B., Chu, D., Ona, E., and Fernandes, P. G. 2015. Target strengths of two abundant mesopelagic fish species. The Journal of the Acoustical Society of America, 137: 989–1000.

Simmonds, J., and MacLennan, D. 2007. Fisheries acoustics: Theory and practice: Second edition. 1–252 pp.

Sobradillo, B., Boyra, G., Martinez, U., Carrera, P., Peña, M., and Irigoien, X. 2019. Target Strength and swimbladder morphology of Mueller's pearlside (Maurolicus muelleri). Scientific Reports, 9.

St.John, M. A. S., Borja, A., Chust, G., Heath, M., Grigorov, I., Mariani, P., Martin, A. P., *et al.* 2016. A dark hole in our understanding of marine ecosystems and their services: Perspectives from the mesopelagic community. Frontiers in Marine Science, 3.

Staby, A., Srisomwong, J., and Rosland, R. 2013. Variation in DVM behaviour of juvenile and adult pearlside (Maurolicus muelleri) linked to feeding strategies and related predation risk. Fisheries Oceanography, 22: 90–101.

Standal, D., and Grimaldo, E. 2020. Institutional nuts and bolts for a mesopelagic fishery in Norway. Marine Policy, 119: 104043.

Tomaru, T., Murakami, H., Niizato, T., Nishiyama, Y., Sonoda, K., Moriyama, T., and Gunji, Y. P. 2016. Information transfer in a swarm of soldier crabs. Artificial Life and Robotics, 21: 177–180.

Torgersen, T., and Kaartvedt, S. 2001. In situ swimming behaviour of individual mesopelagic fish studied by split-beam echo target tracking. ICES Journal of Marine Science, 58: 346–354.

Utne-Palm, A. C. 2002. Visual feeding of fish in a turbid environment: Physical and behavioural aspects. Marine and Freshwater Behaviour and Physiology, 35: 111–128.

Volterra, V. 1926. Variazioni e fluttuazioni del numero d'individui in specie animali conviventi. Memoria della regia accademia nazionale del lincei ser.

Webb, T. J., vanden Berghe, E., and O'Dor, R. 2010. Biodiversity's big wet secret: The global distribution of marine biological records reveals chronic under-exploration of the deep pelagic ocean. PLoS ONE, 5.

10 Paper III

Deviations from functional predation responses

Light and anti-predator behaviour are more important than density in encounters between the mesopelagic fish and its prey

Kjetil Gjeitsund Thorvaldsen , Stefan Neuenfeldt, Helena Hauss, Patrizio Mariani & J. Rasmus Nielsen

Abstract

Understanding trophic interactions in the mesopelagic zone is important in both ecological and potential commercial exploitation context. Trophic interactions between mesopelagic fish *Maurolicus muelleri* and their prey *C. finmarhicus*, as well as the large scale behaviour of both species, have been studied together with light intensity and prey density. However, there is only limited knowledge on how individual *in situ* 3D-behaviour of *C. finmarhicus* is influencing encounters when co-occuring with the predator *Maurolicus muelleri*. We successfully tracked single individuals of *C. finmarchicus* in situ, parametrized their different swimming behaviour at different depths, and calculated their scale dependent self-overlap (ψ) based on the specific paths generated by their movement. We found that swimming activity were higher in the surface layers ($\psi<0.1$) with higher ambient light levels and where predation of *C. finmarhicus* typically occur. This explains

why juvenile *Maurolicus* chose to migrate to a depth layer with lower *C. finmarhicus* density to forage.

Key words: Encounters, Target tracking, *Calanus Finmarchicus, Maurolicus Muelleri*

Introduction

Encounters play a critical role in animals' life histories and behaviour, facilitating feeding, mating and predation (Rothschild *et al.*, 1988; Nathan, 2008). However, quantifying encounter rates is challenging. Another approach to understand predator-prey relationships is theoretical modelling (Lotka, 1920; Volterra, 1926; Fasham *et al.*, 1990; Berryman, 1992), where encounters are assumed proportional to the product of predator and prey densities. In typical functional response models, density and prey-handling time are the main parameters (Holling, 1959, 1966; Rothschild et al., 1988). Yet, it is widely known both from terrestrial (Tablado et al., 2014) and marine ecology that encounter rates are influenced by many factors (Eiane et al., 1999; Aksnes et al., 2004; Neuenfeldt and Beyer, 2006). Light has for example been included in some visual predation models as explanatory variable to modify encounter rates as the size of the effective search volume depends on it (Huse and Fiksen, 2010; Staby et al., 2013). The factors that determine encounters and hence ultimately predator growth and prey mortality, vital parameters shaping their respective population dynamics, are still challenging to measure in situ in the ocean. However, we need a mechanistic understanding of interactions

between predator and prey, and how different internal and external factors influences this, to improve our encounter models. Here, state of the art acoustic technologies provide new opportunities in previously unaccessible habitats.

Mesopelagic layers layers (from the base of the euphotic zone to 1000m depth) are an almost global zone in all the world's oceans, and are presumed to be one of the world's largest habitat in volume (Duvall and Christensen, 1946; Dietz, 1962; Knutsen et al., 2017), likely holding the world's largest vertebrate biomass (Gjøsaeter and Kawaguchi, 1980; Lam and Pauly, 2005; Irigoien et al., 2014; Proud et al., 2019). The mesopelagic zone is conveyed as important for key ecosystem services (Davison *et al.*, 2013; St.John *et al.*, 2016; Proud *et al.*, 2017) and also potentially in commercial and food provisioning context (Standal and Grimaldo, 2020; Paoletti et al., 2021; Grimaldo et al., 2022), serving both as an ecological link between primary production and commercially important species such as for example blue whiting *(Micromesistius poutassou*), as well as a potential source of fishmeal as well as protein and lipids for human consumption (Olson *et al.*, 2014; Howey *et al.*, 2016; Duffy *et al.*, 2017; Battaglia *et al.*, 2018) Mesopelagic fish also play a significant role in active carbon sequestering between the atmosphere, surface layers and the deep sea, and thus in regulating the global climate (Davison *et al.*, 2013; St.John *et al.*, 2016).

In mesopelagic communities, light conditions determine the depth distribution and densities of the biological acoustic back-scattering layers on a global scale(Bianchi and Mislan, 2016), with large variations according to regional and seasonal ambient light levels

(Kaartvedt *et al.*, 2019). Mesopelagic fishes use the so called anti-predator window for efficient foraging while hiding at depth, since light and turbidity play large roles in successful foraging for visual predators (Aksnes and Utne, 1997; Utne-Palm, 2002).

The predator-prey relationship between the pearlside *Maurolicus muelleri,* an abundant mesopelagic fish, and the dominant large copepod *C. finmarhicus* is varying throughout the year in Norwegian fjords. During spring and summer, some *Calanus finmarchichus* are vertically migrating from darker waters to the surface feeding on phytoplankton (Falk-Petersen *et al.*, 2009), and being preyed upon in the surface by visually foraging mesopelagic fishes, pearlside and glacier lanternfish *(Benthosema glaciale*) , mostly during dusk and dawn(Gjøsæter, 1973, 1981; Giske *et al.*, 1990; Balino and Aksnes, 1993; García-Seoane *et al.*, 2013; Staby *et al.*, 2013; Thorvaldsen *et al.*, 2022a). During winter, *Calanus finmarchichus* enter diapause and migrate permanently to deeper waters, staying inactive throughout the winter at larger depths to reduce predation (Kaartvedt, 1996; Bagøien *et al.*, 2001). However, it is known that many species of copepods have flexibility in their feeding strategies (Kleppel, 1993; Campbell *et al.*, 2009; Hobbs *et al.*, 2020) feeding on protists (Campbell *et al.*, 2009) or cannibalism (Bonnet *et al.*, 2004; Basedow and Tande, 2006), enabling foraging in the surface during winter. Pearlside have different strategies for feeding throughout the year. During summer, adult pearlside migrate towards the surface between dawn and dusk to feed on mainly *C. finmarhicus* (Kinzer, 1977; Gjøsæter, 1981; Roe *et al.*, 1984; Staby *et al.*, 2013), while during winter the juvenile pearlside form a layer above the adults at typically 70 meters, feeding throughout the winter(Balino and Aksnes, 1993; Prihartato *et al.*, 2015;

Thorvaldsen *et al.*, 2022a). form a layer above the adults, potentially as they can afford to prevail in a higher ambient light intensity, as smaller fish are harder to visually detect (Giske *et al.*, 1990; Aksnes and Utne, 1997; Staby *et al.*, 2013) Both pearlside and many species of copepods are known to move in convoluted patterns that can provide both protection and forage opportunities (Bianco *et al.*, 2014; Thorvaldsen *et al.*, 2022a). Vertical movement patterns have been studied widely both on population scale (Staby and Aksnes, 2011; Staby *et al.*, 2013; Prihartato *et al.*, 2015) and individual scale (Torgersen and Kaartvedt, 2001; Kaartvedt *et al.*, 2008; Christiansen *et al.*, 2019, 2021). However, individual copepod behaviour experiments are usually conducted in a laboratory setup (Visser and Kiørboe, 2006; Bianco *et al.*, 2014; Michalec *et al.*, 2015; Chen and Hwang, 2018), as observing behaviour in situ have been historically challenging. .Methodologies observing feeding and predation in marine fishes consist usually of fishery or survey catches combined with stomach samples (Kristoffersen and Salvanes, 1998; Staby et al., 2013). However, Mesopelagic fishes are also challenging to observe in a laboratory as they can't handle either the capture process or survive in the laboratory (Salvanes and Kristoffersen, 2001).

In the current study, for different depth layers representing variable light conditions, we acoustically followed individual *C. finmarhicus* in the vicinity of individuals of their predator pearlside, measured their respective densities, and quantified their behaviour in terms of self-overlap of their swimming trajectories, and velocity. Based on these measurements, we calculated relative encounter probabilities for predator and prey

between depth layers and prioritised the relative roles of light, prey density and spatial behaviour of the prey.

Material & Methods

Despite their often very shallow sill depth of a few tens of meters, many Norwegian fjords enclose mesopelagic habitats that contain a community encompassing mesopelagic fishes and other micro nekton. Due to the calm surface conditions, they are an ideal environment to deploy in situ observational gear. The study site, Sørfjorden, is a fjord in western Norway (N 60.43, E 5.62) and a part of the fjord system covering Osterøy, with maximum depth of 425 meters. This fjord has a widely studied ecosystem and the populations of mesopelagic organisms and mesozooplankton are studied both with regards to biological composition, and trophic interactions on several occasions (Salvanes *et al.*, 1995; Bagøien *et al.*, 2001; Kaartvedt *et al.*, 2008; Folkvord *et al.*, 2016, Thorvaldsen et al.,2022). Environmental properties and hydrographical parameters of the fjord water layers were measured with a seabird- CTD profiler (Supplementary Material, SM, Figure 1). Relative light intensities were calculated theoretically using prescribed light extinction in water.

Biological sampling

Vertically stratified zooplankton samples were collected using a Hydrobios Multinet Mammoth (1 m^2 mouth area, mesh size 300µm, nine nets) in an oblique tow

(2kn) during darkness from 242 m to the surface. The surface net was twisted, and therefore eight samples analysed in the depth strata 242-210-180-150-125-100-75-50-25m. The catch were scanned on an Epson V750 flatbed scanner at 2400 dpi, and further processed using the ImageJ macro set Zooprocess (Gorsky *et al.*, 2010) before being uploaded to the Ecotaxa web-based classification and archive platform (Picheral *et al.*, 2017.), where a deep learning prediction into 14 taxonomic categories (Actinopterygii, Amphipoda, Chaetognatha, Decapoda, Euphausiacea, Hydrozoa, Siphonophorae, Ostracoda, *Oithona*, *Oncaea*, *Centropages*, *Calanus*, Metridinidae and unidentified calanoid copepods) as well as detritus and artifacts (such as air bubbles), followed by manual validation, was carried out. Images are available on https://ecotaxa.obs-vlfr.fr/prj/6145. Exported data were used to estimate individual biomass of zooplankton based upon individual image area using taxon-specific functions according to Lehette & Hernandez-Leon (2006) and aggregated to depth layers by sample. Code used is available on Github (https://github.com/lenihauss/GOSars_multinet). There were no measurements in the upper 25 meters. Both biomass and numerical density (ind. m^{-3} *)* were calculated for all taxonomic groups. For comparison between net samples and acoustic observationsdensity was also estimated by counting accepted acoustic "Calanus" trajectories within the effective sampling volume where where number of counted targets in 2m vertical depth bins were divided on the beamvolume giving individuals m^{-3}.

Collecting acoustic single tracks of *Calanus finmarchicus* with the TS-probe

Trajectories of *C. finmarhicus* were collected with a Simrad EK80 ('EK80 Scientific wide-band echo sounder - Kongsberg Maritime', 2022) echosounder mounted on an acoustic probe that from now on is referred to as the TS-probe (for target strength probe). The TS-probe is an observation platform equipped with echosounders used to measure acoustic properties of aquatic organisms at close range (Dias Bernardes *et al.*, 2020, Thorvaldsen 2022). The applied frequencies on this study were 160-260 kHz using broadband echosounders, looking downward (so, dorsally on horizontally swimming targets) with a ping-rate of 4 Hz (Figure 1). The transducers were calibrated after ICES-standards (Sm table 1). The TS-Probe was deployed from the hangar of research vessel G.O Sars, and were controlled by a hydraulic winch and a fibre-optic cable attached to the TS-Probe to transfer signals (Figure 1). Mean volume backscattering strength (Sv (dB re 1 m^{-1})) used for echo integration (Simmonds and MacLennan, 2007), and Target strength which is the reflectivity of a single target (dB re 1 m^{-1}))(Simmonds and MacLennan, 2007), were measured *in situ*. Backscatter properties were observed in real time on the vessel trough the fibre optic cable.

After collection of raw acoustic data, trajectories were initially created applying a target tracking algorithm (Handegard *et al.*, 2005; Handegard, 2007) which is included in the acoustic data post processing software LSSS (Large Scale Survey System, Korneliussen, 2010; Korneliussen *et al.*, 2016) . Acoustic target tracking was performed in

all three depth layers with measurements from 5-25 meter vertical distance from the transducer which means that each depth layer covered were (25-45 m, , 75-95 (Figure 1) and 125-45 meters (Figure 1), from now on referred as depth layers 1, 2 and 3, respectively. Each depth layer was monitored for approximately 10 minutes. Angular positions of each track calculated by the split beam echosounder (alongship, atwarthship, depth and TS per ping) were further used to create trajectories. All echograms were initially inspected visually before applying the tracking algorithm. The applied TS threshold range for analyses were set to between 70-130 dB (supplementary table 2) to be able to observe all groups of zooplankton as *C. finmarhicus* are known to be weak scatterers (Sakinan *et al.*, 2019), and after observing large deviations in TS after initial trials on the data, where TS meausurements have large individual variations when *C.finmarchicus* are moving upwards and downwards (SM, figure 2).

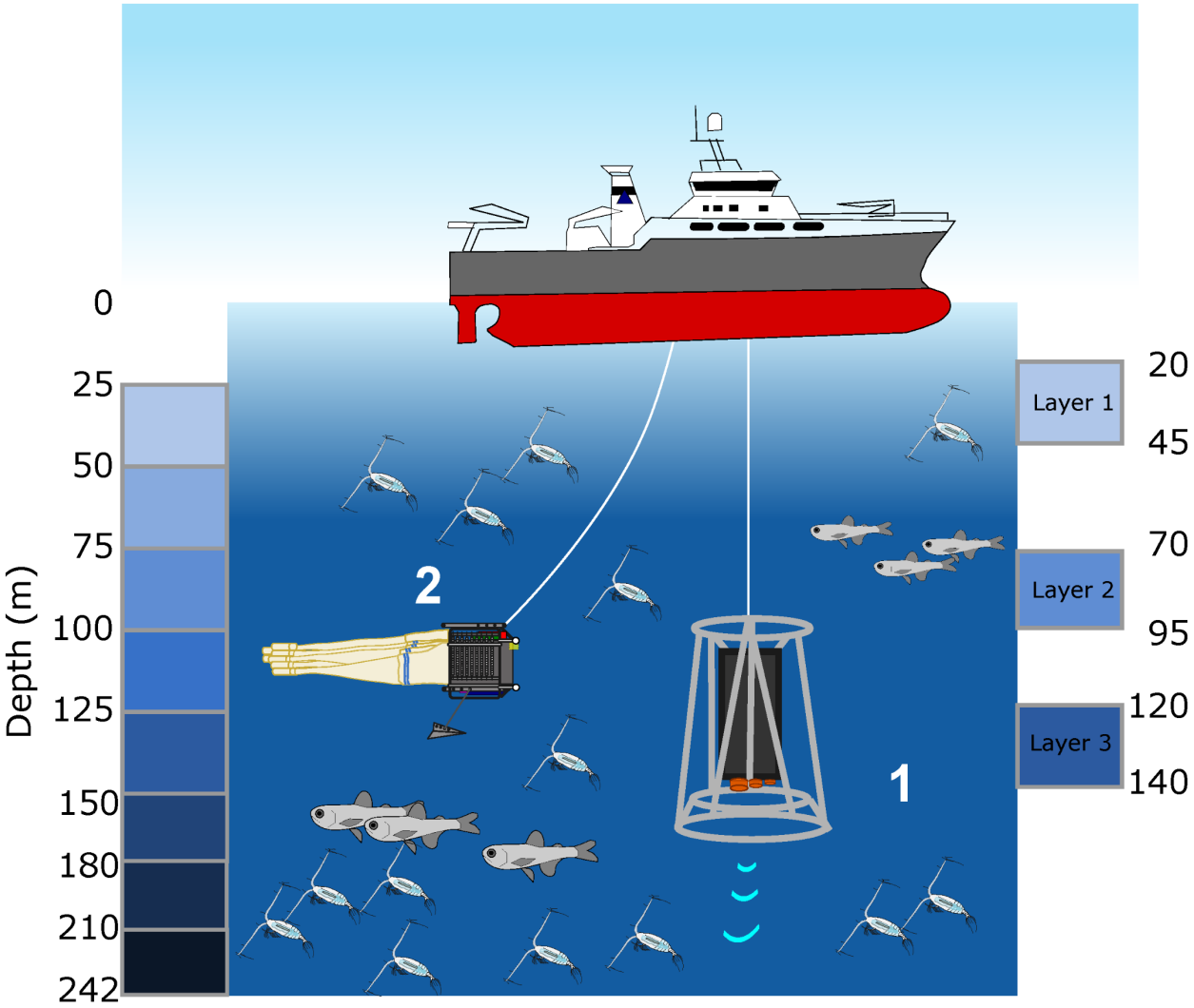

Figure 1: Simplified illustration of the deployment of the TS-probe (1), where the TS-probe is lowered to three depth layers of 20-45 meters, 70-95 meters and 120-145 meters which are marked on the right y-axis. The Hydrobios Mammoth multinet (2) were deployed and depth bins-sampled are seen on the left y-axis. The animal illustrations represent pearlside and *C.finmarchicus*.

The main two steps in the tracking algorithm are initiation and association. Initiation is the creation of new tracks based on the range from a previous terminated track to a new track (r_g), along (α_0) and atwartship angles (β_0) within the acoustic beam, as well variation in dB between a new initiated track and a previous terminated track (I_0). The next

step is to assosciate the track for each subsequent ping. The track assosciation settings follow the same principles but for subsequent detections within the track (r_g α_g , β_g and I_g). The initiation and association along α_0, α_G and atwarthship β_0 ,β_G cut off angles for target tracking were set to 2.8 degrees. The initiation range were set to r_0 =0.44 m, while the association range were set lower r_g =0.2m after observing the tracks.

I_0 and I_g were set to 30 dB, as the algorithm initially failed to track the C.finmarhicus while moving downwards (SM Figure 2), this was done as initial inspection of TS per ping for the trajectories had large variation when the *C. finmarhicus* where migrating upwards vs downwards(SM Figure 2). These large value for TS-deviation were justified to observe the tracks for longer periods, capturing more of the behaviour. For all tracks, the maximum number of missing detections and samples within a track was set to 8, and the maximum ratio of missing detections to the total number of detections in a track was set to 0.8.

Scrutinizing of acoustic data

Acoustic trajectories were allocated to species *C. finmarhicus* after scrutinizing TS-measurements. Echo-counting derived densities was compared with the densities of *C. finmarhicus* caught in the multinet (Figure 2b, orange line for *C. finmarhicus* density from multinet and purple dots for densities derived from echo counting). The target strength values derived from the trajectories were compared with a theoretical estimations of TS for *C. finmarhicus* predicted by a DWBA-model (Distorted Wave Born Approximation) estimating TS for *C. finmarhicus* with and without a lipid deposit. Predicted backscatter values of the model and *C. finmarhicus* target strength was predicted to be higher when the lipid deposits are high, estimating TS close to -90 dB at 200 kHz (Sakinan *et al.*, 2019),

agreeing with the in situ TS-measurements. Most specimens classified as *C. finmarhicus* from the multinet samples were between 1.5 and 3mm (Figure 2b) total length and between 200 and 300µg calculated dry weight. On many images, lipid reserves were visible (Fig. 1c). Densities derived from the oblique haul was compared with densities derived from the acoustic echo counting. The only species that were in the same order of magnitude between the two measurement methods was *C. finmarhicus* (Figure 2a). After studying both 2D and 3D trajectories, it was concluded that many of the swimming patterns were typical of copepods in a hop-and-sink mode (Figure 3d and e)).

Quantifying 3D behaviour by measuring self-overlap

After applying the tracking algorithm, trajectories were visually inspected in LSSS. Track split errors occurred with some frequency, and tracks were re-joined by using the "merge tracks" function in LSSS based on visual inspection of fragmented tracks in the echogram and by checking angular positions and TS of the track. Erroneous measurements seen as spikes in x,y or z value >30 cm and or large changes in TS probably stemming from accidental measurements of other targets were manually removed. Along and athwartship angular positions are more prone to positional errors (Simmonds and MacLennan, 2007), hence a smoothing spline over time was used to compute the final positions in x, y and z direction. A piece-wise polynomial smoothing spline in MatLab (MathWorks, 2020) was used with smoothing parameter $p = 0.1$.

These 3D tracks were used in a self-overlap analyses using the method developed in (Bianco *et al.*, 2014) . The scale dependent self-overlap, $\psi(r)$ was calculated for a range of detective radiuses (r) as:

$$\psi(r) = 1 - \frac{V(r)}{V_{max}(r)} \qquad (1)$$

Here, r is the distance from the track position which is also a measure of the encounter radius. $V(r)$ is the effective swept volume by the organism based on different encounter radius, and $V_{max}(r)$ is the maximum volume that can be scanned as function of r. The maximum volume is computed as:

$$V_{max}(r) = \pi r^2 L + \frac{4}{3}\pi r^3 \qquad (2)$$

If the trajectory is a complete straight line then $V(r) = V_{max}(r)$. Howerver, usually animals' trajectories are convoluted and there is some portion of the swept volume, V(r), which is overlapping with volumes of water that were already scanned. The self-overlap is then providing a scale dependent function bounded within the range of zero (no overlap) and one (full overlap), i.e., $0 \leq \psi(r) \leq 1$.

A Monte-Carlo method was used to calculate $V(r)$ (Bianco et al. 2014). We first introduced a maximum radius for the calculation, i.e. the visual range $r\_max = 100\ cm$, and then for each trajectory computed the bounding box $x_{min} - r_{max} < x < x_{max} + r_{max}$ where x_{min}, x_{max} are respectively the minimum and the maximum value of the trajectory along the x coordinate. Similarly, minimum and maximum values are used for the other coordinates on the y and z axes, and finally the volume of the box V_{box} is calculated. We then drawed $NP = 2 \cdot 10^9$ random points within the bounding box and calculated the histogram of the number of points, i.e., $n(r)$, falling within a distance less than a given radius r from the trajectories with the minim radius at $r_{min} = 1\ cm$, and $r_{min} \leq r < r_{max}$. Note that the

distance is measured using the interpolating segment between two consecutive points on the trajectory. Given the large number of random points we can then effectively estimate the volume as:

$$V(r) = \frac{n(r)}{NP} V_{box}. \quad (3)$$

When applying the method to the dataset, we checked that the trajectories had sufficient high number of pings, and for sufficient length of time, so that the results are stationary and not too influenced by the behaviour at the endpoints of the tracks.

Scrutinizing of acoustic data

Acoustic trajectories were allocated to species *C. finmarhicus* after scrutinizing TS-measurements. Echo-counting derived densities was compared with the densities of *C. finmarhicus* caught in the multinet (Figure 2b, orange line for *C. finmarhicus* density from multinet and purple ”x” for densities derived from echo counting). The target strength values derived from the trajectories were compared with a theoretical estimations of TS for *C. finmarhicus* predicted by a DWBA-model (Distorted Wave Born Approximation) estimating TS for *C. finmarhicus* with and without a lipid deposit. Predicted backscatter values of the model and CF target strength was predicted to be higher when the lipid deposits are high, estimating TS close to -90 dB at 200 kHz(Sakinan *et al.*, 2019), agreeing with the in situ TS-measurements. All specimen caught in the multi-net had a high degree of lipid depositsDensities derived from the oblique haul was compared with densities derived from the acoustic echo counting. The only species that were in the same order of

magnitude between the two measurement methods was *C. finmarhicus* (Figure 2a). After studying both 2D and 3D trajectories, it was concluded that many of the swimming patterns were typical for copepods (SM Figure 2).

Calculating relative values influencing encounters

In an attempt to observe how different parameters might impact encounters for *C.finmarchicus* relative density, relative irradiance at depth and relative self overlap were calculated. For light intensity, the surface irradiance were set to 1 and irradiance were a relative value between 0 and 1. And calculated by using the exponential decay model for irradiance in sea-water

$$I_z = I_0 e^{(-k_z)} \quad (4)$$

Where I_z is relative irradiance at the depth z, I_0 is surface irradiance which equals 1 and k is the attenuation factor. The attenuation factor were set to 0.05, 0.025, 0.0125 and 0,00625, where previous estimates from norwegian fjords in winter is close to .

Relative values of light intensity $R(I_z)$, density $R(\rho)$, and self overlap $R(\psi)$ were calculated

$$R(I_z) = \frac{I_{layer(x)}}{I_{layer(1)}} (5)$$

$$R(\rho) = \frac{\rho_{layer(x)}}{\rho_{layer(1)}} (6)$$

$$R(\psi) = \frac{\psi_{layer(x)}}{\psi_{layer(1)}} (7)$$

3 Results

Biological composition derived from oblique hauls and acoustic echocounting

The fish-component in the acoustic backscattering has already been resolved to be consisting of juvenile pearlside, adult pearlside and lanternfish and echo-traces from larger fish (Thorvaldsen *et al.*, 2022a)where only juvenile pearlside were migrating towards the surface. The mesozooplankton was dominated in numbers by copepods (small unspecified calanoid copepods, *Oithona sp.* and *C. finmarhicus* , with *C. finmarhicus* dominating total mesozooplankton biomass. *Oithona* was mainly found in the upper part of the water column (25-75 m), and small calanoids were numerically dominating in all depth layers, while *C. finmarhicus* was dominating in total biomass. In lower abundances (less than 1 m^{-3}), other large copepods such as *Metridia* sp., *Centropages* sp. and *Pareuchaeta* sp. were found. *C. finmarhicus* was present in all depth layers with low densities in the surface and higher densities below 125 meters dominating in biomass here with individuals between 1.5 and 3 mm body length (supplementary Figure 3). The numerical abundance of all other taxa at the study site was low (Figure 2a). The echocounting-derived densities were 3, 4.3 and 5.6 tracks per cubic meter at 20-45, 70-95 and 120-145 meters depth, respectively (Figure 2a).

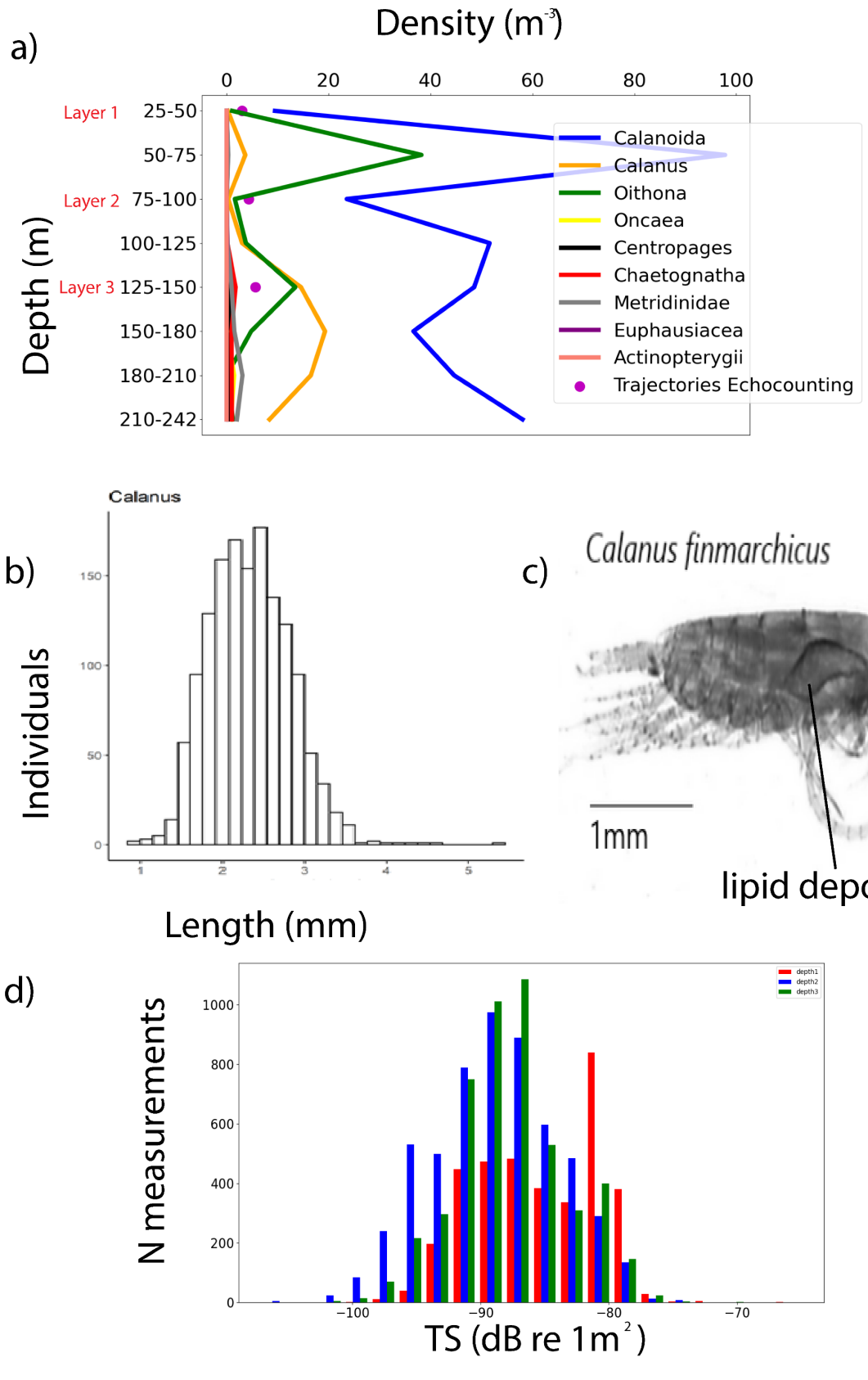
a)
Density (m-3)
0
20
40
60
80
100
Depth (m)
Layer 1
25-50
50-75
Layer 2
75-100
100-125
Layer 3
125-150
150-180
180-210
210-242
Calanoida
Calanus
Oithona
Oncaea
Centropages
Chaetognatha
Metridinidae
Euphausiacea
Actinopterygii
Trajectories Echocounting
b)
Calanus
Individuals
Length (mm)
c)
Calanus finmarchicus
1mm
lipid deposit
d)
N measurements
TS (dB re 1m2)
depth1
depth2
depth3

Figure 2. Panel a shows the density of mesozooplankton and micronekton groups (ind. m^{-3})caught with the multinet oblique hauls for each 25-mm depth bin, except the surface, as well as the three mean densities estimates for *C. finmarhicus* by echo counting. Panel b shows the length distribution for the caught specimen of *C. finmarchicus*. Panel c shows a specimen of *Calanus finmarchicus* with a lipid reserve representative for the total catch. Panel d shows the TS-distribution (dB re m^{-1}) compiled for all trajectories obtained by the target tracking algorithm where layer 1,2 and 3 is shown as red, blue and green bars respectively

Acoustic track characteristics

The average TS of the accepted–trajectories from the acoustic target tracking algorithm was -83 dB (20-45 m), -86 dB (70-95 m) and -85.6 dB (120-145m) with some higher measurements in layer 1 (Figure 2b, red bars), and showed a clear bell shaped distribution around -90 dB for all depth bins (Figure 2b). The accepted trajectories of *C. finmarhicus* showed distinct characteristic swimming patterns in all 3 layers: Present in all layers, but especially present in layer 1 and 2, *C. finmarhicus* were swimming in a very specific manner in the vertical plane. *C. finmarhicus* were performing ascents and descents of 20 cm where ascents and descents were equally long both in time and vertical change (Figure 3d-e). The sharp transition between ascent and descent, combined by visual inspection of fish trajectories (Figure 3e) excludes the possibility of the trajectories being caused by waves. During ascents and descents the TS varies as much as 20 dB (SM Figure 2) usually reaching a peak in TS when *C. finmarhicus* stops swimming upwards and start to sink or swim downwards. Most of the accepted tracks was large both in the horizontal and vertical dimension (Figure 3a-c, Figure 4), which should be seen in context of most trajectories were longer than one meter (Figure 4). In the upper layer, there were some *C.*

finmarhicus individuals that moved downwards more than 2 meters (Figure 4, track No.1, 3 & 11) while most *C. finmarhicus* inviduals move less than 1 meter vertically. Many *C. finmarhicus* individuals were performing loops (Figure 4 Track nr 1,2 and 4). While other *C. finmarhicus* moved almost on a straight line over long distances followed by some more convoluted behaviour with examples in Figure 4 (tracks No. 5, 6 & 9).

In layer 1, *C. finmarhicus* on average performed more sink and swim behaviour ("jumps") compared to layer 2 and 3. The jump frequency at the upper layer were on average 2.54 jumps minute^{-1} compared to 1.5 and 1.1 jumps minute^{-1} in layer 2 and 3 (Table 1). The vertical behaviour were varying both between individuals and different depth layers (Figure 3 d-f). Some individuals moved vertically with vertical speeds as high as 1.7 m/min. This swimming behaviour was observed both for individuals swimming upwards and downwards. The largest changes in vertical speed were observed in the upper layer with an average downwards movement of -0.27 m per minute compared to -0.08713 m downwards movment per minute in layer 2 and 0.055 m upwards movement in layer 3. All values higher than 1m s^{-1} occurred in layer 1. Furthermore, it was evident that all layers had both trajectories of copepods and fish (Figure 3a-c)(Thorvaldsen *et al.*, 2022a).

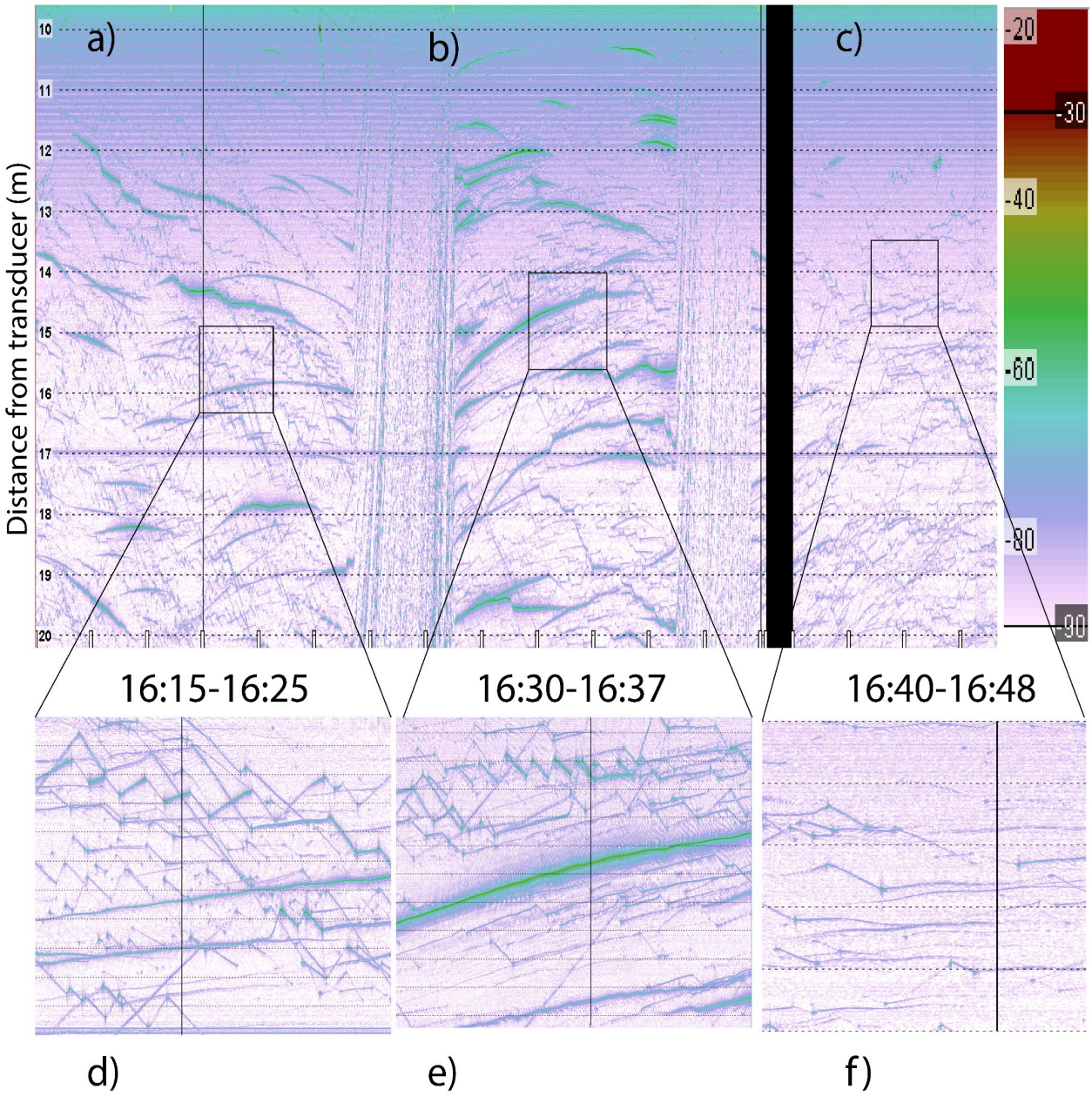

Figure 3. Echogram recorded by the TS-probe. The x-axis of the echogram shows time in hours and minutes and the y-axis the vertical distance from the transducer where the resolution is 4 Hz. Panels a), b) and c) are showing echograms from 30-40 m, 80-90 m, and 130-140 m total water depth, respectively. Panels d) and e) and f) are zoomed in selected parts of each echogram showing *C. finmarhicus* trajectories as thin lines seen in d), e) and f), and fish targets in e) with thicker lines. The parts of the echogram between a), b)

and c), where trajectories appear to move simultaneously upwards is just due to the Probe being lowered to the next depth layer, thus targets moving upwards.

Table 1. Parameterization of *Calanus finmarchicus* trajectories

Depth (m)	Jump frequency average (jumps min^{-1})	Standard deviation(m)	Average change in vertical position	Deviation(m)
20-45	2.54	1.92	-0.27	1.02
70-95	1.50	1.46018	-0.088	0.37
120-145	1.12	1.58	0.056	0.4

Trajetories 20 meters	Trajectories 70 meters	Trajectories 120 meters
1 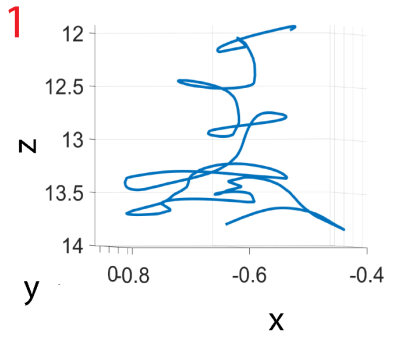	5 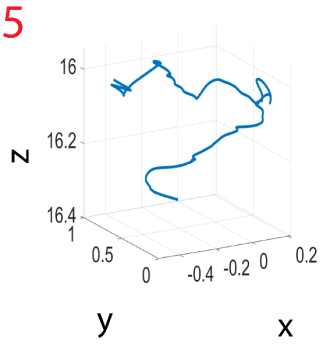	9 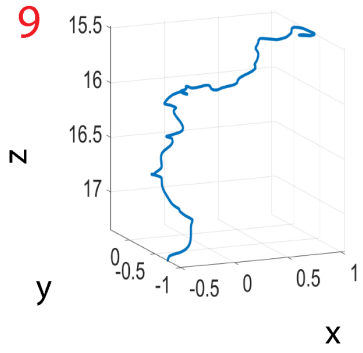
2 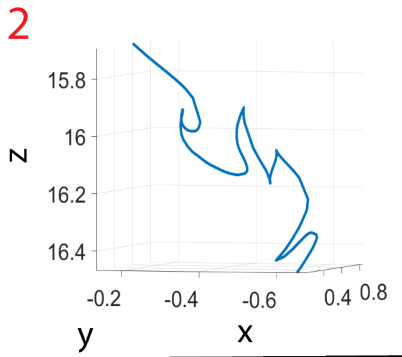	6 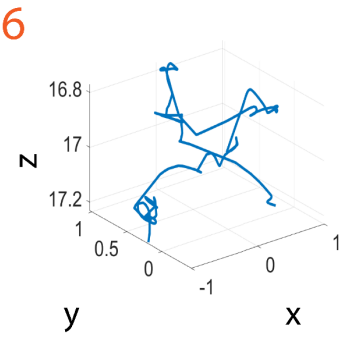	10 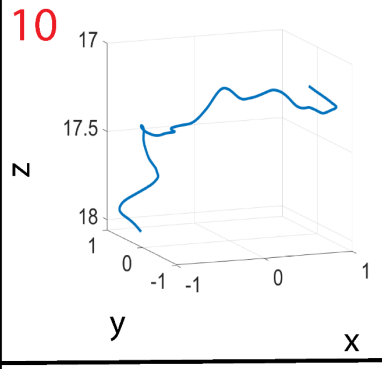
3 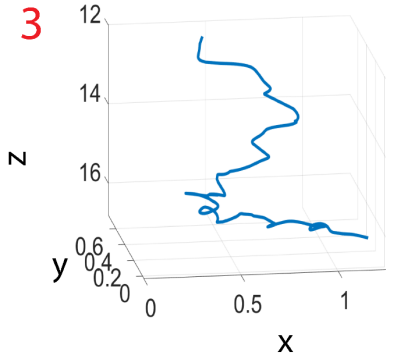	7 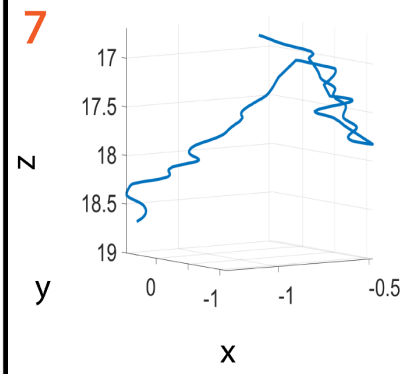	11 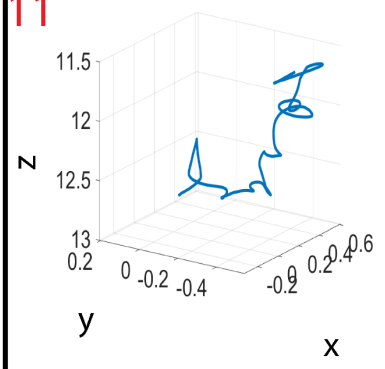
4 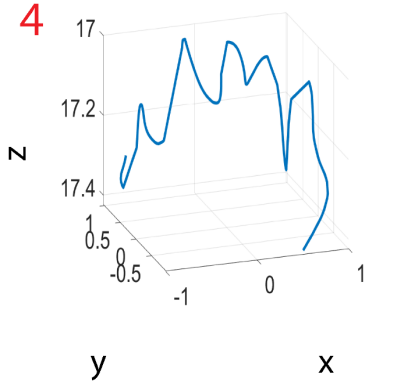	8 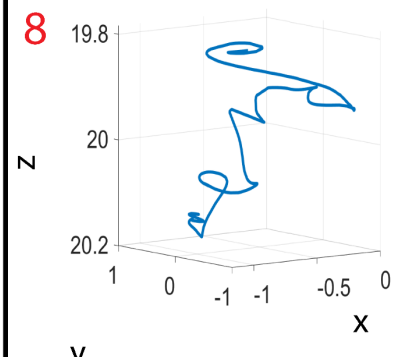	12 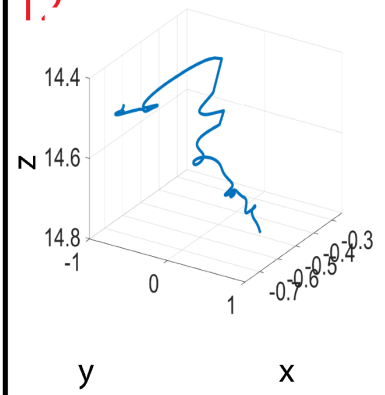

Figure 4. Selected trajectories. The columns show 4 tracks from each depth layer of the TS-probe (20-45 m tracks 1-4, 70-95 m tracks 5-9 and 120-145 m tracks 9-12). The x-axis is alongship position (m), y is athwartship position (m) and z is the vertical distance from transducer (m) with the transducer depth listed on the top of the figure panels providing total water depth when combining transducer depth and vertical position from the transducer.

Self-overlap measurements and relative estimations

The average self-overlap for depth layer 1 was ~0 at a detective radius of 1 cm, 0.05 at 10 cm and 0.15 at 1 m, while the average self-overlap in layer 2 was 0, 0.2 and 0.3 at detective radiuses of 1, 10 and 100 cm, respectively, while self-overlap in layer 3 was 0, 0.1 and 0.2 at 1, 10 and 100 cm. The degree of self-overlap was low in all depth layers and at all measured ranges, but it was higher in especially layer 2 compared to layer 1. The relative values of light intensity were highest in the surface and declining at various rates depending on the light attenuation factor K (Figure 6a), the relative self overlap were 4.5 times higher in layer 2 compared to layer 1 for 10 cm detection radius, while ~2 times higher for detective radiuses for 100 cm in layer 2. While relative self overlap were 2.5 times higher for 10 cm and 1.5 higher for 100 cm in layer 3 compared to layer 1(Figure 6b). The relative density were 1.4 times higher in layer 2 and 1.8 times higher in layer 3 (Figure 6c)

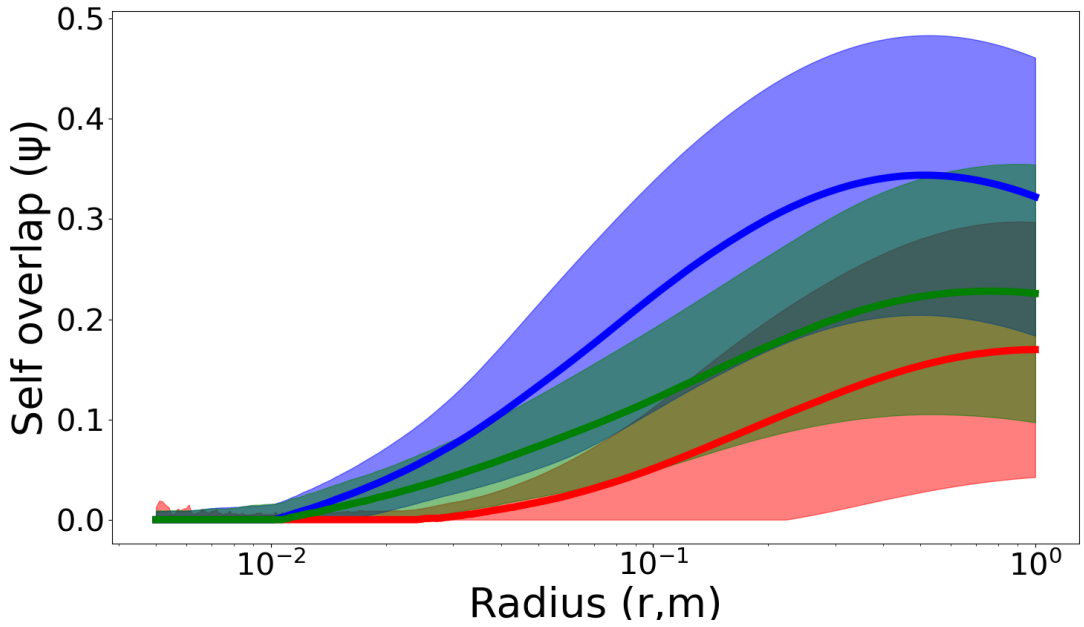

Figure 5. The upper panel a is the derived self-overlap (from Equation 1) for all trajectories. On the x-axis detective radius (r) is displayed on a logarithmic scale and on the y-axis the self-overlap (psi) is shown where 1 is full self-overlap and 0 is no self-overlap. Red, blue and green color lines represent depth layers 1, 2 and 3, respectively. The lower panel b shows mean self-overlap for the tree layers where the thick lines are indicating the mean, and thin lines show the standard deviation.

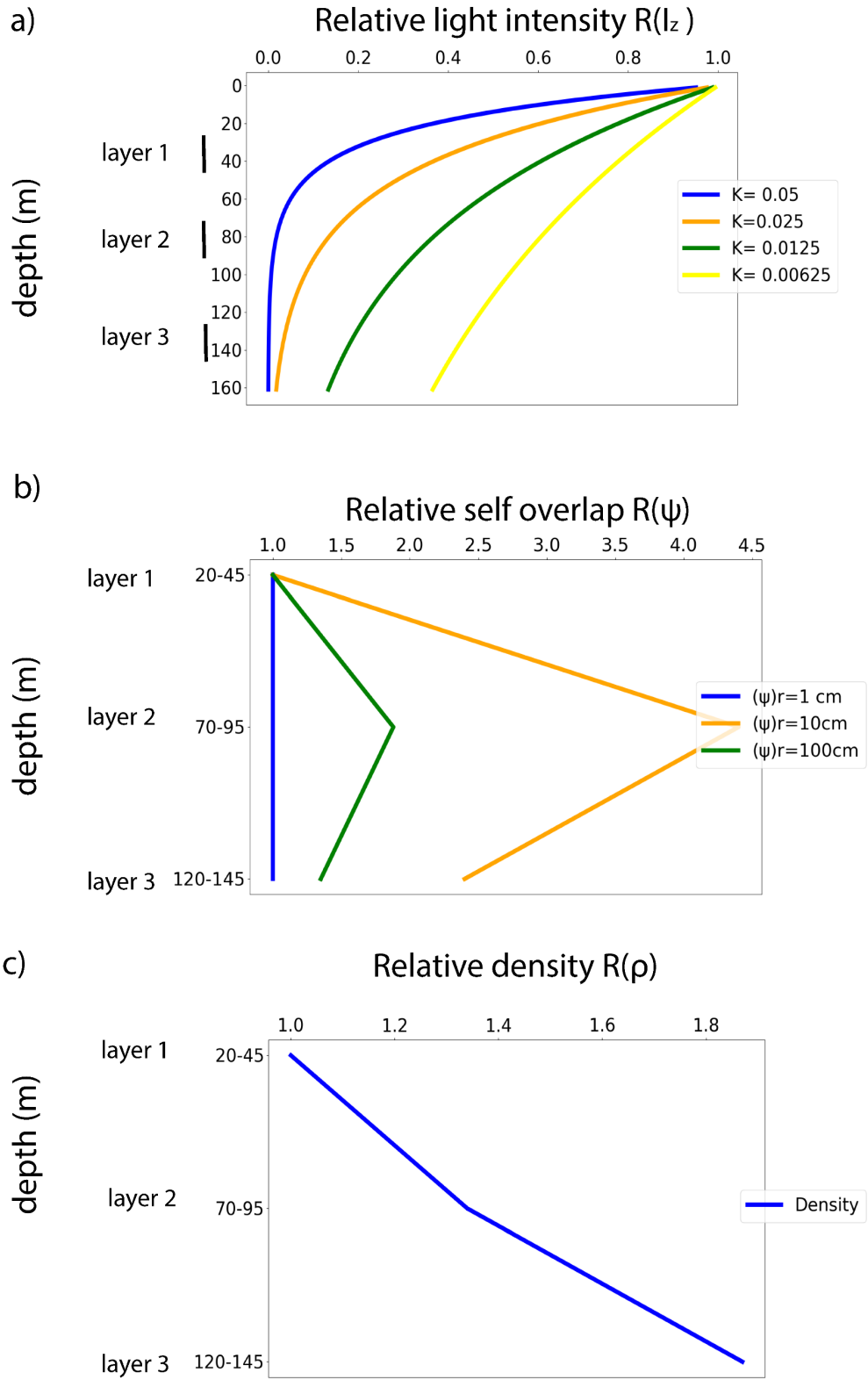
a)
Relative light intensity R(Iz)
depth (m)
layer 1
layer 2
layer 3
K= 0.05
K=0.025
K= 0.0125
K= 0.00625
b)
Relative self overlap R(ψ)
depth (m)
layer 1
layer 2
layer 3
20-45
70-95
120-145
(ψ)r=1 cm
(ψ)r=10cm
(ψ)r=100cm
c)
Relative density R(ρ)
depth (m)
layer 1
layer 2
layer 3
20-45
70-95
120-145
Density

Figure 6: Relative values of measured parameters. A is showing the relative light intensity $R(I_z)$ plotted against depth, for four different values of K. Panel b is showing the relative self-overlap for the three representative layers $R(\psi)$ for detective radiuses of 1, 10 and 100 cm, and finally panel c is showing the relative density $R(\rho)$ from the echo-counting derived densities.

Discussion

Using broadband acoustic observations we provide in-situ accurate descriptions of behavioural responses and predator prey interactions between mesopelagic fish species and their zooplankton prey. In particular, we demonstrate that juvenile pearlside individuals can migrate towards the surface during dusk to forage on *C. finmarhicus* although prey abundance in the surface is significantly lower than abundances found at the depths where pearlside individuals dwell during daytime. We explain this counter-intuitive predation strategy as resulting from the interaction of three factors regulating encounter rates: light availability, prey density, and prey swimming behaviour. Irradiance is generally low in the study area (Norwegian fjord in December) and light availability decreases with depth being very low at the depth where juvenile and adult pearlside individuals are present during daytime. Zooplankton (*C. finmarhicus*) density showed large changes with depth with higher abundances at depth and lower in the surface as most likely resulting because larger predation by fish in the illuminated region. Swimming behaviour of *C. finmarhicus* also shows changes with depth with more convoluted tracks at mid depth. These results in

significant changes in the self-overlap which is always generally low, but markably higher in layer 2. Large values of self-overlap can significantly decrease the encounter between *C.finmarchicus* and its fish predator. We argue that the changes in behaviour of zooplankton in layer 2 could be elicited by the increased presence of fish predators in that layer because of vertical migrations. A process that can be linked the so called ecology of fear (Brown *et al*., 1999; Zanette and Clinchy, 2019).

Light, behaviour and density's contribution to encounters

It is well established that the feeding patterns of pearlside rely on their visual capability to forage successfully (Aksnes and Utne, 1997; Eiane *et al.*, 1999; Staby and Aksnes, 2011; Staby *et al.*, 2013). Given that our acoustic measurements were conducted during dusk/early night, the surface irradiance was already highly reduced. Furthermore, the relative decrease in light and thus visual was potentially even more pronounced in layer 2 and 3 than assumed in the self-overlap model as TS-probe deployment in layer 2 and 3 were done 10 and 20 minutes later in the evening (Figure 3), potentially rendering the light attenuation rates between layers conservative estimate.

The reactive distance of pearlside is a combination of physical properties of the prey, visual properties of the fish and ambient light levels, which makes this value hard to quantify *in situ* (Aksnes and Utne, 1997; Utne-Palm, 2002; Huse and Fiksen, 2010), although irradiance and attenuation are parameters that are measurable(Aksnes and Utne, 1997; Staby and Aksnes, 2011; Staby *et al.*, 2013; Christiansen *et al.*, 2019). It is known that that mesopelagic fish have adaptions for very low light levels(De Busserolles *et al.*,

2017). However, it is equally important that increased visual range comes with a cost of predation, and explains why it is suggested that the adult population trade of feeding to decrease mortality during winter(Staby *et al.*, 2013)s.

This study and (Thorvaldsen *et al*., 2022a)highlights how knowledge on small scale behaviours, might provide answer on important topics both in biology, and in fisheries management as encounters feeds directly into parameters of growth, mortality and distribution. Visual foraging has successfully been included in theoretical encounter models for planktivorous fishes and *C. finmarhicus* (Huse and Fiksen, 2010). However, the prey is assumed stationary in this study. Modifications of the experienced prey density inside the search volume caused by prey movements is so far unaccounted for in literature. The *C. finmarhicus* trajectories found in current study strongly suggest that also prey movement is an important factor determining encounters.

C. finmarhicus behaviour in layer 1, 2 and 3 based on acoustic target trajectories and self overlap

The *C. finmarchicus* behaviour derived from the current acoustic trajectories differed in the three water depth layers. The jump-frequency, vertical movement, (table 1) and overall swimming behaviour (Figure 3a and d) suggest higher *C. finmarchicus* activity closer to the surface compared to the deeper layers. The higher activity is within the layer with the highest ambient light levels, i.e. the surface, and simultaneously highest predation risk (Giske *et al*., 1990; Giske and Aksnes, 1992; Balino and Aksnes, 1993; Staby*et al*., 2013). The sink and swim behaviours found in the current trajectories can be related to foraging as similar foraging behaviour have been seen in different species of copepods in

controlled condition(Bianco *et al.*, 2014; Chen and Hwang, 2018), or the increased vertical movement is used to increase unpredictability (Humphries and Driver, 1970) or both. This increased movement seen in the surface might suggest that the remaining Calanus trade off predation for increased feeding opportunities. However, the nature of the behaviour is uncertain, and should be explored further. The self-overlap observed in the layers 1, 2 and 3 are different, where the degree of self-overlap is very low in layer 1, higher in layer 2 and highest in layer 3 at all detective radiuses. (Figure 5a-b, 6b). However, in contrast to the copepod trajectories observed in Bianco et al., (2014) under laboratory conditions, the current *in situ C. finmarhicus* -trajectories would all categorized as ballistic at all scales (1,10 and 100cm)(Visser and Kiørboe, 2006; Visser, 2008; Bianco *et al.*, 2014). Self-overlap with a value of 0 means that the organism is moving in a straight line, never intersecting itself, while a self-overlap of 1 means that the animal does not move at the given visual range. All the *in situ* trajectories had extremely low values for self-overlap at the narrow range (1 cm). Generally for all three layers, self-overlap was increasing with visual range with some degree of taper towards the highest visual ranges between 10-100 cm. Small scale turbulence are likely playing a role in shaping the trajectories. The convoluted patterns seen in laboratory set-ups are under controlled conditions(Bianco *et al.*, 2014) and currents will change their motion strategy drastically (Michalec *et al.*, 2015), even if capable to resist vertical currents to some degree (Weidberg *et al.*, 2021).

There are many unknowns tied in with the deviations we observe. Both foraging, anti-predator behaviour and turbulence are possible factors shaping the trajectories. It has been reported in other groups of copepods that low food concentrations can increase their

swimming activity drastically to long ballistic trajectories in search for patches of food, while helical behaviour were only observed in a setting with food present (Chen and Hwang, 2018). The assumption for optimal behaviour (Bianco *et al.*, 2014) where self-overlap is close to 0 at *C. finmarhicus* 's detective radius and 1 at pearlside detective radius. might be too simple in an environment where feeding opportunities are possibly not evenly distributed zooplankton distribution is known to be patchy(Ashjian *et al.*, 1994; Folt and Burns, 1999).

There could be several explanations to why self-overlap is higher in layer 2. Typically foraging are happening in the surface (Ringelberg, 2010) , and by sensing the presence of fish with their range of sensory organs (Fields and Yen, 1997; Burdick *et al.*, 2007; Strickler and Balázsi, 2007; Abrahamsen *et al.*, 2010; Yen *et al.*, 2015). In layer 2, C.finmarchicus respond by moving with a higher degree of protection (Figure 5), and the difference are especially visible at detective radiuses of 10 cm(Figure 6a). During DVM, mesopelagic fishes passes by this layer, and this might be sensed by the *C. finmarhicus*, leading to increased anti-predator behaviour I.e The ecology of fear(Brown *et al.*, 1999). There were also small vertical movements observed in layer 3 (Figure 3f). This means that there is a small degree of movement, even within the layer assumed to be mostly in diapause.

Some of the trajectories resemble in many ways the nature of *Lévy* flights (Viswanathan *et al.*, 1996) (Figure 4, track nr 6) with long ballistic transitions and some search behaviour followed by a new transition, and *C. finmarhicus* might switch strategies

between ballistic searches, and convoluted feeding patterns. In other studies, other copepods are swimming in a circling or spiralling pattern in vicinity of food (Mazzocchi and Paffenhöfer, 1999), and moving in this way within the patch may increase foraging efficiency (Gerritsen and Strickler, 1977). A high degree of movement may also be an anti-predator strategy, where increased movement creates higher unpredictability for the predator to locate the prey also known as protean movement (Humphries and Driver, 1970). Moving at high speeds and long distances, there is a possibility, if the visual range is short, *C. finmarhicus* may leave the reactive distance of the fish before the fish are able to locate and attack the prey.

. The highest proportion of biomass is found in deeper waters and these *C. finmarhicus* are potentially performing diapause (Kaartvedt, 1996; Bagøien *et al.*, 2001; Hobbs *et al.*, 2020), and the fact found in current study that pearlside still vertically migrate towards the surface(Thorvaldsen *et al.*, 2022a)to feed on a lower biomass proves that the conditions in the surface layers are favourable for juvenile pearlside for other reasons than just prey density alone. Our study highlights the need to measure behaviour in situ and compare with laboratory studies

Ecological impacts

Both mesopelagic fish and micro nekton are important contributors to the carbon and lipid pumps, and knowing interactions in the mid-trophic levels in both regards are crucial to their role in linking primary production and higher trophic levels (Kloser *et al.*, 2009;

Battaglia *et al.*, 2013; St.John *et al.*, 2016; Duffy *et al.*, 2017), as well as binding organic matter to greater depths (Davison *et al.*, 2013; Jónasdóttir *et al.*, 2015)

To our knowledge there are, yet, no acoustic studies looking at single trajectories of *copepods in situ* in context of feeding and predator avoidance. Obtaining trajectories *in situ* is important, as there are oceanic and biological conditions that are very complex and difficult to mimic in an *ex situ* laboratory setup. Measuring of movement patterns of several taxa at different life stages is crucial as one of the goals in movement ecology is to observe "end-to-end movement" from birth to death of an organism to understand its ecology.

Combining movement with environmental parameters such as light, will increase knowledge on life history parameters of several trophic levels. In this context it is crucial to investigate which factors beyond density influences encounters and hence predation rate as well as predator growth. The relationship between light attenuation and visual predator range is important. Darkening of coastal areas due to increased riverine inflow as a consequence of climate change, and a parallel increase of gelatinous zooplankton populations(Eiane *et al.*, 1999; Aksnes *et al.*, 2004; Condon *et al.*, 2012) might hence so far unaccounted consequences for population- and ecosystem dynamics.

Using movement data to identify organisms

Ground truthing of acoustic data is challenging, especially in mesopelagic habitats(Kaartvedt *et al.*, 2012; Davison *et al.*, 2015; Kloser *et al.*, 2016; Proud *et al.*, 2019; Thorvaldsen *et al.*, 2022b). There is some uncertainty with regards to translating acoustic trajectories to the correct group or species. There are to date no *in situ* TS-measurements of *Calanus finmarchicus* in the lipid-filled state we observed in our study. However,

DWBA-models (Distorted Wave Born Approximation) predicting backscatter from small zooplankton suggest that they are capable of producing similar backscatter (TS ~-90dB) at 200 kHz, in scenarios were lipid content is high (Sakinan *et al.*, 2019). This study suggests that there are large possibilities to observe trophic interactions in the mesopelagic given that the micronekton and mesozooplankton is measured with acoustic platforms pinging at a short range.

Another critical parameter in determining the species identity of the trajectories were the observed movement patterns of the trajectories. The ascend-descend movement or' Hop-and-sink" behaviour is typical of copepods (Bianco *et al.*, 2014; Chen and Hwang, 2018; Weidberg *et al.*, 2021). We suggest using biological knowledge on movement patterns of different taxa paired with scattering properties and biological sampling)(Thorvaldsen *et al.*, 2022a).There are still challenges in the phase-deviation derived angular position estimates also known as along- and athwartship (x and y), but we observe that the characteristic vertical changes (z) are determined by using the timing of the echo (Simmonds and MacLennan, 2007) which is seen as a more precise measure, and here was the main parameter determining *C. finmarhicus* behaviour.

Conclusion

As seen in this study and many others, movement is not random and highly influences encounter rates between predator and prey. In our case, encounters are tightly linked to light. Even as prey density is lower, juvenile mesopelagic fish migrate to shallow waters to be able to see their prey. Furthermore, the behaviour of *C. finmarhicus* is different

in likely a trade-off between feeding and predation risk in the surface, while anti-predator behaviour is more present in layer 2 and 3, where feeding possibly do not occur. We find that non-invasive acoustic telemetry data have the potential to fill some important gaps in understanding trophic interactions.

Acknowledgements

We thank the crew of G.O Sars for the help in data collection, and Professor Egil Ona for making sure the TS-probe were collecting data properly. The production of the manuscript was funded by the project H2020-MEESO ("Ecologically and economically sustainable mesopelagic fisheries" grant agreement No. 817669).

References

Abrahamsen, M. B., Browman, H. I., Fields, D. M., and Skiftesvik, A. B. 2010. The three-dimensional prey field of the northern krill, Meganyctiphanes norvegica, and the escape responses of their copepod prey. Marine Biology, 157: 1251–1258.

Aksnes, D. L., and Utne, A. C. W. 1997. A revised model of visual range in fish. Sarsia, 82: 137–147.

Aksnes, D. L., Nejstgaard, J., Sædberg, E., and Sørnes, T. 2004. Optical control of fish

and zooplankton populations. Limnology and Oceanography, 49: 233–238.

Ashjian, C. J., Smith, S. L., Flagg, C. N., Mariano, A. J., Behrens, W. J., and Lane, P. V. Z. 1994. The influence of a Gulf Stream meander on the distribution of zooplankton biomass in the Slope Water, the Gulf Stream, and the Sargasso Sea, described using a shipboard acoustic Doppler current profiler. Deep-Sea Research Part I, 41: 23–50.

Bagøien, E., Kaartvedt, S., Aksnes, D. L., and Eiane, K. 2001. Vertical distribution and mortality of overwintering Calanus. Limnology and Oceanography, 46: 1494–1510.

Balino, B. M., and Aksnes, D. L. 1993. Winter distribution and migration of the sound scattering layers, zooplankton and micronekton in Masfjorden, western Norway. Marine Ecology Progress Series, 102: 35–50.

Basedow, S. L., and Tande, K. S. 2006. Cannibalism by female Calanus finmarchicus on naupliar stages. Marine Ecology Progress Series, 327: 247–255.

Battaglia, P., Andaloro, F., Consoli, P., Esposito, V., Malara, D., Musolino, S., Pedà, C., *et al.* 2013. Feeding habits of the Atlantic bluefin tuna, Thunnus thynnus (L. 1758), in the central Mediterranean Sea (Strait of Messina). Helgoland Marine Research.

Battaglia, P., Ammendolia, G., Esposito, V., Romeo, T., and Andaloro, F. 2018. Few But Relatively Large Prey: Trophic Ecology of Chauliodus sloani (Pisces: Stomiidae) in Deep Waters of the Central Mediterranean Sea. Journal of Ichthyology, 58: 8–16.

Berryman, A. A. 1992. The origins and evolution of predator-prey theory. Ecology, 73: 1530–1535.

Bianchi, D., and Mislan, K. A. S. 2016. Global patterns of diel vertical migration times and velocities from acoustic data. Limnology and Oceanography, 61: 353–364.

Bianco, G., Mariani, P., Visser, A. W., Mazzocchi, M. G., and Pigolotti, S. 2014. Analysis of self-overlap reveals trade-offs in plankton swimming trajectories. Journal of the Royal Society Interface, 11.

Bonnet, D., Titelman, J., and Harris, R. 2004. Calanus the cannibal. Journal of Plankton Research, 26: 937–948.

Brown, J. S., Laundré, J. W., and Gurung, M. 1999. The ecology of fear: Optimal foraging, game theory, and trophic interactions. Journal of Mammalogy, 80: 385–399.

Burdick, D. S., Hartline, D. K., and Lenz, P. H. 2007. Escape strategies in co-occurring calanoid copepods. Limnology and Oceanography, 52: 2373–2385.

Campbell, R. G., Sherr, E. B., Ashjian, C. J., Plourde, S., Sherr, B. F., Hill, V., and Stockwell, D. A. 2009. Mesozooplankton prey preference and grazing impact in the western Arctic Ocean. Deep Sea Research Part II: Topical Studies in Oceanography, 56: 1274–1289.

Chen, M. R., and Hwang, J. S. 2018. The Swimming Behavior of the Calanoid Copepod Calanus sinicusUnder Different Food Concentrations. Zoological Studies, 57.

Christiansen, S., Titelman, J., and Kaartvedt, S. 2019. Nighttime Swimming Behavior of a Mesopelagic Fish. Frontiers in Marine Science, 6.

Christiansen, S., Klevjer, T. A., Røstad, A., Aksnes, D. L., and Kaartvedt, S. 2021. Flexible behaviour in a mesopelagic fish (Maurolicus muelleri). ICES Journal of Marine Science.

Condon, R. H., Graham, W. M., Duarte, C. M., Pitt, K. A., Lucas, C. H., Haddock, S. H. D., Sutherland, K. R., *et al.* 2012. Questioning the rise of gelatinous Zooplankton in the world's oceans. BioScience, 62: 160–169.

Davison, P. C., Checkley, D. M., Koslow, J. A., and Barlow, J. 2013. Carbon export mediated by mesopelagic fishes in the northeast Pacific Ocean. Progress in Oceanography, 116: 14–30.

Davison, P. C., Koslow, J. A., and Kloser, R. J. 2015. Acoustic biomass estimation of mesopelagic fish: Backscattering from individuals, populations, and communities. ICES Journal of Marine Science, 72: 1413–1424.

De Busserolles, F., Cortesi, F., Helvik, J. V., Davies, W. I. L., Templin, R. M., Sullivan, R. K. P., Michell, C. T., *et al.* 2017. Pushing the limits of photoreception in twilight conditions: The rod-like cone retina of the deep-sea pearlsides. Science Advances, 3: 4709.

Dias Bernardes, I., Ona, E., and Gjøsæter, H. 2020. Study of the Arctic mesopelagic layer with vessel and profiling multifrequency acoustics. Progress in Oceanography, 182: 102260.

Dietz, R. S. 1962. The Sea's Deep Scattering Layers, 207: 44–51.

Duffy, L. M., Kuhnert, P. M., Pethybridge, H. R., Young, J. W., Olson, R. J., Logan, J. M., Goñi, N., *et al.* 2017. Global trophic ecology of yellowfin, bigeye, and albacore tunas: Understanding predation on micronekton communities at ocean-basin scales. Deep Sea Research Part II: Topical Studies in Oceanography, 140: 55–73.

Duvall, G. E., and Christensen, R. J. 1946. Stratification of Sound Scatterers in the Ocean. The Journal of the Acoustical Society of America, 18: 254–254.

Eiane, K., Aksnes, D. L., Bagøien, E., and Kaartvedt, S. 1999. Fish or jellies - A question of visibility? Limnology and Oceanography, 44: 1352–1357.

EK80 Scientific wide-band echo sounder - Kongsberg Maritime. 2022. .

Falk-Petersen, S., Mayzaud, P., … G. K.-M. B., and 2009, undefined. 2009. Lipids and life strategy of Arctic Calanus. Taylor & Francis, 5: 18–39.

Fasham, M. J. R., Ducklow, H. W., and McKelvie, S. M. 1990. A nitrogen-based model of plankton dynamics in the oceanic mixed layer. Journal of Marine Research, 48: 591–639.

Fields, D. M., and Yen, J. 1997. The escape behavior of marine copepods in response to a quantifiable fluid mechanical disturbance. Journal of Plankton Research, 19: 1289–1304.

Folkvord, A., Gundersen, G., Albretsen, J., Asplin, L., Kaartvedt, S., and Giske, J. 2016. Impact of hatch date on early life growth and survival of Mueller's pearlside (Maurolicus muelleri) larvae and life-history consequences. Canadian Journal of

Fisheries and Aquatic Sciences, 73: 163–176.

Folt, C. L., and Burns, C. W. 1999. Biological drivers of zooplankton patchiness Box 1. Why is scale important?, 14.

García-Seoane, E., Dalpadado, P., and Vázquez, A. 2013. Feeding ecology of the glacier lanternfish Benthosema glaciale (Actinopterygii, Myctophidae) in the Flemish Cap (North Atlantic Ocean). Hydrobiologia, 717: 133–146.

Gerritsen, J., and Strickler, J. R. 1977. Encounter Probabilities and Community Structure in Zooplankton: a Mathematical Model. Journal of the Fisheries Research Board of Canada.

Giske, J., Aksnes, D. L., Baliño, B. M., Kaartvedt, S., Lie, U., Nordeide, J. T., Salvanes, A. G. V., *et al.* 1990. Vertical distribution and trophic interactions of zooplankton and fish in Masfjorden, Norway. Sarsia, 75: 65–81.

Giske, J., and Aksnes, D. L. 1992. Ontogeny, season and trade-offs: Vertical distribution of the mesopelagic fish maurolicus muelleri. Sarsia, 77: 253–261.

Gjøsaeter, J., and Kawaguchi, K. 1980. A review of the world resources of mesopelagic fish. FAO Fisheries Technical Paper, 193: 123–134.

Gjøsæter, J. 1973. The food of the mygtophid fish, benthosema glaciale (reinhardt), from Western Norway. Sarsia, 52: 53–58.

Gjøsæter, J. 1981. Variation in Growth Rate and Age at First Maturation in Rainbow Trout; Growth, Production and Reproduction of the Myctophid Fish Benthosema

Glaciale From Western Norway and Adjacent Seas; Life History and Ecology of Maurolicus Muelleri (Gonostomatidae) i. 109–131 pp.

Gorsky, G., Ohman, M. D., Picheral, M., Gasparini, S., Stemmann, L., Romagnan, J. B., Cawood, A., *et al.* 2010. Digital zooplankton image analysis using the ZooScan integrated system.

Grimaldo, E. ;, Herrmann, B. ;, Bri, J., Cerbule, K. ;, Brinkhof, J. ;, Grimsmo, L. ;, and Jacques, N. 2022. Prediction of potential net panel selectivity in mesopelagic trawls. Ocean Engineering, 260.

Handegard, N. O., Patel, R., and Hjellvik, V. 2005. Tracking individual fish from a moving platform using a split-beam transducer. The Journal of the Acoustical Society of America, 118: 2210–2223.

Handegard, N. O. 2007. Observing individual fish behavior in fish aggregations: Tracking in dense fish aggregations using a split-beam echosounder. The Journal of the Acoustical Society of America, 122: 177–187.

Hobbs, L., Banas, N. S., Cottier, F. R., Berge, J., and Daase, M. 2020. Eat or Sleep: Availability of Winter Prey Explains Mid-Winter and Spring Activity in an Arctic Calanus Population. Frontiers in Marine Science.

Holling, C. S. 1959. Some Characteristics of Simple Types of Predation and Parasitism. The Canadian Entomologist, 91: 385–398.

Holling, C. S. 1966. The Functional Response of Invertebrate Predators to Prey Density.

The Memoirs of the Entomological Society of Canada, 98: 5–86.

Howey, L. A., Tolentino, E. R., Papastamatiou, Y. P., Brooks, E. J., Abercrombie, D. L., Watanabe, Y. Y., Williams, S., *et al.* 2016. Into the deep: the functionality of mesopelagic excursions by an oceanic apex predator. Ecology and Evolution, 6: 5290–5304.

Humphries, D. A., and Driver, P. M. 1970. Protean defence by prey animals. Oecologia 1970 5:4, 5: 285–302.

Huse, G., and Fiksen, Ø. 2010. Modelling encounter rates and distribution of mobile predators and prey. Progress in Oceanography, 84: 93–104.

Irigoien, X., Klevjer, T. A., Røstad, A., Martinez, U., Boyra, G., Acuña, J. L., Bode, A., *et al.* 2014. Large mesopelagic fishes biomass and trophic efficiency in the open ocean. Nature communications, 5: 3271.

Jónasdóttir, S. H., Visser, A. W., Richardson, K., and Heath, M. R. 2015. Seasonal copepod lipid pump promotes carbon sequestration in the deep North Atlantic. Proceedings of the National Academy of Sciences of the United States of America.

Kaartvedt, S. 1996. Habitat preference during overwintering and timing of seasonal vertical migration of Calanusï¿¿finmarchicus. Ophelia, 44: 145–156.

Kaartvedt, S., Torgersen, T., Klevjer, T. A., Røstad, A., and Devine, J. A. 2008. Behavior of individual mesopelagic fish in acoustic scattering layers of Norwegian fjords. Marine Ecology Progress Series, 360: 201–209.

Kaartvedt, S., Staby, A., and Aksnes, D. L. 2012. Efficient trawl avoidance by mesopelagic fishes causes large underestimation of their biomass. Marine Ecology Progress Series, 456: 1–6.

Kaartvedt, S., Langbehn, T. J., and Aksnes, D. L. 2019. Enlightening the ocean's twilight zone. ICES Journal of Marine Science, 76: 803–812.

Kinzer, J. 1977. Observations on feeding habits of the mesopelagic fish Benthosema glaciale (Myctophidae) off NW Africa.

Kleppel, G. S. 1993. On the diets of calanoid copepods. Marine Ecology Progress Series, 99: 183–195.

Kloser, R. J., Ryan, T. E., Young, J. W., and Lewis, M. E. 2009. Acoustic observations of micronekton fish on the scale of an ocean basin: Potential and challenges. *In* ICES Journal of Marine Science, pp. 998–1006.

Kloser, R. J., Ryan, T. E., Keith, G., and Gershwin, L. 2016. Deep-scattering layer, gas-bladder density, and size estimates using a two-frequency acoustic and optical probe. *In* ICES Journal of Marine Science, pp. 2037–2048.

Knutsen, T., Wiebe, P. H., Gjøsæter, H., Ingvaldsen, R. B., and Lien, G. 2017. High Latitude Epipelagic and mesopelagic scattering layers-a reference for future Arctic ecosystem change. Frontiers in Marine Science, 4.

Korneliussen, R. J. 2010. Large Scale Survey System – LSSS. Database.

Korneliussen, R. J., Heggelund, Y., Macaulay, G. J., Patel, D., Johnsen, E., and Eliassen,

I. K. 2016. Acoustic identification of marine species using a feature library. Methods in Oceanography, 17: 187–205.

Kristoffersen, J. B., and Salvanes, A. G. V. 1998. Life history of Maurolicus muelleri in fjordic and oceanic environments. Journal of Fish Biology, 53: 1324–1341.

Lam, V. W. M., and Pauly, D. 2005. Mapping the global biomass of mesopelagic fishes. 4 pp.

Lotka, A. J. 1920. Analytical Note on Certain Rhythmic Relations in Organic Systems. Proceedings of the National Academy of Sciences.

MathWorks. 2020. Curve Fitting Toolbox - MATLAB.

Mazzocchi, M. G., and Paffenhöfer, G. A. 1999. Swimming and feeding behaviour of the planktonic copepod Clausocalanus furcatus. Journal of Plankton Research, 21: 1501–1518.

Michalec, F. G., Souissi, S., and Holzner, M. 2015. Turbulence triggers vigorous swimming but hinders motion strategy in planktonic copepods. Journal of the Royal Society Interface, 12.

Nathan, R. 2008, December 9. An emerging movement ecology paradigm.

Neuenfeldt, S., and Beyer, J. E. 2006. Environmentally driven predator-prey overlaps determine the aggregate diet of the cod Gadus morhua in the Baltic Sea. Marine Ecology Progress Series, 310: 151–163.

Olson, R. J., Duffy, L. M., Kuhnert, P. M., Galván-Magaña, F., Bocanegra-Castillo, N., and Alatorre-Ramírez, V. 2014. Decadal diet shift in yellowfin tuna Thunnus albacares suggests broad-scale food web changes in the eastern tropical Pacific Ocean. Marine Ecology Progress Series, 497: 157–178.

Paoletti, S. ;, Rasmus Nielsen, J. ; R., Sparrevohn, R. ;, Bastardie, C. ;, and Vastenhoud, M. J. 2021. Potential for Mesopelagic Fishery Compared to Economy and Fisheries Dynamics in Current Large Scale Danish Pelagic Fishery. Citation.

Picheral, M., Colin, S., and Irisson J-O. (n.d.). EcoTaxa.

Prihartato, P. K., Aksnes, D. L., and Kaartvedt, S. 2015. Seasonal patterns in the nocturnal distributionand behavior of the mesopelagic fish Maurolicus muelleri at high latitudes. Marine Ecology Progress Series, 521: 189–200.

Proud, R., Cox, M. J., and Brierley, A. S. 2017. Biogeography of the Global Ocean's Mesopelagic Zone. Current Biology, 27: 113–119.

Proud, R., Handegard, N. O., Kloser, R. J., Cox, M. J., Brierley, A. S., and Demer, D. 2019. From siphonophores to deep scattering layers: Uncertainty ranges for the estimation of global mesopelagic fish biomass. ICES Journal of Marine Science, 76: 718–733.

Ringelberg, J. 2010. Diel vertical migration of zooplankton in lakes and oceans: Causal explanations and adaptive significances. Diel Vertical Migration of Zooplankton in Lakes and Oceans: Causal Explanations and Adaptive Significances: 1–356.

Roe, H. S. J., Angel, M. V., Badcock, J., Domanski, P., James, P. T., Pugh, P. R., and Thurston, M. H. 1984. The diel migrations and distributions within a Mesopelagic community in the North East Atlantic. 1. Introduction and sampling procedures.

Rothschild, B., Research, T. O.-J. of plankton, and 1988, undefined. 1988. Small-scale turbulence and plankton contact rates. academic.oup.com, 10: 465–474.

Sakinan, S., Lawson, G. L., Wiebe, P. H., Chu, D., and Copley, N. J. 2019. Accounting for seasonal and composition-related variability in acoustic material properties in estimating copepod and krill target strength. Limnology and Oceanography: Methods, 17: 607–625.

Salvanes, A. G. V., and Kristoffersen, J. B. 2001. Mesopelagic Fishes. *In* Encyclopedia of Ocean Sciences.

Salvanes, A. G. V., Aksnes, D., Fosså, J. H., and Giske, J. 1995. Simulated carrying capacities of fish in Norwegian fjords. Fisheries Oceanography, 4: 17–32.

Simmonds, J., and MacLennan, D. 2007. Fisheries acoustics: Theory and practice: Second edition. 1–252 pp.

St.John, M. A. S., Borja, A., Chust, G., Heath, M., Grigorov, I., Mariani, P., Martin, A. P., *et al.* 2016. A dark hole in our understanding of marine ecosystems and their services: Perspectives from the mesopelagic community. Frontiers in Marine Science, 3.

Staby, A., and Aksnes, D. L. 2011. Follow the light-diurnal and seasonal variations in

vertical distribution of the mesopelagic fish Maurolicus muelleri. Marine Ecology Progress Series, 422: 265–273.

Staby, A., Srisomwong, J., and Rosland, R. 2013. Variation in DVM behaviour of juvenile and adult pearlside (Maurolicus muelleri) linked to feeding strategies and related predation risk. Fisheries Oceanography, 22: 90–101.

Standal, D., and Grimaldo, E. 2020. Institutional nuts and bolts for a mesopelagic fishery in Norway. Marine Policy, 119: 104043.

Strickler, J. R., and Balázsi, G. 2007, November 29. Planktonic copepods reacting selectively to hydrodynamic disturbances.

Tablado, Z., Fauchald, P., Mabille, G., Stien, A., and Tveraa, T. 2014. Environmental variation as a driver of predator-prey interactions. Ecosphere.

Thorvaldsen, K. G., Neuenfeldt, S., Mariani, P., and Nielsen, J. R. 2022a. Hiding in plain sight: Predator avoidance behaviour of mesopelagic Maurolicus muelleri during foraging.

Thorvaldsen, K. G., Neuenfeldt, S., Kubilius, R., and Ona, E. 2022b. Towards identifying broadband signatures of the Norwegian shelf's sound scattering layers.

Torgersen, T., and Kaartvedt, S. 2001. In situ swimming behaviour of individual mesopelagic fish studied by split-beam echo target tracking. ICES Journal of Marine Science, 58: 346–354.

Utne-Palm, A. C. 2002. Visual feeding of fish in a turbid environment: Physical and

behavioural aspects. Marine and Freshwater Behaviour and Physiology, 35: 111–128.

Visser, A. W., and Kiørboe, T. 2006. Plankton motility patterns and encounter rates. Oecologia, 148: 538–546.

Visser, A. W. 2008. Lagrangian modelling of plankton motion: From deceptively simple random walks to Fokker-Planck and back again. Journal of Marine Systems, 70: 287–299.

Viswanathan, G. M., Afanasyev, V., Buldyrev, S. V., Murphy, E. J., Prince, P. A., and Stanley, H. E. 1996. Lévy flight search patterns of wandering albatrosses. Nature, 381: 413–415.

Volterra, V. 1926. Variazioni e fluttuazioni del numero d'individui in specie animali conviventi. Memoria della regia accademia nazionale del lincei ser.

Weidberg, N., DiBacco, C., Pezzola, C., Rebiffe, E., and Basedow, S. 2021. Swimming performance of subarctic Calanus spp. facing downward currents. Marine Ecology Progress Series.

Yen, J., Murphy, D. W., Fan, L., and Webster, D. R. 2015. Sensory-Motor Systems of Copepods involved in their Escape from Suction Feeding. *In* Integrative and Comparative Biology, pp. 121–133.

Zanette, L. Y., and Clinchy, M. 2019. Ecology of fear. Current Biology, 29: R309–R313.

11 Supplementary material paper II

Supplementary table 1: Results from the calibration of the echosounders.

	Simrad EK80 TS-Probe, FM pulses			
Transducer type	ES70-7CD		ES120-7CD	ES200-7CD
Frequency (kHz)	56-87	97-160	160-260	280-450
Power (W)	500	400	150	50
Gain (dB)	27.59	26.79	26.2	24.85
Equivalent beam angle (dB)	-20.7	-20.7	-20.7	-20.7
Taper (%)	1.74	1.0	0.60	0.34
Absorption coefficient (dB km^{-1})	23.8	40.02	55.55	86.63
Pulse duration (ms)	2.048	2.048	2.048	2.048
Half power beam widths (along/athwart ship) (deg))	6.96/6.87	7.26/7.28	6.86/6.91	6.73/6.77
Transducer angle sensitivity (deg))((along ship and athwart ship)	23.0	23.0	23.0	23.0
Sound speed (measured) (m s^{-1})	1500	1500	1500	1500

SED-Filters for target tracking using broadband pulses	
Min TS (dB)	-75

Pulse length determination level (dB)	6
Max one-way gain compensation (dB)	6

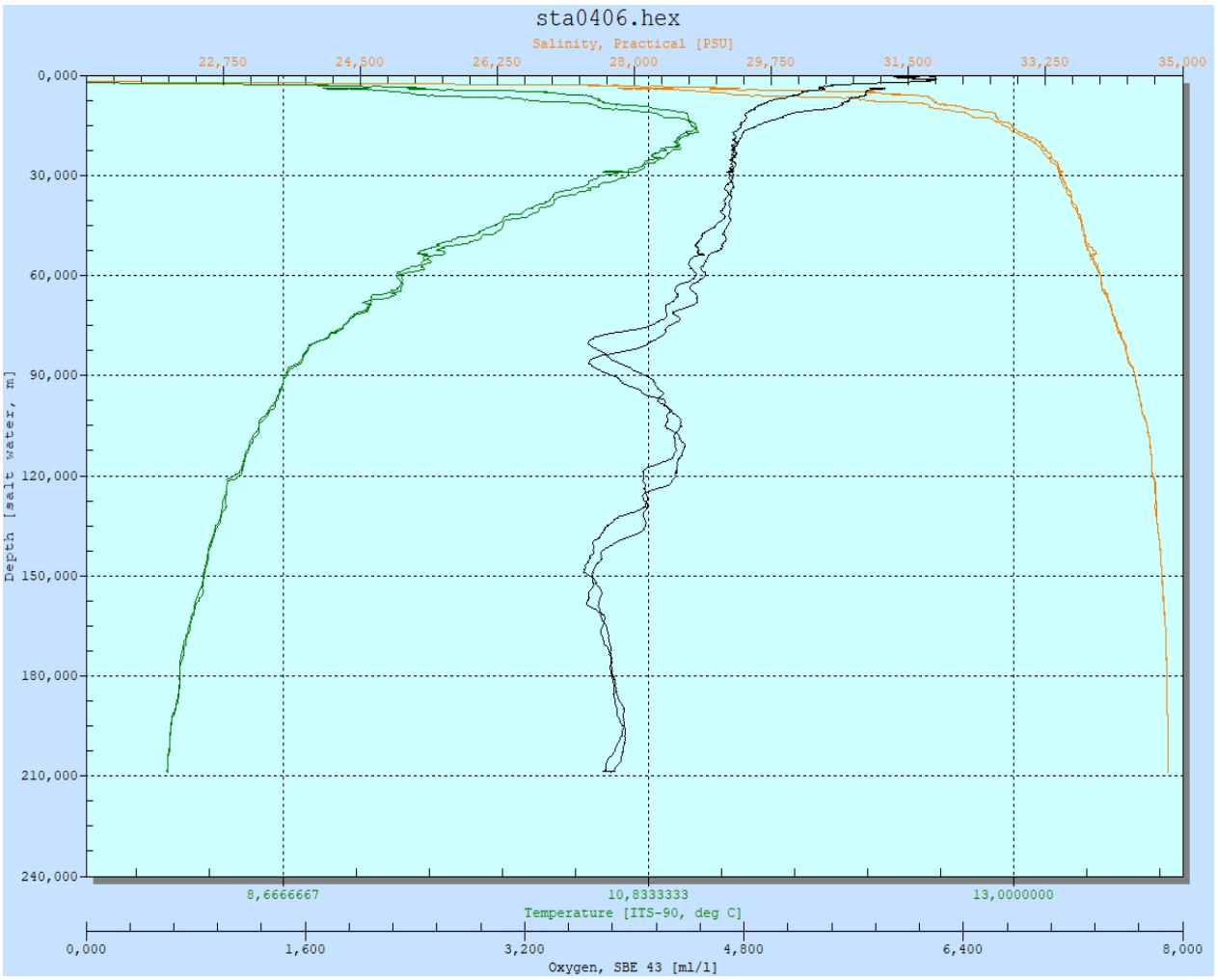

Figure 1. Results from CTD profile, showing temperature (green (celsius), salinity (psu), and oxygen (black(ml/l) measured from the surface down to 210 meters.

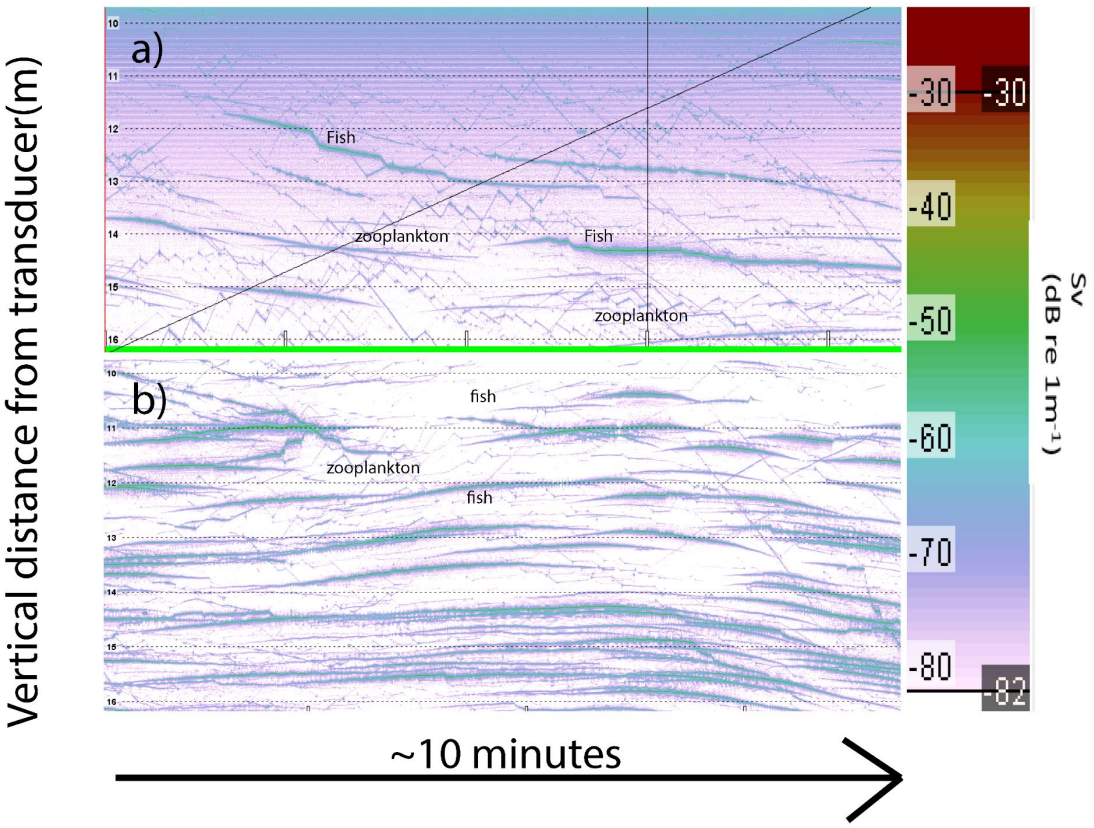

Supplementary figure 2. Panel a is showing an echogram of approximately 10 minutes of TS-probe measurements in SSL1. Panel b is showing a similar time interval in SSL2. Strong echoes, here seen as large green lines were labelled to be fish, while the weaker echoes with the characteristic vertical movement, especially seen in panel a is labelled to be zooplankton. Zooplankton and fish are seen in both echograms.

12 Supplementary paper III

Supplementary paper 3

Supplementary table 1: Results from the calibration of the echosounders.

	Simrad EK80 TS-Probe, FM pulses			
Transducer type	ES70-7CD		ES120-7CD	ES200-7CD
Frequency (kHz)	56-87	97-160	160-260	280-450
Power (W)	500	400	150	50
Gain (dB)	27.59	26.79	26.2	24.85
Equivalent beam angle (dB)	-20.7	-20.7	-20.7	-20.7
Taper (%)	1.74	1.0	0.60	0.34
Absorption coefficient (dB km^{-1})	23.8	40.02	55.55	86.63
Pulse duration (ms)	2.048	2.048	2.048	2.048
Half power beam widths (along/athwart ship) (deg))	6.96/6.87	7.26/7.28	6.86/6.91	6.73/6.77
Transducer angle sensitivity (deg))((along ship and athwart ship)	23.0	23.0	23.0	23.0
Sound speed (measured) (m s^{-1})	1500	1500	1500	1500

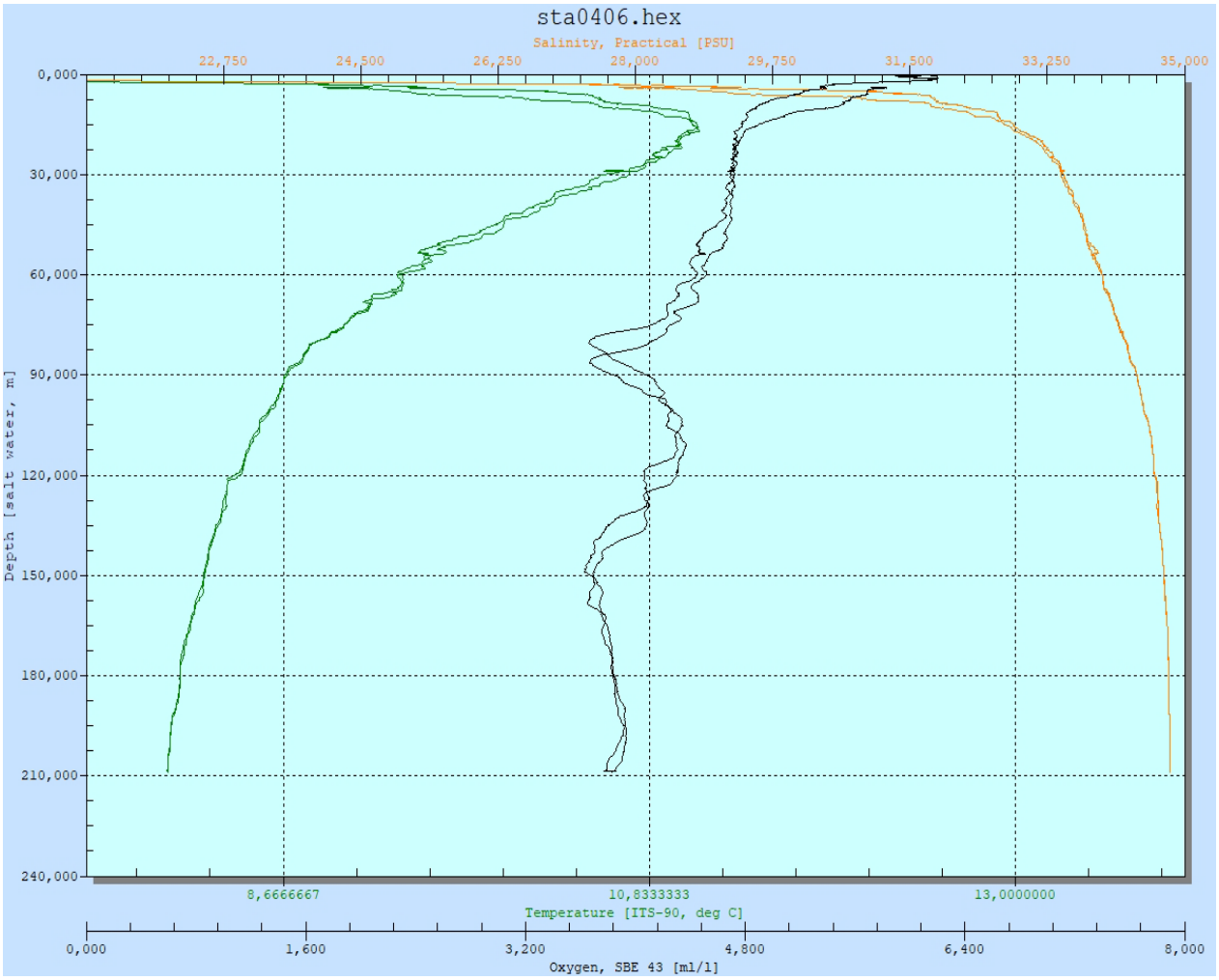

Figure 1. Results from CTD profile, showing temperature (green (celsius), salinity (psu), and oxygen (black(ml/l) measured from the surface down to 210 meters.

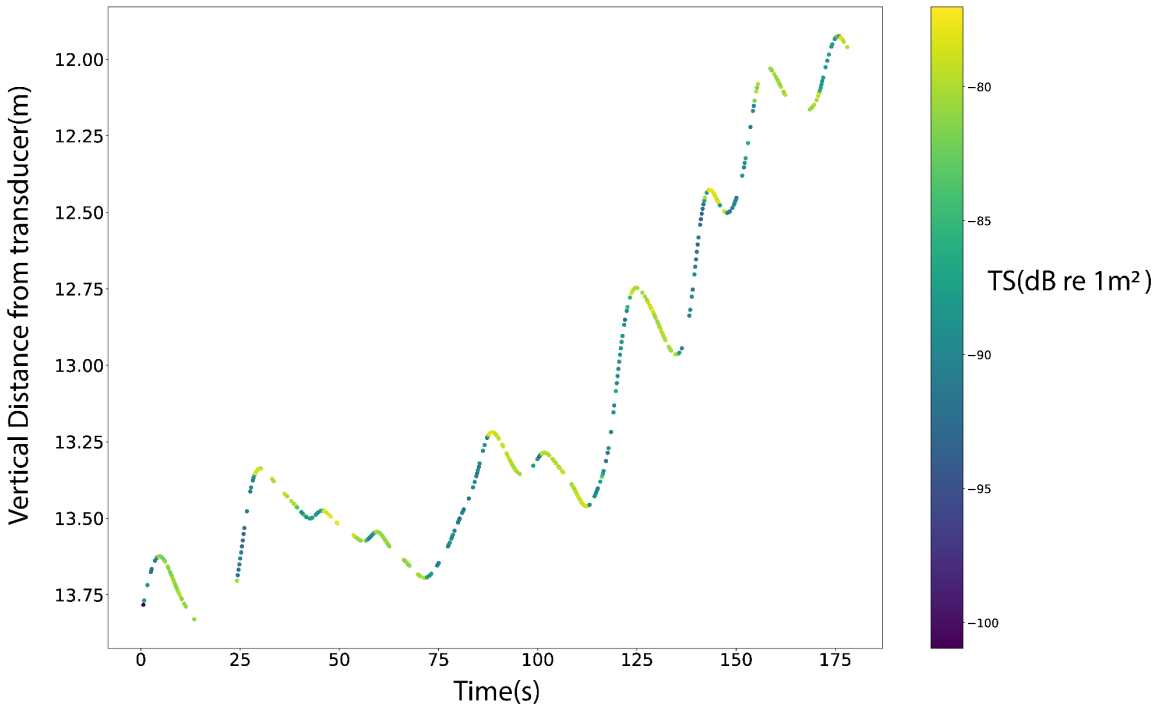

Supplementary figure 2: vertical positions of a tracked copepod as a function of time. The y axis are showing vertical position of the targets and the x-axis are showing time (s). The color bar shows TS, and TS generally increases when the *C.Finmarchicus* were moving downwards.

Table x SED-filters for target tracking using broadband pulses.

SED-Filters for target tracking using broadband pulses

Min TS (dB)	-130
Pulse length determination level (dB)	6
Max one-way gain compensation (dB)	6

Technical
University of
Denmark

DTU Aqua
Kemitorvet
DK-2800 Kgs. Lyngby

www.aqua.dtu.dk